

Adjoint Methods as Design Tools in Thermoacoustics

In a thermoacoustic system, such as a flame in a combustor, heat release oscillations couple with acoustic pressure oscillations. If the heat release is sufficiently in phase with the pressure, these oscillations can grow, sometimes with catastrophic consequences. Thermoacoustic instabilities are still one of the most challenging problems faced by gas turbine and rocket motor manufacturers. Thermoacoustic systems are characterized by many parameters to which the stability may be extremely sensitive. However, often only few oscillation modes are unstable. Existing techniques examine how a change in one parameter affects all (calculated) oscillation modes, whether unstable or not. Adjoint techniques turn this around: They accurately and cheaply compute how each oscillation mode is affected by changes in all parameters. In a system with a million parameters, they calculate gradients a million times faster than finite difference methods. This review paper provides: (i) the methodology and theory of stability and adjoint analysis in thermoacoustics, which is characterized by degenerate and nondegenerate nonlinear eigenvalue problems; (ii) physical insight in the thermoacoustic spectrum, and its exceptional points; (iii) practical applications of adjoint sensitivity analysis to passive control of existing oscillations, and prevention of oscillations with ad hoc design modifications; (iv) accurate and efficient algorithms to perform uncertainty quantification of the stability calculations; (v) adjoint-based methods for optimization to suppress instabilities by placing acoustic dampers, and prevent instabilities by design modifications in the combustor's geometry; (vi) a methodology to gain physical insight in the stability mechanisms of thermoacoustic instability (intrinsic sensitivity); and (vii) in nonlinear periodic oscillations, the prediction of the amplitude of limit cycles with weakly nonlinear analysis, and the theoretical framework to calculate the sensitivity to design parameters of limit cycles with adjoint Floquet analysis. To show the robustness and versatility of adjoint methods, examples of applications are provided for different acoustic and flame models, both in longitudinal and annular combustors, with deterministic and probabilistic approaches. The successful application of adjoint sensitivity analysis to thermoacoustics opens up new possibilities for physical understanding, control and optimization to design safer, quieter, and cleaner aero-engines. The versatile methods proposed can be applied to other multiphysical and multiscale problems, such as fluid–structure interaction, with virtually no conceptual modification. [DOI: 10.1115/1.4042821]

1 Introduction

Thermoacoustic oscillations are a challenging problem that affects aircraft and industrial gas turbines, as well as rocket and heat-exchanger manufacturing [1–7]. In gas turbines, the chemical energy contained in the fuel is converted into thermal energy via controlled combustion with air. During the combustion process, the flame releases unsteady heat, which is a powerful monopole source of sound waves [8] propagating back and forth within the combustion chamber. When they echo and return to the flame, sound waves may enhance the heat released by the flame, which, in turn, generates even stronger sound waves. These are called thermoacoustic instabilities or oscillations, which are also known as combustion instabilities.² For this to occur, three macro subsystems—hydrodynamics,³ acoustics, and the flame (Fig. 1)—constructively interact with each other. Hydrodynamic instabilities (e.g., shear layer instabilities) unsteadily change the flame shape, which, in turn, changes the heat release rate, thereby generating acoustic perturbations. The latter, in turn, excite hydrodynamic instabilities at the flame's base, which closes the feedback loop. The essence of this feedback mechanism was explained by Rayleigh [16] and mathematically formalized in Refs. [17] and [18] by defining the acoustic energy as

$$\tilde{E}_{\text{ac}} \equiv \frac{1}{2} \int_{\tilde{V}} \left(\tilde{\rho} \tilde{\mathbf{u}}' \cdot \tilde{\mathbf{u}}' + \frac{\tilde{p}'^2}{\tilde{\rho} \tilde{c}^2} \right) d\tilde{V} \quad (1)$$

where $\tilde{\cdot}$ denotes a dimensional quantity; $\bar{\cdot}$ is the mean-flow quantity; $'$ is the small fluctuation; $\tilde{\rho}$ is the density; $\tilde{\mathbf{u}}$ is the velocity; \tilde{p} is the pressure; \tilde{c} is the speed of sound; and \tilde{V} is the space domain, i.e., the volume of the combustion chamber. By combining the acoustic momentum and energy equations (Sec. 2), the instantaneous change in the acoustic energy reads

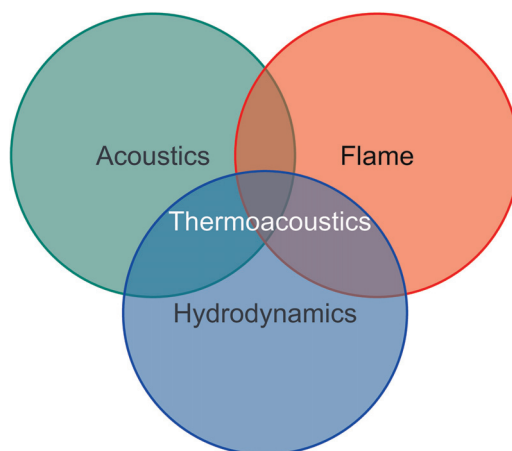


Fig. 1 Three main subsystems interact with each other to give rise to thermoacoustic instabilities

¹Corresponding author.

²Additionally, there exist thermoacoustic instabilities that occur in anechoic systems, which are called intrinsic thermoacoustic instabilities [9–15].

³Nonreacting flow phenomena governed by low-Mach number equations.

Manuscript received October 8, 2018; final manuscript received February 5, 2019; published online March 13, 2019. Editor: Harry Dankowicz.

$$\frac{\partial \tilde{E}_{ac}}{\partial \tilde{t}} = \int_{\tilde{V}} \left(\frac{\gamma - 1}{\gamma \tilde{p}} \right) \tilde{p}' \tilde{Q}' d\tilde{V} - \int_{\tilde{S}} \tilde{p}' \tilde{\mathbf{u}}' \cdot \mathbf{n} d\tilde{S} \quad (2)$$

where γ is the gas heat-capacity ratio; \tilde{Q} is the heat release rate from a generic source; and \mathbf{n} is the unit vector normal to the boundary \tilde{S} . When the left-hand side of Eq. (2) is positive over an acoustic period, the acoustic energy, \tilde{E}_{ac} , increases in time. Physically, this occurs when the heat release rate is sufficiently in phase with the acoustic pressure such that the source of power (first integral on the right-hand side) exceeds the acoustic radiation from the boundary (second integral on the right-hand side). This is called the *Rayleigh criterion* [16],⁴ which is pedagogically explained in Refs. [3] and [7]. The growth of the acoustic energy over a cycle results in a noisy (often tonal) thermoacoustic oscillation. In jet engines and afterburners, where the power density is $\sim 0.1 \text{ GW/m}^3$, detrimental consequences of thermoacoustic oscillations are mechanical fatigue, noise pollution, and increase in the engine emissions. In the worst-case scenario, uncontrolled thermoacoustic oscillations can extinguish the flame or bring about structural failure, especially in rocket motors where the power density is $\sim 1 \text{ GW/m}^3$ in solid rockets, and $\sim 50 \text{ GW/m}^3$ in liquid rockets [1,4]. It is, therefore, paramount for engineers to understand, predict, and control these oscillations, and suppress them when they occur. Eigenvalue analysis is a widely used tool in industry and academia for the calculation of thermoacoustic stability, as detailed in Sec. 1.1.

1.1 Eigenvalue Analysis. In the preliminary design of an aero-engine combustor, the first objective is to guarantee that the configuration is linearly stable to small perturbations over the desired operating range. A necessary condition for thermoacoustic oscillations not to occur is that the growth rates of the eigenvalues are negative, i.e., the eigenvalues lie in the stable semiplane. Eigenvalue analysis is attractive because it is computationally cheaper than testing, high-fidelity computations, and nonlinear analysis.

1.1.1 Transient Growth. The stability of eigenvalues is a necessary but not sufficient condition for the combustor not to experience nonlinear oscillations. Indeed, if the transient growth is sufficiently large, even small perturbations, such as background noise, can be amplified and trigger nonlinearities. This phenomenon is particularly dangerous in subcritical bifurcations, within the hysteresis region in which a finite-amplitude solution co-exists with an eigenvalue stable fixed point. If the degree of non-normality is large⁵ in the hysteresis region, a linearly stable solution can be driven to an oscillating attractor. This phenomenon is therefore called *triggering* or *bypass transition*⁶ [30,34–39].

In general, thermoacoustic systems are non-normal because their eigenfunctions are not orthogonal to each other [40]. As reviewed by Sujith et al. [39], non-normality in thermoacoustics was investigated in ducted diffusion flames [36,37] and heat sources [34,35,41–45]; solid rocket motors [46,47]; and premixed flames [48]. Later on, the authors of Ref. [38] showed that thermoacoustic non-normality in ducted diffusion flames is not as influential as it was thought to be. The calculations were performed by both singular value decomposition [38] and seminorm Lagrangian optimization [49]. In ducted premixed flames, the level of non-normality was shown to be small [50]. The small

⁴In the original Rayleigh criterion, the dissipation integral, $\int_S \tilde{p}' \tilde{\mathbf{u}}' \cdot \mathbf{n} d\tilde{S}$, is not accounted for, but it can be found in Chu [18]. Other sources of acoustic damping, such as dissipation in the thermal/viscous boundary layer, are not taken into account to a first approximation. As a side note, as shown by Chu [19], the acoustic energy can support spurious growth even in the absence of sources and presence of dissipation. This aspect is discussed by defining other thermoacoustic norms to measure the acoustic energy [20–28].

⁵A linear operator that does not commute with its adjoint is called non-normal. A property of non-normal systems is that their eigenfunctions are not orthogonal to each other.

⁶An example occurs in incompressible hydrodynamics of the Poiseuille flow, where the eigenvalue becomes unstable at a Reynolds number $Re \approx 5772$, but in experiments, transition to turbulence is observed at $Re \approx 1000$ [29–33]. In this case, eigenvalue analysis fails because the system is highly non-normal.

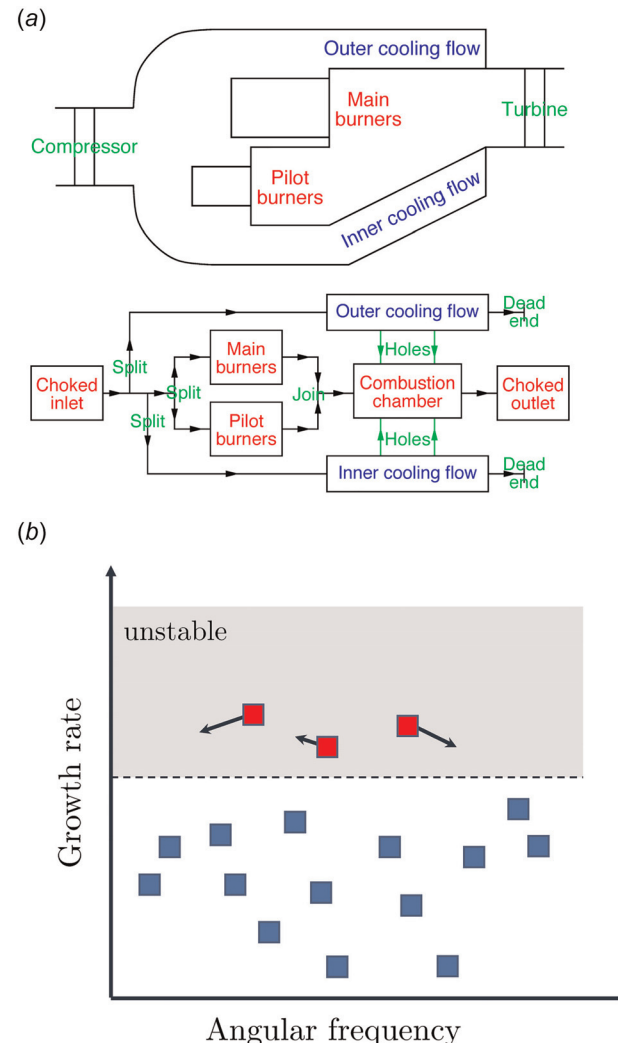


Fig. 2 (a) An example of a gas-turbine thermoacoustic network reduction taken from Ref. [51]. **(b)** The squares pictorially denote the eigenvalues. If the thermoacoustic network system has some eigenvalues with positive growth rate (red squares), the system is linearly unstable. Adjoint methods quantify how eigenvalues of interest change due to a small modification of any parameter (arrows). (Panel (b) is a pictorial figure and does not contain any results from calculations.)

degree of non-normality justifies the use of eigenvalue analysis in thermoacoustic stability. Non-normal effects are ignored accordingly in this review.

1.2 Adjoint-Based Methods: A Literature Review. Figure 2(a) shows a typical low-order thermoacoustic network of an aeronautical gas turbine [51]. When stability analysis is performed, some thermoacoustic eigenvalues may be found to be unstable. To study the influence of a small change in one of the many parameters of the network, the naive approach is to re-run the stability analysis for every parameter and calculate how every eigenvalue is affected. This is called the *finite difference approach*. When the parameters are more than the quantities of interests, an inverse approach turns this procedure around. One single adjoint calculation provides the gradient of the quantity of interest with respect to all the parameters of the network⁷ (Fig. 2(b)). This is called the *adjoint approach*.

⁷In the same vein, adjoint methods can be applied to the calculation of the optimal position where to place an external passive device, thereby reducing the number of computations by a factor equal to the number of grid points, which can be millions in numerical simulations.

In other words, the solution of the adjoint system provides the gradient of the quantity of interest to *all* the parameters of the system. Computationally, adjoint methods require fewer computations than finite difference methods when the number of parameters is larger than the number of quantities of interest, which is a typical situation in many engineering problems. Furthermore, adjoint methods enable the calculation of the forced response (receptivity) of the flow to external open-loop forcing.

1.2.1 Nonreacting Flows. In nonreacting fluid mechanics, adjoint methods were first applied to shape optimization problems. Pironneau [52] analytically derived the optimal shape of a unit-volume body with smallest drag in a Stokes flow. This technique was subsequently used to calculate the shape derivative of a hump to minimize the drag [53]. Notably, adjoint methods were developed and integrated into the wing-design cycle of aircraft by Jameson and coworkers [54–56], as acknowledged in Ref. [57].

This section offers an overview of adjoint methods used in non-reacting hydrodynamic stability, i.e., the blue portion of the circle in Fig. 1. Adjoint techniques were applied to boundary-layer receptivity by Tumin and Fedorov [58]. In order to map out the regions where to insert a second small cylinder to stabilize the vortex shedding instability of a cylinder flow at $Re = 50$, Hill [59] combined direct⁸ and adjoint eigenfunctions. The sensitivity maps obtained from this theoretical analysis compared favorably with the experimental data of Strykowski and Sreenivasan [60]. In a subsequent study, inspired by the spectral theory of the Orr-Sommerfeld operator [61,62], Hill [63] used the adjoint eigenfunctions to calculate the receptivity of Tollmien-Schlichting waves in Blasius boundary layers to forcing of the momentum, mass, vorticity, boundary conditions, and to acoustic waves. Adjoint sensitivity studies were performed by Luchini and Bottaro [64], to calculate the receptivity of the Görtler instability, and by Pralits et al. [65] to calculate the wall and momentum forcing sensitivity of compressible boundary layers. The leading-edge receptivity of flat plates using adjoint eigenfunctions was investigated by Giannetti and Luchini [66]. Notably, the work by Hill [59] was revisited by Giannetti and Luchini [67], who introduced the concept of structural sensitivity to estimate the wavemaker region, i.e., the region of absolute instability in local analysis [68], with a global approach.⁹ The first-order eigenvalue drift formula of Giannetti and Luchini [67] was also used in flow instability in Refs. [69–71]. Sensitivity analysis to base-flow¹⁰ modifications and steady forcing acting on the steady equations was proposed by Bottaro et al. [72] in a local-analysis framework. The analysis was generalized to a global approach by Marquet et al. [73–75], who reproduced the results of Ref. [60] with a good agreement.

The above pioneering studies laid out the foundations of many other applications in hydrodynamic stability. In incompressible flows, examples of applications are, among others, the forward-facing step [76]; disks and spheres [77–79]; rotating cylinders [80]; wake flows [81]; non-Newtonian cylinder flows [82]; a channel with a sudden expansion [83]; oblate spheroidal bubbles [84]; a T-junction [85,86] and X-junction [87] relevant to microfluid dynamics; two side-by-side cylinders [88]; the sensitivity of the recirculation length to steady forcing in separated flows [89]; cavities in Newtonian [90] and non-Newtonian fluids [91]. The first-order sensitivity theories were extended to second-order analysis by Tammissola et al. [92], who used adjoint eigenfunctions to study the effect that spanwise wavy blowing-suction perturbations of a semi-infinite plate have on stability. A second-order framework was employed to compute the optimal spanwise periodic flow modifications in a

parallel shear flow [93]. In low-Mach number flows, where the density changes with the temperature but not the pressure, adjoint methods were applied by Qadri et al. [94–96] to understand the physical mechanism of the spiral vortex breakdown of swirling flows and design control strategies in jets. In compressible flows, the structural and base-flow sensitivity were applied by Meliga et al. [77,97,98], who studied the stability of axisymmetric wakes past disks, spheres, and rocket-shaped bodies; and by Fedorov [99], who calculated the receptivity of a supersonic boundary layer.

In nonreacting fluid mechanics, the theory was extended by Giannetti et al. [100] to calculate the sensitivity of a limit-cycle stability, in particular the secondary instability of the cylinder flow, by Floquet theory. This framework was applied to investigate the secondary instability of a rotating flow [101]; and the origin of the flip-flop instability of two side-by-side cylinder wakes [102]. The effect that base-flow modifications have on the secondary instability of a cylinder wake was investigated in Ref. [103].

Adjoint sensitivity methods can be applied to time-averaged flows taking the mean flow as the input of the analysis, instead of the base flow. Eigenvalue analysis on time-averaged turbulent flows [104] provide useful and accurate results on the frequency of coherent structures in a wide range of flows, although such an analysis is not be mathematically justified a priori because the mean flow may not be a fixed point of the governing equations. Inspired by the results of the cylinder flow of Barkley [105], the conditions under which mean-flow analysis is valid were found by Sipp and Lebedev [106] via weakly nonlinear analysis of laminar flows, and by Beneddine et al. [107] via resolvent analysis of turbulent flows, who extended the studies of McKeon and Sharma [108] and Turton et al. [109]. Crouch et al. [110] successfully investigated the stability and global modes of the aerofoil transonic buffet including the Spalart-Allmaras eddy viscosity at the perturbation level. Fosas de Pando et al. [111] proposed a matrix-free algorithm to extract the discrete direct and adjoint solutions from a nonlinear code, which was applied to calculate the stability and receptivity of turbulent aerofoil tonal noise [112]. Meliga et al. [113] applied adjoint-based analysis to a D-shaped object to find the optimal locations at which to place a small cylinder to control the coherent structure frequency at a high Reynolds number by unsteady Reynolds-averaged Navier-Stokes (URANS) equations. Mettot et al. [114] revisited the case of Ref. [113] at a lower Reynolds number by decomposing the variables in time-averaged, phase-averaged, and turbulent components [115]. Importantly, they found that to improve the accuracy of stability calculations on mean flows, the eddy viscosity should be extracted from the unsteady simulation. By extracting the eddy viscosity from direct numerical simulation, the sensitivity of the coherent structure oscillations to the shape of the injector in a helicopter engine combustion chamber (cold flow) was calculated in Ref. [116]. When the Reynolds number was based on the combined molecular and eddy viscosity, the prediction of the coherent structure frequency and shapes was markedly improved. In experiments, adjoint analysis was performed by Camarri et al. [117] on mean flows of the wake past a porous cylinder and a thick plate to design a passive control strategy [118].

Although beyond eigenvalue sensitivity, it is worth summarizing some applications of adjoint sensitivity analysis in unsteady nonreacting flows. When the drag is the quantity of interest, a physical interpretation of the unsteady adjoint field of the incompressible cylinder flow was proposed by Wang and Gao [119]. The adjoint field was interpreted as the transfer function between small forces applied to the fluid and the resulting drag on the cylinder. By deploying the shadowing lemma [120,121], sensitivity analysis of time-averaged cost functionals was developed by Wang [122]. Such a technique was made more computationally feasible by the least-square shadowing method [123–126] and its improved versions [127–129]. The discussion of Larsson and Wang [130] is particularly relevant to fluid dynamics simulations. In aeroacoustics, turbulent jet noise was controlled via adjoint-based optimization by Kim et al. [131], and the optimal shape of a

⁸The word *direct* is used to denote the eigenproblem derived from the governing equations to distinguish it from the *adjoint* eigenproblem.

⁹In the hydrodynamic-stability jargon, global stability analysis denotes eigenvalue analysis performed on a base-flow solution without any particular symmetry assumptions, in contrast to local analysis, which assumes the base flow to be parallel.

¹⁰The base flow is the solution of the steady equations, i.e., it is a fixed point.

Helmholtz resonator to maximize acoustic damping was found by Caeiro et al. [132].

The excellent articles by Sipp et al. [133], Luchini and Bottaro [134], and Camarri [135] review adjoint analysis for flow control of nonreacting fluids in depth.

1.2.2 Reacting Flows. This section offers an overview of adjoint methods used in reacting flows at the intersection between the red (flame) and blue (hydrodynamics) circles in Fig. 1. Eigenvalue sensitivity analysis was applied to a low-Mach number combusting flow by Chandler et al. [136]. The wavemaker region of a low-Mach number flame was calculated in Ref. [137], where a passive control strategy to suppress a jet flame oscillation was designed. The eigenvalue sensitivity of reacting bluff-body wakes was investigated by local analysis by Emerson et al. [138].

Although beyond eigenvalue sensitivity, it is worth summarizing some applications of adjoint sensitivity analysis in reacting flows. In the calculation of sensitivities in chemical kinetics, adjoint methods were reviewed by Sandu et al. [139]. An implementation of these methods can be found in the open-source solver for chemical kinetics, thermodynamics, and transport processes CANTERA [140]. In Reynolds-averaged Navier-Stokes simulations, Wang et al. [141] accelerated Monte Carlo assessment for uncertainty quantification of the scramjet unstart by adjoint methods. The sensitivity of the flame tip temperature and NO_x emissions in hydrogen flames to chemistry model parameters was investigated in Ref. [142]. Other implementations of adjoint methods in steady reacting flow solvers can be found in Refs. [143–145]. In time-dependent problems, Lemke et al. [146,147] showed that adjoint equations of one- and two-dimensional compressible reacting flows provide accurate gradient information even with stiff nonlinear reaction rates. The sensitivities and optimal initial conditions to maximize the integrated heat release were computed for a three-dimensional reacting jet crossflow [148]. In laminar flames, adjoint looping was implemented by Qadri et al. [149] to calculate the optimal location where to spark a diffusion flame to maximize the nonlinear integrated heat release. Linearly optimal initial conditions that maximize the acoustic output of a radially imploding flame were calculated in Ref. [150]. The sensitivity of the optimal frequency response to swirling of M-flames was investigated by Skene and Schmid [151]. In turbulent flames, adjoint methods enabled the calculation of the sensitivity of localized ignition in nonpremixed mixing layers [152].

1.2.3 Thermoacoustics. This section offers an overview of adjoint methods for thermoacoustic stability at the intersection of the three circles in Fig. 1. Adjoint methods for thermoacoustic eigenvalue sensitivity analysis were developed in a longitudinal $n\tau$ combustor model by Magri and Juniper [153]. A pedagogical explanation of the method can be found in Ref. [154]. Using Galerkin methods, they studied the eigenvalue sensitivity to (i) any of the design parameters of the system and (ii) generic passive control devices (feedback sensitivity, also known as structural sensitivity). The latter was tested experimentally in a Rijke tube in Refs. [155–157], who measured the growth rate and the frequency shift in the presence of the passive control device. The growth-rate shift was predicted accurately by adjoint sensitivity analysis applied to an open-ended duct flame model [153]. Adjoint analysis was extended to a ducted compact diffusion flame in Refs. [158] and [159] to calculate the thermoacoustic sensitivity to the flame parameters, and to a premixed flame modeled by a flame front tracking equation [160]. By multiple-scale analysis, Magri et al. [161] proposed a thermoacoustic model that simulates the three-way interactions between all subsystems (Fig. 1). The individual influence of the hydrodynamic and acoustic fields on the thermoacoustic stability were identified and calculated by an adjoint method. The adjoint sensitivity framework was applied in Ref. [162] to thermoacoustic networks, which are used in the preliminary design of aero-engines and gas turbines for power generation. Adjoint methods were developed to accelerate uncertainty quantification of thermoacoustic stability in an annular-combustor network [163] and in a turbulent swirled combustor [164], where

first- and second-order corrections for nonlinear degenerate eigenproblems were used [165]. The first implementations of an adjoint Helmholtz solver can be found for a turbulent swirl combustor in Ref. [164] and a two-dimensional annular combustor in Ref. [166]. Monte Carlo free methods were developed by Mensah et al. [167], who calculated the probability that a dump combustor becomes unstable by deriving an adjoint-based algebraic expression for the stability margin. To reduce the cost of computations in rotationally symmetric annular combustors, Mensah et al. [166] computed the thermoacoustic modes by applying Bloch wave theory [168,169] to only one sector of the combustor. By using adjoint methods, they calculated the sensitivity of the degenerate eigenvalue to asymmetries in the flame transfer function due, for example, to an azimuthal mean flow. They extended their analysis to flame describing functions for the calculation of limit cycles [170]. Different symmetry-breaking perturbations to the burners were studied with higher order perturbation adjoint theory in Ref. [171]. In eigenvalue optimization, Mensah and Moeck [172] calculated the optimal placement and tuning of acoustic dampers in an annular combustor, while Aguilar and Juniper [173,174] eliminated thermoacoustic oscillations by shape optimization. Recently, Silva et al. [175] applied adjoint methods to calculate the critical flame index with relevance to intrinsic thermoacoustic (ITA) modes. The receptivity and sensitivity to different thermoacoustic source terms, as applied to the quasi-one-dimensional Helmholtz equation, were recently studied in Ref. [176].

Beyond eigenvalue sensitivity, adjoint gradient-based optimization was used to find the optimal initial perturbation that could cause triggering in an electrically heated Rijke tube [34,42]. In a stochastic framework, Boujo and Noiray [177] used the adjoint Fokker–Planck equation to identify the parameters of a stochastic harmonic oscillator, such as the linear growth rate and damping, with relevance to output-only system identification of thermoacoustic oscillations from noisy time series [178–180]. In weakly nonlinear analysis, Orchini et al. [181] calculated the unstable solution of subcritical bifurcations in a Rijke tube by expanding the Stuart–Landau equation up to fifth order, where adjoint equations were used to enforce solvability conditions [106,182–185].

1.3 Conventions. Depending on the convention used in the original papers, the complex plane is plotted either with the growth rate on the vertical axis or the horizontal axis. In the former case, the unstable semiplane is at the top; in the latter case, the unstable semiplane is on the right. Readers who are new to thermoacoustics will soon familiarize with, and even sooner may get frustrated by, the different conventions used in stability analysis. To help with visualization, the unstable plane is shaded in a gray color. Note that σ denotes both a complex variable (i.e., the Laplace variable) an eigenvalue. This is a slight abuse of notation because, in general, an eigenvalue is a complex variable but the converse is not necessarily true. To avoid confusion, care has been taken to make the distinction between an eigenvalue and a Laplace variable clear in the relevant sections.

Glossary

- **Adjoint:** Or dual. It could be used as an adjective or a noun.
- **Base flow:** A steady solution of the governing equations. With abuse of terminology, sometimes it is used interchangeably with “mean flow”
- **Direct eigenfunction:** Eigenfunction
- **Direct solution:** The solution of the problem, as opposed to the adjoint solution
- **Drift:** Or perturbation, or shift, or small change
- **Defective eigenvalue:** A degenerate eigenvalue with fewer independent eigenfunctions than its algebraic multiplicity
- **Degenerate eigenvalue:** A defective eigenvalue or a semi-simple eigenvalue with multiplicity greater than unity
- **Eigenfunction:** Also known as eigenmode, eigenshape, eigensolution, eigenvector, mode, global mode

- **Eigenpair:** Eigenvalue with the corresponding eigenfunction
- **Eigenproblem:** Or eigenvalue problem
- **Eigenvalue splitting:** The splitting of a degenerate eigenvalue in different trajectories
- **Exceptional point:** A defective eigenvalue that is a branch-point solution of the characteristic function
- **Jump:** Or discontinuity
- **Mean flow:** A time-averaged solution of the governing equations. Note that a base flow is a mean flow, but the converse is true only if the solution of the governing equations is steady.
- **Mode:** It could refer to either an eigenpair, or an eigenfunction, or an eigenvalue
- **N -fold degenerate eigenvalue:** A degenerate eigenvalue with multiplicity N
- **Sensitivity:** Or gradient. Sometimes referred to as a higher order derivative (second-order sensitivity, etc.)
- **Semi-simple eigenvalue:** An eigenvalue with the number of independent eigenfunctions equal to its algebraic multiplicity
- **Simple eigenvalue:** A semi-simple eigenvalue of unit multiplicity
- **Small:** A non-rigorous term that often refers to a first-order quantity, unless otherwise specified

1.4 Dimensional and Nondimensional Parameters. This review paper wishes to show the versatility of adjoint-based methodology to tackle thermoacoustic stability. In so doing, a variety of configurations are reviewed. Unless otherwise stated, the exact parameters and operating points used in the applications taken from the literature can be found in the original publications, as referenced in each section or caption. Unless otherwise specified, (i) the spatial coordinate is nondimensionalized by the length of the combustor for longitudinal configurations, or the length of the circumference for annular combustors; and (ii) the time is nondimensionalized by the acoustic time, which is the ratio between the characteristic length and the reference speed of sound. It follows that the eigenvalue is nondimensionalized by the acoustic frequency.

1.5 Objectives and Structure. This paper reviews the theory and applications of adjoint methods in thermoacoustics. Because adjoint models are, by definition, tied up with the physical models, this paper also reviews modeling approaches in thermoacoustics starting from the general, compressible, multicomponent, reacting governing equations. Different thermoacoustic models ($n-\tau$ model, flame transfer function, diffusion, and premixed flames), numerical approaches (Galerkin method, wave approach, Helmholtz solver, multiple scales), and configurations (longitudinal and annular combustors) are presented in Sec. 2.

The theory of adjoint sensitivity analysis is mathematically formalized and reviewed in Sec. 3. In low-order thermoacoustic networks and Helmholtz solvers, the stability problem is typically governed by nonlinear eigenproblems (NEPs). In rotationally symmetric combustors, such as annular and can-annular combustors, these nonlinear eigenproblems can be degenerate with one eigenvalue being associated with two independent eigenfunctions. First, the stability problem is presented for time-delayed models. Emphasis is given on nonlinear eigenproblems, which govern the stability of most thermoacoustic systems. Second, the adjoint problem is explained and physically interpreted as the receptivity of thermoacoustic linear oscillations. Both continuous, discrete, and automatic differentiation adjoint approaches are explained. Third, the adjoint-based calculation of the eigenvalue sensitivity is shown for higher order perturbations, both for nondegenerate eigenvalues, which are typically relevant to longitudinal configurations, and degenerate eigenvalues, which are typically relevant to rotationally symmetric annular and can-annular configurations.

A more general model of thermoacoustic stability by multiple scales is presented in Sec. 4, which is a standalone section. In thermoacoustics, hydrodynamic instabilities influence the dynamics of the flow field around the flame. Acoustic perturbations, in turn, may excite hydrodynamic instabilities at the flame's base (e.g., shear layer

instabilities). However, in most thermoacoustic systems, the hydrodynamics-acoustics dynamics is one-way coupled; the hydrodynamics is usually modeled with simple models and the acoustics develop on top of it. By multiple scales, a model is devised such that the hydrodynamics and acoustics are two-way coupled in a mathematically robust manner. Physical insight between the coupling of the subsystems is enabled by the concept of intrinsic sensitivity.

Key features of the thermoacoustic spectrum are shown in Sec. 5, as relevant to longitudinal configurations. The interaction between acoustic modes and intrinsic thermoacoustic modes is shown by varying the flame gain and time delay. An exceptional point is found at the intersection of the trajectories of the acoustic and intrinsic modes.

The remainder of the paper shows applications of adjoint analysis. Both deterministic and probabilistic approaches are reviewed. Section 6 reviews deterministic approaches, where no uncertainty is assumed in the system's parameters. The objectives are to (i) calculate the sensitivity of thermoacoustic stability to the design parameters of the system and the insertion of passive devices to control oscillations; and (ii) physically explain the coupling mechanisms between the hydrodynamic and acoustic subsystems. A comparison with experimental results is shown. Section 7 reviews probabilistic approaches, where the flame parameters are assumed uncertain. The objective is to develop adjoint-based methods to calculate the probability that a system will become unstable. Two adjoint-based methods are reviewed. In the first method, an adjoint code enables the accurate calculation of the probability of instability by reducing the number of computations by a factor of $\sim \mathcal{O}(M)$, where M is the number of Monte Carlo samples, which, in this case, is 10,000. In the second method, an adjoint method avoids the Monte Carlo sampling altogether. The uncertainty present in the flame parameters can markedly affect the predictions from deterministic stability analysis. It is advised that uncertainty quantification should be run along with traditional stability analysis for robust design.

Optimization of thermoacoustic configurations is enabled when the sensitivity information obtained by an adjoint method is embedded in a gradient-update routine. Section 8 reviews adjoint-based optimizations by placing acoustic dampers and making passive changes in the geometry. Effects of symmetry-breaking perturbations on annular combustors are shown in Sec. 9. A Bloch wave approach is used to (i) reduce the number of computations by taking advantage of the discrete rotational symmetry of the problem, and (ii) gain physical insight on a stabilization mechanism (the inclination rule).

The last two sections include nonlinear thermoacoustic effects: Section 10 shows how to accurately approximate the amplitude of the oscillations by weakly nonlinear analysis, where adjoint equations enforce solvability conditions. Finally, Sec. 11 presents a method to accurately calculate the drift of the Floquet exponents of a periodic oscillation in time, which extends eigenvalue analysis from fixed points to limit cycles.

Conclusions and future directions end the paper.

2 Thermoacoustic Models

Thermoacoustics is a multiphysical phenomenon that ensues from the interaction between three subsystems, i.e., acoustics, hydrodynamics, and the flame (Fig. 1) [1,3–5,7,187]:

- **Acoustics.** This subsystem includes the fluid phenomena that are characterized by wave propagation. In low-Mach number mean flows, the acoustics are chiefly influenced by the (i) impedances of the combustor's boundaries; (ii) propagation with the mean-flow speed of sound; and (iii) refraction due to mean-flow gradients. Acoustics are damped mainly by radiation/convection out of the domain; vortical dissipation where the flow separates; and vortical/entropic coupling at the thermoviscous boundary layer.
- **Hydrodynamics.** This subsystem includes all the nonreacting fluid phenomena that are characterized by low-Mach convection, which is the typical regime of gas-turbine combustion assumed in this paper. In particular, unsteady coherent

Table 1 Road map of the thermoacoustic models, numerical methods, and configurations reviewed in this paper.

Methodology	Physical model			Application	
	Acoustics	Flame	Hydrodynamics	Configuration	DOFs
Multiple-scale Helmholtz equation	Multidimensional Multidimensional	Chemistry Eqns. Flame response	Low-Mach number Eqns. Flame response	Dump combustor • Dump combustor • Annular combustor • Choked ducted flame • Open ducted flame • Annular combustor Open ducted flame	$\mathcal{O}(10^6)$ $\mathcal{O}(10^5)$ $\mathcal{O}(10^5)$ $\mathcal{O}(10)$ $\mathcal{O}(10^2)$ $\mathcal{O}(10)$ $\mathcal{O}(10^3)$
Wave approach	One-dimensional	• Flame response • Kinematic model	• Flame response • Disturbance phase velocity		
Galerkin method	One-dimensional	Chemistry Eqns.	Uniform		

Note: DOFs stands for degrees of freedom.

structures generated by hydrodynamic instabilities are important to thermoacoustic stability, such as shear-layer instability of two different fluid streams (also known as Kelvin–Helmholtz instability); vortex shedding behind bluff bodies used to stabilize flames (also known as Bénard–von-Kármán instability); jet instabilities, such as vortex breakdown in swirling jets; backward-facing steps and cavities [187]; to name a few.¹¹

- **Flame.** This subsystem includes all the phenomena that are characterized by chemical processes and their interaction with the flow dynamics. In the calculation of thermoacoustic stability, the most important output of the combustion process is the heat release rate of the flame. Aeronautical gas turbines typically work in a rich-burn quick-quench lean-burn regime, which is a mixing-controlled process. In order to lower NO_x emissions, industrial technology is moving toward partially premixed flames. Therefore, two limit cases of flames will be considered in this paper: A diffusion flame, whose dynamics are governed by mixing, and a premixed flame, whose dynamics are governed by flame propagation.¹²

2.1 Nonlinear, Multicomponent, Compressible, Reacting Flow Equations. The general, nonlinear equations of compressible, reacting, multicomponent flows are presented. Throughout the paper, it is assumed that the flow can be modeled as a continuum, Newtonian fluid. The problem is governed by the dimensional equations of continuity, momentum, energy, and conservation of species, respectively [189–192]

$$\frac{D\tilde{\rho}}{D\tilde{t}} + \tilde{\rho}\tilde{\nabla} \cdot \tilde{\mathbf{u}} = 0 \quad (3a)$$

$$\tilde{\rho} \frac{D\tilde{\mathbf{u}}}{D\tilde{t}} + \tilde{\nabla}\tilde{p} = \tilde{\nabla} \cdot \tilde{\boldsymbol{\tau}} + \tilde{\rho} \sum_{i=1}^{N_s} Y_i \tilde{\mathbf{f}}_i \quad (3b)$$

$$\begin{aligned} \tilde{\rho} \frac{D\tilde{h}}{D\tilde{t}} &= \frac{D\tilde{p}}{D\tilde{t}} + \tilde{Q} + \tilde{\nabla} \cdot (\tilde{\lambda}\tilde{\nabla}\tilde{T}) - \tilde{\nabla} \cdot \left(\tilde{\rho} \sum_{i=1}^{N_s} \tilde{h}_i Y_i \tilde{\mathbf{V}}_i \right) \\ &+ \tilde{\boldsymbol{\tau}} \cdot \tilde{\nabla} \cdot \tilde{\mathbf{u}} + \tilde{\rho} \sum_{i=1}^{N_s} Y_i \tilde{\mathbf{f}}_i \cdot \tilde{\mathbf{V}}_i \end{aligned} \quad (3c)$$

$$\tilde{\rho} \frac{DY_i}{D\tilde{t}} + \tilde{\nabla} \cdot (\tilde{\rho} \tilde{\mathbf{V}}_i Y_i) = \tilde{\omega}_i \quad (3d)$$

where \sim denotes a dimensional variable; $\tilde{\rho}$ is the density; $\tilde{\mathbf{u}}$ is the velocity; \tilde{p} is the pressure; \tilde{T} is the temperature; \tilde{h} is the enthalpy; $\tilde{\boldsymbol{\tau}}$ is the viscous stress tensor; N_s is the number of

¹¹Other important hydrodynamic phenomena that can bring about thermoacoustic instabilities, in particular in aero-engines, are droplet formation, jet impingement, secondary breakup, and coalescence.

¹²In real aero-engines, flames are often imperfectly premixed and the evaporation of sprays is another mechanism that leads to thermoacoustic instabilities [187]. Imperfectly premixed flames and sprays will not be considered in this review.

species; the subscript i denotes the i th species; $\tilde{\mathbf{f}}_i$ is a volume force; $\tilde{\mathbf{V}}_i$ is the diffusion velocity, which, adopting Fick's law, is $\tilde{\mathbf{V}}_i = -\tilde{D}\tilde{\nabla} \log(Y_i)$; \tilde{D} is the diffusion coefficient; $\tilde{\lambda}$ is the thermal diffusivity; Y_i is the mass fraction; $\tilde{\omega}_i$ is the production rate; and \tilde{Q} is the external-source heat release rate. The material derivative is $D(\cdot)/D\tilde{t} \equiv \partial(\cdot)/\partial\tilde{t} + \tilde{\mathbf{u}} \cdot \tilde{\nabla}(\cdot)$, where $\tilde{\nabla}$ is the nabla operator and $(\cdot) \cdot \tilde{\nabla}(\cdot) \equiv (\cdot)_j \partial/\partial\tilde{x}_j(\cdot)_i$ in Einstein's notation. \tilde{t} is the time. Vector quantities are denoted in bold, tensors are denoted in bold with an underline. The entropy \tilde{s} is defined by Gibbs' relation for a multicomponent gas

$$\tilde{T}d\tilde{s} = d\tilde{h} - \frac{d\tilde{p}}{\tilde{\rho}} - \sum_{i=1}^{N_s} \frac{\tilde{\mu}_i}{\tilde{W}_i} dY_i \quad (4)$$

where $\tilde{\mu}_i$ is the chemical potential and \tilde{W}_i is the molar mass. By combining Gibbs' equation (4) and the energy equation (3c), the latter can be reformulated with the entropy variable, as follows

$$\begin{aligned} \tilde{T} \frac{D\tilde{s}}{D\tilde{t}} &= - \sum_{i=1}^{N_s} \frac{\tilde{\mu}_i}{\tilde{W}_i} \frac{DY_i}{D\tilde{t}} + \frac{1}{\tilde{\rho}} \left[\tilde{Q} + \tilde{\nabla} \cdot (\tilde{\lambda}\tilde{\nabla}\tilde{T}) \right] \\ &+ \frac{1}{\tilde{\rho}} \left[-\tilde{\nabla} \cdot \left(\tilde{\rho} \sum_{i=1}^{N_s} \tilde{h}_i Y_i \tilde{\mathbf{V}}_i \right) + \tilde{\boldsymbol{\tau}} \cdot \tilde{\nabla} \cdot \tilde{\mathbf{u}} + \tilde{\rho} \sum_{i=1}^{N_s} Y_i \tilde{\mathbf{f}}_i \cdot \tilde{\mathbf{V}}_i \right] \end{aligned} \quad (5)$$

In a mixture of gases, the enthalpy and entropy are defined as

$$\tilde{h} = \sum_{i=1}^{N_s} \tilde{h}_i Y_i, \quad \tilde{s} = \sum_{i=1}^{N_s} \tilde{s}_i Y_i \quad (6)$$

where

$$\tilde{h}_i = \tilde{h}_{s,i} + \Delta\tilde{h}_{f,i}^\circ, \quad \tilde{s} = \tilde{s}_{s,i} + \Delta\tilde{s}_{f,i}^\circ \quad (7)$$

where $\tilde{h}_{s,i}$ and $\tilde{s}_{s,i}$ are the species' sensible enthalpy and entropy, respectively. $\Delta\tilde{h}_{f,i}^\circ$ and $\Delta\tilde{s}_{f,i}^\circ$ are the formation enthalpy and entropy, respectively, at standard condition \circ . Equations (3a)–(3d) govern the nonlinear thermoacoustic problem when a state equation is chosen and initial/boundary conditions are imposed. Low-order models for the acoustics (Sec. 2.2), flame (Sec. 2.3) and hydrodynamics (Sec. 2.4) are presented with their simplifying assumptions. Table 1 summarizes the thermoacoustic models, numerical methods, and configurations reviewed in this paper.

2.2 Acoustics. The acoustic subsystem and its interaction with the heat released by the flame are often characterized by the following assumptions [193,194]:

- there is no external source of heat, $\tilde{Q} = 0$;
- species-diffusion effects are negligible, $\tilde{\mathbf{V}}_i = 0$;
- viscous effects are negligible, $\tilde{\boldsymbol{\tau}} = 0$;
- thermal diffusivity is negligible, $\tilde{\lambda} = 0$;
- volume forces are negligible, $\tilde{\mathbf{f}}_i = 0$;

- the gas is calorifically perfect, i.e., $\tilde{c}_{p,i}$ and $\tilde{c}_{v,i}$ are constant and

$$\tilde{h} = \tilde{c}_p(\tilde{T} - \tilde{T}^\circ) + \sum_{i=1}^{N_s} \Delta \tilde{h}_{f,i}^{\circ} Y_i \quad (8)$$

where $\tilde{c}_p = \sum_{i=1}^{N_s} \tilde{c}_{p,i} Y_i$;

- the gas is ideal

$$\tilde{p} = \tilde{\mathcal{R}} \tilde{\rho} \tilde{T} \quad (9)$$

where $\tilde{\mathcal{R}} = \tilde{\mathcal{R}}_u (\sum_{i=1}^{N_s} (Y_i / \tilde{W}_i))$, with $\tilde{\mathcal{R}}_u$ being the universal gas constant.

Under these assumptions, the nonlinear dimensional equations (3) simplify to

$$\frac{D\tilde{\rho}}{Dt} + \tilde{\rho} \tilde{\nabla} \cdot \tilde{\mathbf{u}} = 0 \quad (10a)$$

$$\frac{D\tilde{\mathbf{u}}}{Dt} + \frac{\tilde{\nabla} \tilde{p}}{\tilde{\rho}} = 0 \quad (10b)$$

$$\frac{D\tilde{p}}{Dt} + \gamma \tilde{p} \tilde{\nabla} \cdot \tilde{\mathbf{u}} = (\gamma - 1) \tilde{\omega}_T + \frac{\tilde{p} - \tilde{\rho} \tilde{p}^{\circ}}{\gamma - 1} \frac{D\gamma}{Dt} \quad (10c)$$

$$\tilde{\rho} \frac{DY_i}{Dt} = \tilde{\omega}_i \quad (10d)$$

where $\tilde{\omega}_T = - \sum_{i=1}^{N_s} \Delta \tilde{h}_{f,i}^{\circ} \tilde{\omega}_i$ is the volumetric heat release rate due to reaction, and γ is the heat capacity ratio. Gibbs' relation (4) simplifies to [195]

$$\frac{d\tilde{s}}{\tilde{c}_p} = \frac{d\tilde{p}}{\gamma \tilde{p}} - \frac{d\tilde{\rho}}{\tilde{\rho}} - \sum_{i=1}^{N_s} (\psi_i + \aleph_i) dY_i \quad (11)$$

where

$$\psi_i \equiv \frac{1}{\tilde{c}_p \tilde{T}} \left(\frac{\tilde{\mu}_i}{\tilde{W}_i} - \Delta \tilde{h}_{f,i}^{\circ} \right) \quad (12)$$

$$\aleph_i \equiv \frac{1}{\gamma - 1} \frac{d \log(\gamma)}{dY_i} + \frac{\tilde{T}^{\circ}}{\tilde{T}} \frac{d \log(\tilde{c}_p)}{dY_i} \quad (13)$$

are the species' chemical potential function and heat-capacity factor, respectively [195,196]. The energy equation formulated with the entropy variable (5) simplifies to

$$\frac{1}{\tilde{c}_p} \frac{D\tilde{s}}{Dt} = - \sum_{i=1}^{N_s} \left(\psi_i + \frac{\Delta \tilde{h}_{f,i}^{\circ}}{\tilde{c}_p \tilde{T}} \right) \frac{DY_i}{Dt} \quad (14)$$

2.2.1 Linearization. Assuming that the acoustics are small perturbations evolving on top of a mean flow, a generic flow variable is decomposed as

$$(\bar{\cdot}) = (\tilde{\cdot}) + \varepsilon (\cdot)' \quad (15)$$

where $\varepsilon \ll 1$ is the arbitrary perturbation parameter; the overbar $\bar{\cdot}$ denotes the steady mean-flow variable ($\partial(\bar{\cdot})/\partial\tilde{t} = 0$), and the prime $'$ denotes the unsteady fluctuation. The equations are nondimensionalized with reference quantities denoted by the subscript *ref*: $\tilde{\nabla} = \nabla/\tilde{L}_{\text{ref}}$; where \tilde{L}_{ref} is a length scale; $\tilde{\rho} = \rho \tilde{\rho}_{\text{ref}}$; $\tilde{p} = p \tilde{\rho}_{\text{ref}}$, where $\tilde{\rho}_{\text{ref}} = \tilde{c}_{\text{ref}}^2 \tilde{\rho}_{\text{ref}}$; \tilde{c}_{ref} is the reference speed of sound; and the other variables are nondimensionalized differently according to whether they are mean-flow or acoustic quantities, as explained in Secs. 2.2.2 and 2.2.3, respectively.

The heat capacities are assumed constant; therefore, $d\tilde{c}_p = 0$ and $dy = 0$.

2.2.2 Nondimensional Mean-Flow Equations. The mean-flow velocity scales with the convection velocity, i.e., $\bar{\mathbf{u}} = \tilde{u}_{\text{ref}} \tilde{\mathbf{u}}$. The mean production rate is nondimensionalized as $\bar{\omega}_i = \tilde{\omega}_i \tilde{L}_{\text{ref}} / (\tilde{\rho}_{\text{ref}} \tilde{u}_{\text{ref}})$, such that $\bar{q} = \tilde{\omega}_T \tilde{L}_{\text{ref}} / (\tilde{u}_{\text{ref}} \tilde{\rho}_{\text{ref}})$ is the nondimensional

mean heat release rate due to combustion. On grouping the steady terms, the nondimensional mean-flow continuity, momentum, energy, and species equations read, respectively,

$$\nabla \cdot (\bar{\mathbf{u}} \bar{\rho}) = 0 \quad (16a)$$

$$\nabla(\bar{M}^2 \bar{\rho} \bar{\mathbf{u}} \cdot \bar{\mathbf{u}} + \bar{p}) = 0 \quad (16b)$$

$$\bar{\mathbf{u}} \cdot \nabla \bar{p} + \gamma \bar{p} \nabla \cdot \bar{\mathbf{u}} = (\bar{\gamma} - 1) \bar{q} \quad (16c)$$

$$\bar{\rho} \bar{\mathbf{u}} \cdot \nabla \bar{Y}_i = \bar{\omega}_i \quad (16d)$$

where $\bar{M} = \tilde{u}_{\text{ref}} / \tilde{c}_{\text{ref}}$ is the mean-flow Mach number. In the limit of low-Mach number combustion, Eq. (16b) shows that the mean-flow pressure is constant at first order of \bar{M} , i.e.,

$$\nabla \bar{p} = 0 \quad \text{for } \bar{M} \ll 1 \quad (17)$$

Variations of the mean pressure are neglected accordingly in this paper. The nondimensional mean-flow energy equation with the entropy variable reads

$$\bar{\mathbf{u}} \cdot \nabla \bar{s} = - \sum_{i=1}^{N_s} \left(\bar{\psi}_i + \frac{\Delta \tilde{h}_{f,i}^{\circ}}{\tilde{c}_p \tilde{T}} \right) \bar{\mathbf{u}} \cdot \nabla \bar{Y}_i \quad (18)$$

where $\bar{s} = \tilde{s} \tilde{c}_p$.

2.2.3 Nondimensional Acoustic Equations. The acoustic velocity scales with the speed of sound, $\bar{\mathbf{u}}' = \mathbf{u}' \tilde{c}_{\text{ref}}$; therefore, the time scales with the wave-propagation time, $\bar{t} = t \tilde{L}_{\text{ref}} / \tilde{c}_{\text{ref}}$. The acoustic pressure is nondimensionalized as $\bar{p}' = \tilde{p}_{\text{ref}} p'$. The production-rate fluctuation is nondimensionalized as $\bar{\omega}'_i = \tilde{\omega}'_i \tilde{L}_{\text{ref}} / (\tilde{\rho}_{\text{ref}} \tilde{c}_{\text{ref}})$ such that $\bar{q}' = \tilde{\omega}'_T \tilde{L}_{\text{ref}} / (\tilde{c}_{\text{ref}} \tilde{\rho}_{\text{ref}})$ is the nondimensional heat release rate fluctuation due to combustion. On grouping the terms $\sim \mathcal{O}(\varepsilon)$, the nondimensional linearized continuity, momentum, energy, and species equations read, respectively,

$$\frac{\partial \rho'}{\partial t} + \nabla \cdot (\bar{\rho} \mathbf{u}' + \bar{M} \rho' \bar{\mathbf{u}}) = 0 \quad (19a)$$

$$\frac{\partial \mathbf{u}'}{\partial t} + \bar{M} (\mathbf{u}' \cdot \nabla \bar{\mathbf{u}} + \bar{\mathbf{u}} \cdot \nabla \mathbf{u}') + \frac{\nabla p'}{\bar{\rho}} = 0 \quad (19b)$$

$$\frac{\partial p'}{\partial t} + \bar{M} (\bar{\mathbf{u}} \cdot \nabla p' + \gamma p' \nabla \cdot \bar{\mathbf{u}}) + \gamma \bar{p} \nabla \cdot \mathbf{u}' = (\gamma - 1) \bar{q}' \quad (19c)$$

$$\frac{\partial Y'_i}{\partial t} + \bar{M} \bar{\mathbf{u}} \cdot \nabla Y'_i + \mathbf{u}' \cdot \nabla \bar{Y}_i = \frac{\dot{\omega}'_i}{\bar{\rho}} - \frac{\bar{\omega}_i}{\bar{\rho}^2} \rho' \quad (19d)$$

The nondimensional linearized energy equation expressed with the entropy reads

$$\begin{aligned} \frac{\partial s'}{\partial t} + \bar{M} \bar{\mathbf{u}} \cdot \nabla s' + \mathbf{u}' \cdot \nabla \bar{s} &= - \sum_{i=1}^{N_s} \left(\bar{\psi}_i + \frac{\Delta \tilde{h}_{f,i}^{\circ}}{\tilde{c}_p \tilde{T}} \right) \\ &\times \left(\frac{\partial Y'_i}{\partial t} + \bar{M} \bar{\mathbf{u}} \cdot \nabla Y'_i + \mathbf{u}' \cdot \nabla \bar{Y}_i \right) \dots \\ &- \sum_{i=1}^{N_s} \left(\bar{\psi}_i + \frac{\Delta \tilde{h}_{f,i}^{\circ}}{\tilde{c}_p \tilde{T}} \right)' \bar{M} \bar{\mathbf{u}} \cdot \nabla \bar{Y}_i \end{aligned} \quad (20)$$

where $\bar{s}' = s' \tilde{c}_p$. The hydrodynamics affects the mean flow and its interaction with the heat released by the flame. When the hydrodynamic and flame subsystems are modeled, Eq. (19) are closed and called *thermoacoustic equations*. Three common simplifications and solution methods of the acoustic Eq. (19) are presented.¹³ The pros/cons of each approach are explained. The heat-release term

¹³Ray theory and Green's function techniques to solve the acoustics are not treated in this paper.

in Eq. (19c), which is the monopole source of acoustics, is modeled in Sec. 2.3.

Helmholtz equation: In addition to the assumptions listed in Sec. 2.2, in the Helmholtz-equation model, it is assumed that [40,197]

- the mean-flow Mach number is negligible, $\bar{M} = 0$;
- the gas composition is uniform; therefore, the single-fluid model is adopted. This means that the species equation (3d) is not considered; the heat release rate in Eq. (19c) needs to be specified and $\dot{q} = 0$ in Eq. (16c) [40,197]. The latter is justified providing that $\bar{M} \ll \tilde{L}_f/\tilde{L}_a$, where \tilde{L}_f is the flame spatial length and \tilde{L}_a is the acoustic spatial scale [197,198].

By taking the time derivative of Eq. (19c) and subtracting the divergence of Eq. (19b) multiplied by $\gamma\bar{p}$, an inhomogeneous wave equation is obtained

$$\frac{\partial^2 p'}{\partial t^2} - \gamma\bar{p}\nabla \cdot \left(\frac{\nabla p'}{\bar{\rho}} \right) = (\gamma - 1)\frac{\partial \dot{q}'}{\partial t} \quad (21)$$

which can be expressed with the speed of sound

$$\frac{\partial^2 p'}{\partial t^2} - \nabla \cdot (\bar{c}^2 p') = (\gamma - 1)\frac{\partial \dot{q}'}{\partial t} \quad (22)$$

where $\bar{c} = \tilde{c}/\tilde{c}_{\text{ref}}$ such that $\bar{c}^2 = \gamma\bar{p}/\bar{\rho}$. The Laplace transform¹⁴ of Eq. (21) is the Helmholtz equation¹⁵

$$\sigma^2 \hat{p} - \nabla \cdot (\bar{c}^2 \hat{p}) = \sigma(\gamma - 1) \hat{\dot{q}}' \quad (23)$$

Other conventions for the Laplace variable that are often used in the literature are $\sigma = i\omega$ or $\sigma = -i\omega$, where ω is the complex eigenfrequency and $i^2 = -1$. At fully reflective boundaries, $\hat{p} = 0$, whereas at rigid walls, $\nabla \hat{p} \cdot \mathbf{n} = 0$, where \mathbf{n} is the normal to the boundary. The general boundary condition is prescribed with the acoustic impedance $Z = \hat{p}/(\bar{\rho}\bar{c}\hat{\mathbf{u}} \cdot \mathbf{n})$ such that $\bar{c}Z\nabla \hat{p} \cdot \mathbf{n} + \sigma\hat{p} = 0$, which models the dissipation of energy by acoustic radiation. To model further sources of damping, the reader may refer to Ref. [189]. A detailed explanation of the Helmholtz equation as applied to thermoacoustics is given by Nicoud et al. [40,197]. The advantage of the Helmholtz-equation framework is that it can tackle three-dimensional geometries, with the con that it holds for very small mean-flow Mach numbers and requires numerical discretization, such as finite elements (e.g., see Refs. [40], [166], [172], and [199–202]), finite volumes (e.g., see Ref. [164]), or finite difference. This model is applied in Sec. 7 for uncertainty quantification of the stability of a turbulent swirled combustor.

Traveling-wave approach: The traveling-wave approach (or simply wave approach) is a method to solve the linearized Euler equations based on Riemann decomposition of the primitive variables [203]. Applications of the wave-approach in thermoacoustics are numerous [193,198,204–210], to name only a few. The traveling-wave approach is presented for longitudinal and annular combustors.

Traveling-wave approach in longitudinal acoustics: The main assumptions are:

- the flow is one-dimensional, i.e., the characteristic acoustic frequency, f_{ac} , is smaller than the cut-off frequency;
- the flame is compact, i.e., the flame Helmholtz number, $\text{He} \equiv 2\pi\tilde{f}_{\text{ac}}\tilde{L}/\tilde{c}$, and the flame Strouhal number, $\text{St} \equiv 2\pi\tilde{f}_{\text{ac}}\tilde{L}/\tilde{u}$ are negligible [198], where \tilde{L} is the axial spatial extent of the flame;

- the mean flow is one-dimensional and uniform (but not necessarily zero);
- the flame is a perfectly premixed flame front moving at speed u'_s with respect to the laboratory frame, and it is anchored to the burner, i.e., $\bar{u}_s = 0$; and
- the fluid is modeled as a single-component mixture.

Here, it is customary to nondimensionalize the convection mean flow speed with the speed of sound, $\tilde{u} = \bar{u}\tilde{c}_{\text{ref}}$; hence, $\bar{q} = \tilde{\omega}_T\tilde{L}_{\text{ref}}/(\tilde{c}_{\text{ref}}\tilde{p}_{\text{ref}})$.

By combining Eqs. (19b) and (19c) in their homogeneous forms, the acoustic pressure reads

$$\left(\frac{\partial}{\partial t} + \bar{u} \frac{\partial}{\partial x} \right)^2 p' - \bar{c}^2 \frac{\partial^2 p'}{\partial x^2} = 0 \quad (24)$$

From Eq. (20), the entropy fluctuation reads

$$\frac{\partial s'}{\partial t} + \bar{u} \frac{\partial s'}{\partial x} = 0 \quad (25)$$

The acoustic density, ρ' , and velocity, u' , are governed by a convective wave equation, the form of which is equal to Eq. (24). By integrating the linearized Gibbs' relation along a path line, the entropy fluctuation can be related to the acoustic pressure and density as

$$s' = p' - \rho' \quad (26)$$

The partial differential equations (24) and (25) are hyperbolic and can be solved with the method of characteristics, yielding

$$p' = f\left(t - \frac{x}{\bar{c} + \bar{u}}\right) + g\left(t + \frac{x}{\bar{c} - \bar{u}}\right) \quad (27a)$$

$$s' = \mathcal{S}_e\left(t - \frac{x}{\bar{u}}\right) \quad (27b)$$

$$\rho' = p' - \mathcal{S}_e\left(t - \frac{x}{\bar{u}}\right) \quad (27c)$$

$$u' = \frac{1}{\bar{\rho}\bar{c}} \left[f\left(t - \frac{x}{\bar{c} + \bar{u}}\right) - g\left(t + \frac{x}{\bar{c} - \bar{u}}\right) \right] \quad (27d)$$

where u' originates from the linearized momentum equation, and ρ' comes from Eq. (26). The solutions are the forward, f , and backward, g , acoustic waves (Riemann invariants), which travel at speeds $\bar{c} + \bar{u}$ and $\bar{c} - \bar{u}$, respectively.¹⁶ In addition, there exists an entropy wave, \mathcal{S}_e , which is convected with the mean flow at speed \bar{u} , which generates an excess density [211]. Modeling a multicomponent mixture creates additional excess density [195]. Figure 3 shows a schematic of the longitudinal combustor modeled with the wave approach.

The assumption of a compact heat source physically signifies that there is no accumulation rate of mass, momentum, and energy at the heat source location. Therefore, the heat source creates a discontinuity in the mean flow, and jump conditions can be derived by the integral form of the governing equations, accordingly. When linearized, the jump conditions at the nondimensional flame location x_f read [212]

$$[\rho'\bar{u} + \bar{\rho}u']_{x_f^-}^{x_f^+} = u'_s(\bar{\rho}_d - \bar{\rho}_u) \quad (28a)$$

$$[p' + 2\bar{\rho}\bar{u}u' + \rho'\bar{u}^2]_{x_f^-}^{x_f^+} = 0 \quad (28b)$$

¹⁴For a generic function f , the Laplace transform is defined as $\mathcal{L}\{f\} \equiv \hat{f}(\sigma) \equiv \int_0^\infty f(t)\exp(-\sigma t)dt$.

¹⁵Technically, this is an inhomogeneous Helmholtz equation; however, the adjectice inhomogeneous is dropped for brevity.

¹⁶In other words, the characteristic lines are given by $dx/dt = \bar{c} \pm \bar{u}$.

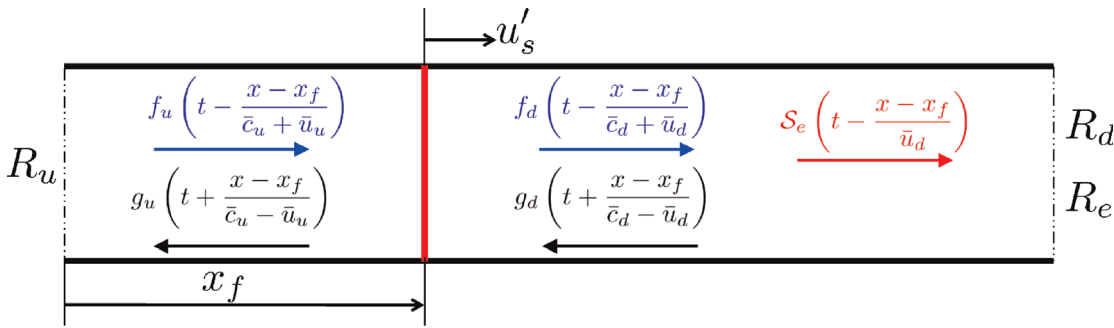


Fig. 3 Traveling-wave approach as applied to a longitudinal combustor with upstream (downstream) acoustic reflection coefficient R_u (R_d) and entropic reflection coefficient, R_e . The Mach number at the outlet is sonic, i.e., the combustor is choked. f is the downstream-traveling acoustic wave, g is the upstream-traveling acoustic wave, and S_e is the entropic perturbation generated by the unsteady flame, whose flame front fluctuates with velocity u'_s .

$$\left[\frac{\gamma}{\gamma-1} (p' \bar{u} + \bar{p} u') + \frac{3}{2} \bar{\rho} \bar{u}^2 u' + \frac{1}{2} \rho' \bar{u}^3 \right]_{x_f^-}^{x_f^+} = \dot{q}' + u'_s \left(\frac{\bar{p}_d - \bar{p}_u}{\gamma-1} + \frac{1}{2} \bar{\rho}_u \bar{u}_u (\bar{u}_d - \bar{u}_u) \right) \quad (28c)$$

$$\tau_d = \frac{2(1-x_f)\bar{c}_d}{\bar{c}_d^2 - \bar{u}_d^2} \quad (33d)$$

$$\tau_e = \frac{(1-x_f)\bar{c}_d}{\bar{u}_d(\bar{c}_d - \bar{u}_d)} \quad (33e)$$

where the flame front speed, u'_s , reads [212,213]

$$u'_s = \bar{u}_u \left(\frac{\rho'(x_f^-)}{\bar{\rho}_u} + \frac{u'(x_f^-)}{\bar{u}_u} - \frac{\dot{q}'}{\dot{q}} \right) \quad (29)$$

The subscript u denotes a condition upstream of the flame, whereas subscript d denotes a condition downstream of the flame. On Laplace transforming, the upstream acoustic wave reads

$$F_u(\sigma) = R_u G_u(\sigma) \exp(-\sigma \tau_u) \quad (30)$$

where $R_u = -1$ is the upstream reflection coefficient for an ideal open end, and

$$\tau_u = \frac{2x_f \bar{c}_u}{\bar{c}_u^2 - \bar{u}_u^2} \quad (31)$$

The downstream boundary is modeled as a choked outlet, where the flow is sonic. The acoustic variables are constrained by [214]

$$2 \frac{u'}{\bar{u}} + \frac{\rho'}{\bar{\rho}} - \frac{p'}{\bar{p}} = 0 \quad (32)$$

which physically corresponds to ensuring that the critical mass flow rate is maximal. Therefore, the downstream reflected acoustic wave reads

$$G_d(\sigma) = R_d F_d(\sigma) e^{-s\tau_d} + R_e A_e(\sigma) e^{-\sigma\tau_e} \quad (33a)$$

where

$$R_d = \frac{1 - \frac{1}{2}(\gamma-1)\bar{M}_d}{1 + \frac{1}{2}(\gamma-1)\bar{M}_d} \quad (33b)$$

$$R_e = \frac{\frac{1}{2}\bar{M}_d}{1 + \frac{1}{2}(\gamma-1)\bar{M}_d} \quad (33c)$$

and A_e is the Laplace transform of the entropy disturbance, S_e . Entropy fluctuations are assumed to be generated by the unsteady flame front; therefore, the flow is isentropic upstream of the flame.

Traveling-wave approach in an annular combustor: Annular combustion chambers are used in aircraft gas turbines because of their compactness, low-NO_x emissions, and ability for efficient light round [215,216]. Such configurations, however, suffer from combustion instabilities due to azimuthal modes that often become unstable at low frequencies, at which damping mechanisms are less effective. This low-order model describes a combustion chamber connected by longitudinal burners fed by a common annular plenum (Fig. 4).

The main assumptions are:

- In the plenum and the combustor, the acoustics depend on the azimuthal coordinate. In the burners, the acoustics depend only on the axial coordinate.
- The mean-flow convection speed is zero.
- The external walls of the annular cavities are rigid.
- There is no flame-to-flame interaction from one sector to another.
- Flames are compact.
- The fluid is modeled as a single-component mixture.

The derivation of the model is conceptually similar to the longitudinal-wave approach, but the mathematical expressions are more involved because of the geometry. The acoustics propagate in the plenum, combustor, and burners as traveling waves. At the intersection between a burner and an annular cavity, (i) the energy jump condition provides the relation between the three pressure waves, and (ii) the momentum jump condition provides the relation between the three velocity waves. Across the flame inside the burner, the acoustic pressure does not change, but the flow rate undergoes a discontinuity induced by the dilation from the heat release rate, which is modeled with a flame transfer function. For more mathematical details, the reader may refer to Refs. [220–222].

Galerkin method: With the Galerkin method, the governing partial differential equations are discretized into a set of ordinary differential equations by choosing a Riesz basis that matches the

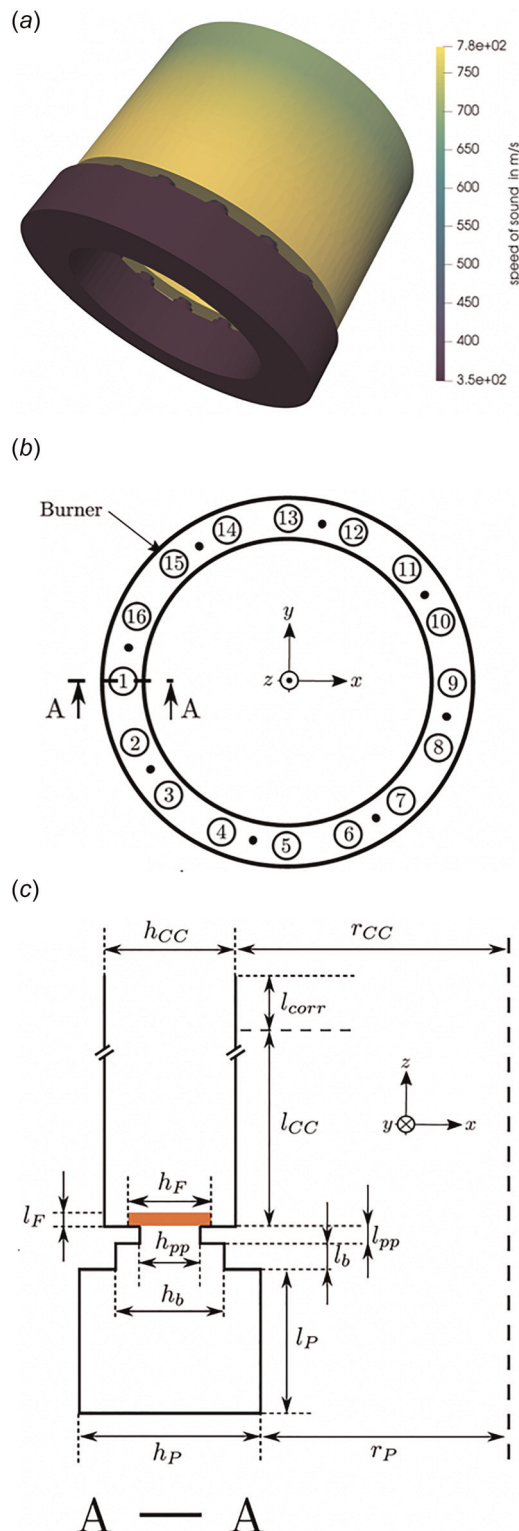


Fig. 4 Schematic of a rotationally symmetric annular combustor, which consists of a plenum and combustion chamber connected by longitudinal burners. In this case, there are 16 burners. (a) mean-flow speed of sound; ((b) and (c)) cross sections of the annular combustor. This represents the MICCA combustor [202,217–219] as modeled in Ref. [171].

boundary conditions and the discontinuity condition at the flame. Here, an open-ended duct, where the acoustic pressure is zero at the ends, is chosen. In this section, the same assumptions as the “Traveling-wave approach” hold, with the additional condition

that the mean-flow convection velocity is zero. Therefore, advected disturbances, such as entropy spots, cannot be modeled. The Galerkin method, which is a weak-form method, ensures that the error is orthogonal to the chosen basis in the subspace in which the solution is discretized, so that the solution is an optimal weak-form solution. The pressure, p' , and velocity, u' , are expressed by separating the time and space dependence, as follows [158]

$$p' = \sum_{j=1}^K \begin{cases} \alpha_{u,j}(t)\Psi_{u,j}(x), & 0 \leq x < x_f \\ \alpha_{d,j}(t)\Psi_{d,j}(x), & x_f < x \leq 1 \end{cases} \quad (34)$$

$$u' = \sum_{j=1}^K \begin{cases} \eta_{u,j}(t)\Phi_{u,j}(x), & 0 \leq x < x_f \\ \eta_{d,j}(t)\Phi_{d,j}(x), & x_f < x \leq 1 \end{cases} \quad (35)$$

For an open-ended duct

$$p' = \sum_{j=1}^K \begin{cases} -\alpha_j(t)\sin(\omega_j\sqrt{\rho_u}x), & 0 \leq x < x_f \\ -\alpha_j(t)\left(\frac{\sin\gamma_j}{\sin\beta_j}\right)\sin(\omega_j\sqrt{\rho_d}(1-x)), & x_f < x \leq 1 \end{cases} \quad (36)$$

$$u' = \sum_{j=1}^K \begin{cases} \eta_j(t)\frac{1}{\sqrt{\rho_u}}\cos(\omega_j\sqrt{\rho_u}x), & 0 \leq x < x_f \\ -\eta_j(t)\frac{1}{\sqrt{\rho_d}}\left(\frac{\sin\gamma_j}{\sin\beta_j}\right)\cos(\omega_j\sqrt{\rho_d}(1-x)), & x_f < x \leq 1 \end{cases} \quad (37)$$

where $\gamma_j \equiv \omega_j\sqrt{\rho_u}x_f$ and $\beta_j \equiv \omega_j\sqrt{\rho_d}(1-x_f)$. The spatial dependency of each mode of Eqs. (36) and (37) is shown in Fig. 5. ω_j is calculated through the dispersion relation

$$\sin\beta_j\cos\gamma_j + \cos\beta_j\sin\gamma_j\sqrt{\frac{\rho_u}{\rho_d}} = 0 \quad (38)$$

Note that in the limit $\rho_u = \rho_d$, the nondimensional angular frequencies of the acoustic eigenfunctions are $\omega_j = j\pi$, as it ought to be for an open-ended duct.

2.3 Flame Models. Two simplified flame models are presented to model diffusion and premixed flames.

2.3.1 Diffusion Flame. Diffusion flames are governed by the mixing between the fuel and oxidizer streams. As such, diffusion flames do not propagate. An important geometric parameter that affects the flame shape is the fuel-to-air port ratio. The main assumptions of this simplified model are: (i) the density in the flame domain is uniform; (ii) the Lewis number, defined as the ratio of thermal diffusivity to mass diffusivity, is unitary; (iii) the chemistry is infinitely fast with one-step reaction; (iv) the flame is two-dimensional. In diffusive problems, it is convenient to introduce the mixture fraction, Z [223]

$$Z \equiv \frac{\nu Y_F - Y_O + Y_{O,in}}{\nu Y_{F,in} + Y_{O,in}} \quad (39)$$

where ν is the stoichiometric mass ratio; the subscripts F , O , and in denote fuel, oxidizer, and inlet, respectively; and Y is the mass fraction. The fuel and oxidizer diffuse into each other and, under the infinite-rate chemistry assumption, combustion occurs in an infinitely thin region at the stoichiometric contour, $Z = Z_{sto}$, where $Z_{sto} = (1 + \nu Y_{F,in}/Y_{O,in})^{-1}$. The governing equation for Z is derived

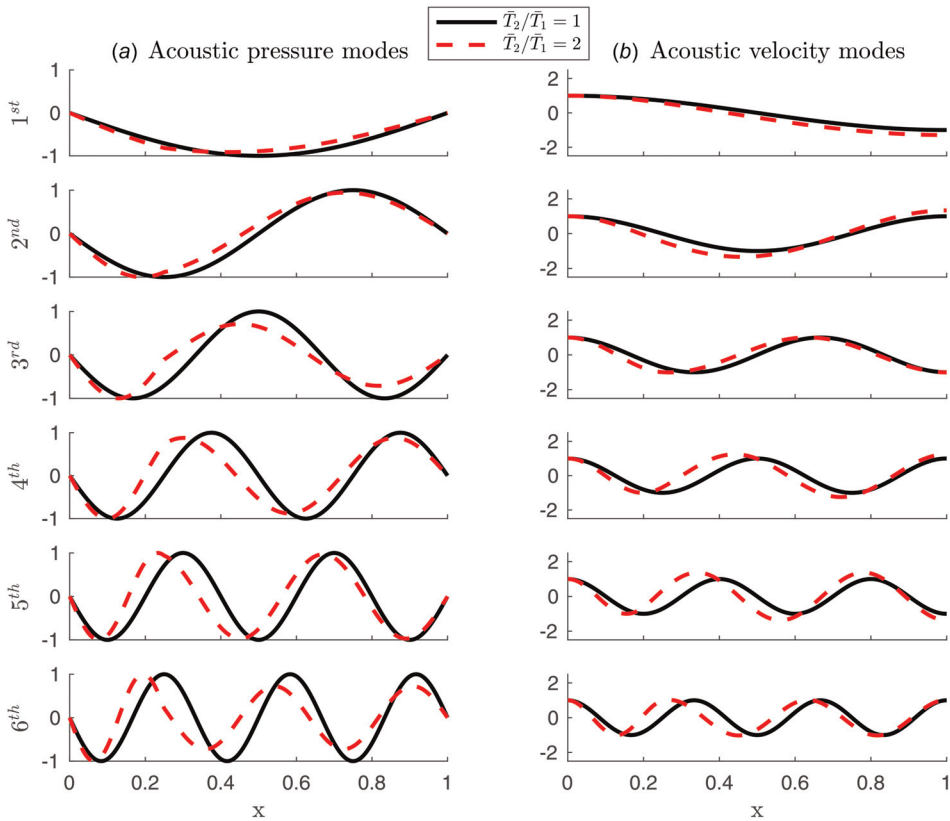


Fig. 5 The acoustic eigenfunctions of an open-ended duct with zero mean flow. (a) Pressure and (b) velocity with temperature jump (red-dashed lines) and without temperature jump (black-solid lines). The position of the mean-flow temperature jump is at $x_f = 0.25$.

from the species equations [224,225] and, in nondimensional form, reads

$$\frac{\partial Z}{\partial t_f} + \left(\bar{u} + u'_f \right) \frac{\partial Z}{\partial x_f} - \frac{1}{Pe} \left(\frac{\partial^2 Z}{\partial X_f^2} + \frac{\partial^2 Z}{\partial Y_f^2} \right) = 0 \quad (40)$$

where t_f is the nondimensional time in the flame domain; u'_f is the acoustic velocity evaluated at the flame location; Pe is the Péclet number, which is the ratio between the diffusion and convective time scales; and X_f and Y_f denote the nondimensional spatial coordinates in the flame domain. In the flame domain, which is separated from the acoustic domain, the time scales with the inverse of the convective velocity. Therefore, the velocities are nondimensionalized by the mean flow convective velocity. More details can be found in Ref. [158]. At the oxidizer port $Z = 1$, whereas at the fuel port $Z = 0$.¹⁷ Neumann boundary conditions are prescribed elsewhere to ensure that there is no diffusion across the walls of the combustor, and that Z is uniform at the end of the flame domain. The variable Z is split into two components, $Z = \bar{Z} + z'$, in which \bar{Z} is the steady solution [158] and z' is the small fluctuation. The nondimensional heat release (rate) is given by the integral of the total derivative of the nondimensionalized sensible enthalpy

$$\dot{Q} \sim \int_{V_f} \frac{d(T_b - T_{in})}{dt} dX_f dY_f \quad (41a)$$

$$T_b = T_{in} + \bar{Z} + z', \quad Z < Z_{sto} \quad (41b)$$

$$T_b = T_{in} + \frac{Z_{sto}}{1 - Z_{sto}} (1 - \bar{Z} - z'), \quad Z \geq Z_{sto} \quad (41c)$$

where V_f is the flame domain, and T_{in} is the nondimensional inlet temperature of both species. The fluctuating heat release, integrated over the flame domain, that feeds into the acoustics is $\dot{q}' \sim \dot{Q} - \bar{Q}$, where the symbol \sim signifies that the exact expression for the quantity depends on the scale factors used [158].

2.3.2 Premixed Flame. The dynamics of a premixed-flame front is modeled here with a kinematic model, the G -equation (see, e.g., Refs. [189] and [227–230]), which is a level-set method that tracks the propagating infinitely thin flame front that separates reactants by products. This is a simplified model for a premixed flame because it does not include reaction mechanisms. Turbulence effects are neglected for simplicity. The nondimensional G -equation reads

$$\frac{\partial G}{\partial t_f} + \mathbf{u} \cdot \nabla G = s_L^0 (1 - \mathcal{L}\kappa) |\nabla G| \quad (42)$$

where \mathbf{u} is the hydrodynamic velocity field; s_L^0 is the flame speed; \mathcal{L} is the Markstein length; and κ is the flame curvature. The flame front is the locus of points for which $G = 0$. The flame is assumed axisymmetric. The G -equation can be linearized around a mean flame shape.¹⁸ Following Ref. [160], on linearization, the flame front is a single-valued function of the radial coordinate of the flame front

$$G(X_{fr}, R_{fr}, t_f) = X_{fr} - \bar{F}_G(R_{fr}) - F'_G(R_{fr}, t_f) \quad (43)$$

¹⁷Axial back diffusion at the port is neglected because the Péclet number is assumed to be large [226].

¹⁸Elaborate flame dynamics, such as pinch-off and flame wrinkling, are nonlinear phenomena, which are not captured by linear analysis.

where the flame shape is defined by the mean function \bar{F}_G and the fluctuation by F'_G , which are provided by Eqs. (6a) and (6b) in Ref. [160]. The subscript *fr* stands for “flame front.” The axial and radial components of the hydrodynamic velocity field are, respectively,

$$u_X = \bar{u} + \Delta u_X \quad (44)$$

$$u_R = -\frac{1}{2}R_f \frac{\partial \Delta u_X}{\partial X_f} \quad (45)$$

In forced flames, the nondimensional axial perturbation Δu_X is prescribed, whereas in self-excited thermoacoustic problems, as those under investigation in this paper, the axial perturbation is provided by the acoustic model. Finally, the total nondimensional heat release rate is obtained by integration [160]

$$\dot{Q} \sim 2\pi \int_0^R (1 - \mathcal{L}\kappa) \sqrt{1 + \left(\frac{d\bar{F}_G}{dR_f} + \frac{\partial F'_G}{\partial R_f} \right)^2} R_f dR_f \quad (46)$$

where the symbol \sim signifies that the exact expression for the quantity depends on the scale factors used.

2.3.3 Flame Response Models. In linear approximation, the total unsteady heat release can be expressed in terms of response functions [187]

$$\frac{\hat{q}'}{\hat{q}}(\omega) = \text{FTF}_u \frac{\hat{u}'}{\hat{u}} + \frac{1}{M} \text{FTF}_p \frac{\hat{p}'}{\hat{p}} + \frac{1}{M} \text{FTF}_\phi \frac{\hat{\phi}'}{\hat{\phi}} \quad (47)$$

where FTF_u , FTF_p , and FTF_ϕ are the transfer functions obtained by harmonically forcing (with a small amplitude) the velocity, pressure, and equivalence ratio, respectively, over a range of angular frequencies, ω , and measuring the heat release output. (The presence of $1/M$ is due to the nondimensionalization used in Secs. 2.2.2–2.2.3.) Transfer functions characterize the behavior of linear time-invariant systems. In this paper, only FTF_u is considered because it is the dominant transfer function in fully premixed flames. The subscript *u* will be dropped from now on. Transfer functions that are measured in a different range of forcing amplitudes are called flame describing functions (see, e.g., Refs. [206], [227], [231], and [232] for more references). In polar notation, the normalized heat release rate is provided by

$$\frac{\hat{q}'}{\hat{q}} = |\text{FTF}| \frac{\hat{u}'}{\hat{u}} \exp(i\angle \text{FTF}) \quad (48)$$

The negative slope of the transfer-function phase is the time delay

$$\tau = -\frac{d\angle \text{FTF}}{d\omega} \quad (49)$$

which, at low-frequencies, can be assumed constant, such that

$$\frac{\hat{q}'}{\hat{q}} = |\text{FTF}| \frac{\hat{u}'}{\hat{u}} \exp(-i\tau\omega) \quad (50)$$

The inverse Fourier-transform of Eq. (50) justifies the time-delayed model (also known as the $n-\tau$ model)

$$\dot{q}' = nu'(t - \tau) \quad (51)$$

where n is the interaction index, which measures the flame gain. The time-delayed model in Eq. (51) was a phenomenological model proposed by Crocco and Cheng [233], after some discussions with Summerfield [234], to explain rocket-engine combustion instabilities [4,235,236].

2.4 Hydrodynamic Models. Accurate hydrodynamic fields can be obtained by computational fluid dynamics; however, this review focuses on simplified qualitative models. First, in the diffusion-flame problem, the hydrodynamic field is assumed uniform for simplicity. Second, in the premixed-flame model, the action of the hydrodynamic field is encapsulated in the nondimensional disturbance phase velocity, K , which modulates the perturbation along the flame, Δu , at the flame’s base as

$$\frac{\partial \Delta u_X}{\partial t_f} + \frac{1}{K} \frac{\partial \Delta u_X}{\partial X_f} = 0 \quad (52)$$

In general, the nondimensional disturbance phase velocity, K , depends on the frequency of oscillation. K was calculated from direct numerical simulations in a conical flame [237]. Here, K is assumed constant, $K = 1.2$, as proposed in Ref. [160]. Third, in the flame response model, the action of the hydrodynamics is absorbed in the interaction index, n , and the time delay, τ , both of which encapsulate combustion and hydrodynamic phenomena.

3 Stability, Receptivity, and Sensitivity Analysis

The theoretical foundations of stability, receptivity, and sensitivity (SRS) analysis of thermoacoustic systems are laid out in the following subsections: The proposed framework and formalism are kept as general as possible such that they can be applied to other problems, such as hydrodynamic stability, time-delayed differential equations, and multiphysical systems. The stability of the system is calculated by eigenvalue analysis, whereas the receptivity to open-loop forcing is calculated by adjoint analysis. Finally, it is shown that the sensitivity can be accurately and cheaply calculated by combining the information from stability and adjoint analyses.

3.1 Stability. In general, the linearized thermoacoustic problem in the time domain is governed by a time-delayed dynamical system

$$\frac{d\mathbf{q}}{dt} = \mathbf{L}\mathbf{q} + \mathbf{L}_\tau\mathbf{q}(t - \tau) + \mathbf{s}, \quad t > 0 \quad (53a)$$

$$\mathbf{q} = \mathbf{g}(t), \quad t < 0 \quad (53b)$$

$$\mathbf{q} = \mathbf{q}_0, \quad t = 0 \quad (53c)$$

where $\mathbf{q} \in \mathbb{R}^N$ is the state vector, which represents a linear perturbation around an unperturbed mean flow; $\mathbf{g} \in \mathbb{R}^N$ is the preshape condition; \mathbf{q}_0 is the initial condition; and \mathbf{s} is an open-loop forcing term, i.e., it does not depend on the state variables and is set to zero except in Sec. 3.2. Although the solution, \mathbf{q} , lives in \mathbb{R}^N , time-delayed systems are infinite dimensional because of Eq. (53b). The linearized problem (53) is also known as *direct problem*.

Physically, the time delay is the time that a flow perturbation at the flame’s base takes to release a heat perturbation into the acoustics. There are two scenarios. In the first scenario, the heat release, \hat{q} , is modeled by a flame response (Sec. 2.3), in which $\tau \neq 0$ (hence $\mathbf{L}_\tau \neq 0$) is a key thermoacoustic parameter. The matrices \mathbf{L} and \mathbf{L}_τ are the spatial discretizations of the partial derivatives of the linear operator and the linear time-delayed operator, respectively, which embed the discretized boundary conditions. Without loss of generality, it is assumed that $\mathbf{q} = 0$ for $t < 0$ and $\mathbf{q} = \mathbf{q}_0$ at $t = 0$, i.e., the flame and acoustics are at rest for $t < 0$. In the second scenario, the heat release is not modeled by a flame response; therefore, the hydrodynamic and flame equations are solved to obtain \hat{q} . The matrix \mathbf{L} contains the hydrodynamic and combustion equations; $\tau = 0$; hence, $\mathbf{L}_\tau = 0$; and $\mathbf{q} = \mathbf{q}_0$ at $t = 0$. The linear time-delayed system becomes a linear initial value problem.

All the remarks that are being made are valid for both time-delayed systems and initial value problems.¹⁹

¹⁹An initial value problem can be viewed as a subset of a time-delayed problem with $\tau = 0$.

3.1.1 Stability Conditions. Time-delayed thermoacoustic systems, which are retarded systems, are asymptotically stable if and only if $\forall \varepsilon > 0$ there exists $\delta > 0$ such that $\forall \mathbf{q}([-\tau, 0])$ with $\|\mathbf{q}([-\tau, 0])\|_\infty < \delta$, $\|\mathbf{q}\|_\infty < \varepsilon$ for $t \geq 0$, where $\|\cdot\|_\infty$ is the infinity norm. Physically, a thermoacoustic system is asymptotically stable if perturbations die out in the long-time limit, i.e., $\mathbf{q} = 0$ for $t \rightarrow \infty$. Crucially, thermoacoustic systems are asymptotically stable if they are exponentially stable. To calculate the exponential stability, a modal decomposition is employed for the state vector

$$\mathbf{q}(\mathbf{x}, t) = \hat{\mathbf{q}}(\mathbf{x}) \exp(\sigma t) \quad (54)$$

where \mathbf{x} are the spatial coordinates, $\sigma \in \mathbb{C}$, and $\hat{\cdot}$ is the Laplace transformed quantity. The system is exponentially stable if $\text{Re}(\sigma) < 0$, i.e., the growth rate is negative. The angular frequency is provided by the imaginary part, $\text{Im}(\sigma)$. If the largest growth rate is zero, the system is marginally stable, i.e., perturbations persist with no amplification/decay. Otherwise, the system is unstable.

3.1.2 Nonlinear Eigenproblem. The substitution of the modal decomposition (54) into the governing equations, in general, results in a NEP [40,163,165], in contrast to most cases in hydrodynamic stability where linear eigenproblems²⁰ govern the stability. The nonlinear eigenproblem reads

$$\mathbf{N}(\sigma, \mathbf{p}) \hat{\mathbf{q}} = 0 \quad (55)$$

where \mathbf{N} is an $N \times N$ complex matrix, which is assumed analytic²¹ with respect to the parameters' vector, \mathbf{p} , and the complex number, σ , in a suitably defined domain of the complex plane.²² The dependence on σ and \mathbf{p} is dropped unless it is necessary for clarity. The size of the matrix has the order of either 1–100, in the case of a network-based model, or 10^3 – 10^6 in Helmholtz solvers. The nonlinear eigenproblem is solved when σ and $\hat{\mathbf{q}} \neq 0$ are found such that (55) is satisfied, which corresponds to the condition

$$\det(\mathbf{N}) = 0 \quad (56)$$

The above condition cannot be directly solved in most problems by cofactor expansion because the determinant has a complexity that grows factorially with the size of the matrix. More numerically efficient methods are typically used (Sec. 3.1.3).

The main sources of nonlinearity in the eigenproblem (55) are (i) the flame response model, which introduces a characteristic time delay τ appearing as $\exp(-\sigma\tau)$ in the frequency space; (ii) and nonideal acoustic boundary conditions, which are functions of frequency-dependent impedances [40]. σ may appear under rational, polynomial, trigonometric, and exponential nonlinearities. In general, such an NEP cannot be recast as a linear eigenproblem. The set of all the eigenvalues of $\mathbf{N}(\sigma, \mathbf{p})$ is the spectrum; and $\hat{\mathbf{q}}$ is the direct²³ eigenfunction, which forms an eigenpair with σ . The eigenfunction is the natural shape with which a small perturbation oscillates around the base state.

3.1.3 Features of Nonlinear Eigenproblems. Nonlinear eigenproblems appear in different applications in science and engineering beyond thermoacoustics, for example, in vibrations of structures, fluid–structure interaction, nanotechnology (quantum dots), time-delayed systems, control theory, to name a few. For more details, the reader may refer to Refs. [238–242]. The key facts of NEPs that are useful for stability, receptivity, and sensitivity analysis of thermacoustic systems and reacting flows are:

²⁰Or nonlinear eigenproblems with quadratic nonlinearities, which can be recast as linear eigenproblems.

²¹Some authors discard the growth rate in the flame transfer function (FTF) and retain only the angular frequency. In this scenario, we can apply analytic continuation to extend the FTF to the complex plane.

²²For example, by leaving out of the domain the singularities of rational functions.

²³Also known as the right eigenvector or, simply, eigenvector.

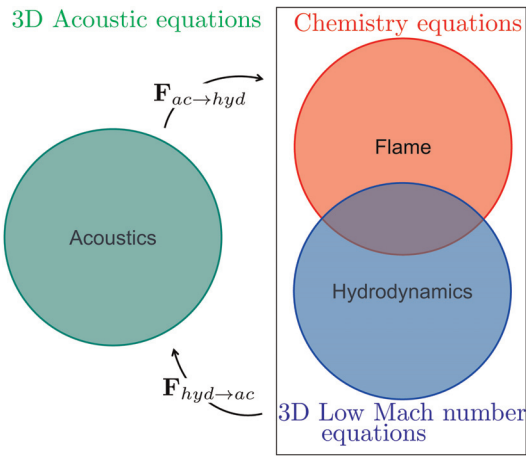


Fig. 6 Coupling between combusting hydrodynamics, governed by the low-Mach number equations and acoustics. Depending on the multiple-scale limit, the coupling terms, $F_{ac \rightarrow hyd}$ and $F_{hyd \rightarrow ac}$, have different expressions (Table 2) [161].

- A linear eigenproblem is a subset of NEPs with $\mathbf{N} = \mathbf{A} - \sigma\mathbf{L}$, where \mathbf{A} and \mathbf{L} may be complex matrices. Some thermoacoustic systems, however, may be governed by linear eigenproblems (e.g., in state space models [243–245] or with time-delayed equations that are linearized in τ [42,153]);
- The spectrum of an NEP is discrete, i.e., it does not have accumulation points. The eigenvalues are isolated and can be countably infinite;
- An eigenvalue has algebraic multiplicity a if $d^j/d\sigma^j \det(\mathbf{N}) = 0$ and $d^j/d\sigma^a \det(\mathbf{N}) \neq 0$, where $j = 0, 1, \dots, a-1$. The geometric multiplicity, g , of an eigenvalue σ is the dimension of the null space of $\mathbf{N}(\sigma)$, i.e., $g = \dim(\text{null}(\mathbf{N}(\sigma)))$. In linear eigenproblems, the algebraic multiplicities add up to the dimension of the problem. However, in NEPs, there may exist an infinite number of eigenvalues, and an eigenvalue may have any algebraic multiplicity greater than the dimension of the problem²⁴;
- An eigenvalue is semisimple if $a = g$. If $a = 1$, the eigenvalue is simple;
- An eigenvalue is defective if $a > g$. An important class of defective eigenvalues are branch-point solutions of the characteristic function,²⁵ which are known as exceptional points [246,247]. Exceptional points have infinite sensitivity to infinitesimal perturbations to the system (as shown later in Fig. 7);
- Eigenvalues that are not simple are degenerate. For example, problems with symmetries, such as rotationally symmetric annular combustors, typically have semisimple, thus degenerate, eigenvalues;
- Eigenvectors corresponding to distinct eigenvalues are linearly independent in linear eigenproblems, whereas this is not necessarily the case in NEPs. Likewise, generalized eigenvectors of linear eigenproblems are linearly independent, whereas this does not necessarily hold in NEPs. All the linearly independent eigenvectors (and generalized eigenvectors) provide a basis for nondefective (defective) NEPs;
- On one hand, algebraic simplicity implies geometric simplicity. On the other hand, geometric simplicity and $\partial\mathbf{N}/\partial\sigma$ -orthogonality (Eq. (60)) imply algebraic simplicity [248];
- Numerically, an NEP can be solved by Newton's methods with iterative projection methods for large-scale problems (Lanczos, rational Krylov, Jacobi-Davidson, etc.), contour integration [242], and linearization methods, to name a few.

²⁴For example, the complex function $F(z) = z^{N+k}$, with N being the space dimension and k being a positive integer, has an eigenvalue $\sigma = 0$ with algebraic multiplicity of $N+k$.

²⁵The solutions of the characteristic function may be complex multivalued functions; hence, they may be branch points.

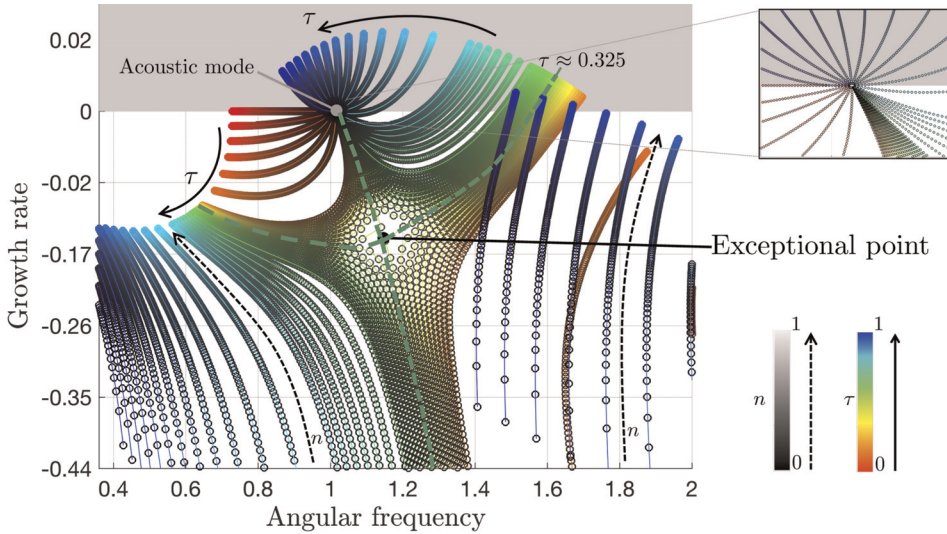


Fig. 7 Locus of eigenvalues as the flame parameters are varied as $n = [0 \rightarrow 1]$ and $\tau = [0 \rightarrow 1]$ with increments of 0.05. Adapted from Ref. [175].

- The references [240,242,249] provide thorough descriptions of existing numerical methods for NEPs. In thermoacoustics, simple gradient-based iteration algorithms are typically utilized (e.g., Ref. [40]). Contour integration was applied to solve dispersion relations in Ref. [250] and to find all the defective and nondefective eigenvalues in a given circle of the complex plane in Refs. [247,251]. The contour integration method proved numerically more robust and stable than gradient-based iteration methods, with the advantage of finding all the eigenvalues in a defined domain in the complex plane;
- The eigenvalues of a state space model (Eqs. (53a)–(53c)) are the poles of the corresponding transfer function.

Appendix A explains the local Smith form of NEPs.

3.2 Receptivity (Adjoint Eigenproblem). The receptivity of a thermoacoustic variable to open-loop forcing or initial conditions is calculated by solving the adjoint problem. The key facts of adjoint NEPs that are useful for receptivity analysis of thermoacoustic systems and reacting flows are:

- The adjoint operator, \mathbf{N}^+ , is defined such that for any vector, $\hat{\mathbf{q}}^+$, the following identity holds

$$\langle \hat{\mathbf{q}}^+, \mathbf{N}\hat{\mathbf{q}} \rangle_{\mathbf{M}} \equiv \langle \mathbf{N}^+ \hat{\mathbf{q}}^+, \hat{\mathbf{q}} \rangle_{\mathbf{M}} \quad (57)$$

where $\langle \cdot, \cdot \rangle_{\mathbf{M}}$ is a bilinear form,²⁶ or a sesquilinear form²⁷ when working with complex numbers. In this paper, an inner product²⁸ is used to define the adjoint operator

$$\langle \mathbf{a}, \mathbf{b} \rangle_{\mathbf{M}} \equiv \mathbf{a}^H \mathbf{M} \mathbf{b} \quad (58)$$

where \mathbf{M} is a positive-definite weight matrix; \mathbf{a} and \mathbf{b} are generic complex vectors; and H is the conjugate transpose. The adjoint operator reads

$$\mathbf{N}^+ = \mathbf{M}^{-1} \mathbf{N}^H \mathbf{M} \quad (59)$$

²⁶i.e., $\langle \mathbf{a} + \mathbf{c}, \mathbf{b} + \mathbf{d} \rangle = \langle \mathbf{a}, \mathbf{b} \rangle + \langle \mathbf{c}, \mathbf{b} \rangle + \langle \mathbf{a}, \mathbf{d} \rangle + \langle \mathbf{b}, \mathbf{d} \rangle$ and $\langle \lambda \mathbf{a}, z \mathbf{b} \rangle = \lambda z \langle \mathbf{a}, \mathbf{b} \rangle$, where $\mathbf{a}, \mathbf{b}, \mathbf{c}$, and \mathbf{d} are arbitrary complex vectors and λ and z are arbitrary complex scalars.

²⁷i.e., $\langle \mathbf{a} + \mathbf{c}, \mathbf{b} + \mathbf{d} \rangle = \langle \mathbf{a}, \mathbf{b} \rangle + \langle \mathbf{c}, \mathbf{b} \rangle + \langle \mathbf{a}, \mathbf{d} \rangle + \langle \mathbf{b}, \mathbf{d} \rangle$ and $\langle \lambda \mathbf{a}, z \mathbf{b} \rangle = \lambda^* z^* \langle \mathbf{a}, \mathbf{b} \rangle$.
²⁸i.e., a sesquilinear form that is symmetric, that is, $\langle \mathbf{a}, \mathbf{b} \rangle = \langle \mathbf{b}, \mathbf{a} \rangle^*$.

The right-hand side of Eq. (59) defines a similarity transformation; therefore, the spectrum of \mathbf{N}^H is the complex conjugate²⁹ of the spectrum of \mathbf{N} . This information serves as a good check when validating adjoint algorithms. Unless otherwise specified, in this paper, $\mathbf{M} = \mathbf{I}$, thus, the subscript \mathbf{M} in Eq. (58) is dropped;

- Importantly to sensitivity analysis (Sec. 3.3), a necessary and sufficient condition for the eigenvalue to be semisimple is that direct and adjoint eigenvectors are $\partial \mathbf{N}/\partial \sigma$ -orthogonal to each other [248]

$$\left\langle \hat{\mathbf{q}}_j^+, \frac{\partial \mathbf{N}}{\partial \sigma} \Big|_{\sigma_j} \hat{\mathbf{q}}_i \right\rangle = C \delta_{i,j} \quad (60)$$

where $\delta_{i,j}$ is the Kronecker delta, and $C \neq 0$ is a user-defined normalization factor, often $C = 1$. Equation (60) is a generalization of the biorthogonality condition of linear eigenproblems that appear in hydrodynamic stability [62];

- From a corollary of the Keldysh theorem [238,242], in a neighborhood of a simple eigenvalue σ_j , the inverse of the operator can be represented as

$$\mathbf{N}^{-1}(\sigma) = \frac{1}{(\sigma - \sigma_j)} \frac{\hat{\mathbf{q}}_j \otimes \hat{\mathbf{q}}_j^{+*}}{\left\langle \hat{\mathbf{q}}_j^+, \frac{\partial \mathbf{N}}{\partial \sigma} \Big|_{\sigma_j} \hat{\mathbf{q}}_j \right\rangle} + \mathcal{O}(\sigma - \sigma_j) \quad (61)$$

where \otimes is the dyadic product, and $\sim \mathcal{O}(\sigma - \sigma_j)$ is an analytic additive term (a remainder from the Laurent series), which is zero in linear eigenproblems. Note that the adjoint eigenfunction projects a vector onto the corresponding direct eigenvector, or, in other words, the adjoint eigenvector is a projector.

3.2.1 Continuous Adjoint, Discrete Adjoint or Automatic Differentiation? To present the different ways and philosophies to obtain the adjoint of a system, a step back is taken to consider the nonlinear problem in time. Three steps are generally taken to simulate problems in thermofluid dynamics. First, under the continuum hypothesis, continuous differential equations are selected to

²⁹Strictly speaking, for general NEPs such that $\det(\mathbf{N}(\sigma))^* \neq \det(\mathbf{N}(\sigma^*))$, the spectrum of $(\mathbf{N}(\sigma))^H$ is the spectrum of $\mathbf{N}(\sigma)$ because σ is the solution of the adjoint problem, i.e., $0 = \det(\mathbf{N}(\sigma)) = \det(\mathbf{N}(\sigma))^* = \det((\mathbf{N}(\sigma))^T)^* = \det((\mathbf{N}(\sigma))^H)$. However, the NEP may be recast as $\mathbf{M}(\sigma)\hat{\mathbf{q}} = \sigma\hat{\mathbf{q}}$, where $\mathbf{M}(\sigma) \equiv \sigma\mathbf{I} - \mathbf{N}(\sigma)$. With this arrangement, the complex conjugate, σ^* , is the eigenvalue of the adjoint eigenproblem $(\mathbf{M}(\sigma))^H \hat{\mathbf{q}}^+ = \sigma^* \hat{\mathbf{q}}^+$, i.e., the solution of $\det(\mathbf{M}(\sigma)^H - \sigma^* \mathbf{I}) = 0$. In this paper, we implicitly use the latter arrangement when referring to the adjoint spectrum as being the complex conjugate of the direct spectrum.

represent the physical problem, e.g., partial differential equations, ordinary differential equations, integro-differential equations. The more skilled the modeler, the more predictive the selected equations. Second, assuming that no closed-form solution exists,³⁰ a discretization scheme is chosen to approximate the continuous equations, e.g., finite differences, finite volumes, finite elements, spectral methods, etc. Third, the discrete equations are implemented in algorithmic instructions in a computer program. The adjoint model can be defined and implemented after any of these three steps: The continuous adjoint (CA) approach defines the adjoint system after the first step; the discrete adjoint (DA) approach defines the adjoint system after the second step; and the automatic (or algorithmic) differentiation (AD) approach defines the adjoint system after the third step.³¹ In this review, the focus is on CA and DA approaches. An example of an AD approach in thermoacoustics can be found in Ref. [252].

Typical applications of adjoint analysis of nonlinear systems in the time domain are variational data assimilation, Bayesian inference, sensitivity analysis, constrained optimization, optimal control, calculation of singular vectors, input/output analysis, inverse modeling. The time-dependent framework is described in Appendix B.1. In this review, the focus is on applications of adjoint analysis to eigenvalues.

A comment on the differences between CA and DA approaches: Continuous adjoint equations were introduced in the second half of the 18th century by the Italian-French mathematician Joseph-Louis Lagrange in the theory of linear ordinary differential equations. Here, the CA approach is analyzed as applied to partial differential equations, and differences with the DA approach are discussed. First, in the CA approach, the solutions live in different spaces, typically Sobolev spaces. For Riesz theorem, the adjoint always exists and is unique in continuous operators in Hilbert spaces, of which a finite dimensional space is a subset. Second, the adjoint boundary conditions explicitly appear as further variables, whereas in the DA approach, they are encapsulated in the discrete operator. Third, the adjoint equations are defined by a bilinear form, or a sesquilinear form when working with complex numbers, that includes the spatial dependency

$$\left[\underline{\mathbf{q}}^+, \left(\frac{\partial}{\partial t} - \mathcal{L} \right) \underline{\mathbf{q}} \right] - \left[\left(\frac{\partial}{\partial t} - \mathcal{L}^+ \right) \underline{\mathbf{q}}^+, \underline{\mathbf{q}} \right] = \text{boundary and initial terms} \quad (62)$$

Here, an inner product is used to define the adjoint equations (see Sec. 3.2)

$$[\underline{\mathbf{a}}, \underline{\mathbf{b}}] \equiv \frac{1}{TV} \int_0^T \int_V \underline{\mathbf{a}}^* \cdot \underline{\mathbf{b}} \, dV dt \quad (63)$$

where \mathcal{L} is the continuous linear thermoacoustic operator, which is a linear combination of the spatial derivatives (see Sec. 2); $\underline{\mathbf{a}}$, $\underline{\mathbf{b}}$ are arbitrary functions in the function space in which the problem is defined³²; V is the space domain; T is the integration time; and $*$ is the complex conjugate. Equation (62) is sometimes referred to as Green's (or Lagrange-Green) identity [134,253]. To find the adjoint operator with the CA approach, integration by parts (with the divergence theorem) of Eq. (62) is performed. The adjoint boundary conditions, which arise from integration by parts of Eq. (62), are defined such that the right-hand side is zero. Importantly, it is straightforward to check the important property that $\partial([\underline{\mathbf{q}}^+, \underline{\mathbf{q}}])/\partial t = 0$, which is used for debugging unsteady adjoint codes (see *dot-product test* in Appendix B.2).

³⁰Alas, this is the case in the vast majority of engineering problems.

³¹In other areas in computational science, no distinction is made between DA and AD. However, the author feels that such a distinction should be made, in particular in thermoacoustic problems.

³²In this section, the underline is used to denote a function that depends on space as well.

Magri et al. [153,162] presented a comparison between the numerical truncation errors between the CA and DA methods as applied to thermoacoustics. Although the two formulations should converge in principle, it has been shown that convergence is actually not guaranteed a priori [134,254–257]. Dual-consistent numerical schemes help improve this convergence (see, e.g., Refs. [258] and [259]). On one hand, the CA approach highlights the physical information carried by the adjoint variables at the boundaries. On the other hand, the DA approach provides the exact gradient (to machine precision) of the discrete objective function. For the thermoacoustic system considered in this paper, the DA method provides more accurate results and is easier to implement. However, the results obtained via the CA method are shown to describe how the method works and interpret the jump conditions in thermoacoustic network models (Sec. 3.5). In Appendices B.2–B.3, other remarks on adjoint equations are listed for keen readers.

3.2.2 Physical Information From Adjoint Eigenfunctions. To show the physical information that can be obtained from the adjoint eigenpairs, here it is assumed that the eigenvalue is simple so that Eq. (61) holds. Similar conclusions can be drawn if the eigenvalue is semisimple.

The spatially discretized linearized time-delayed thermoacoustic problem (53) can be solved by the Laplace transform. By observing that the Laplace transform of $\underline{\mathbf{q}}(t - \tau)$ is $\underline{\mathbf{q}} \exp(-\sigma\tau) + \hat{\mathbf{g}}$, Eqs. (53) are transformed as

$$\underbrace{[\sigma\mathbf{I} - \mathbf{L} - \mathbf{L}_\tau \exp(-\sigma\tau)]}_{\equiv \mathbf{N}} \hat{\mathbf{q}} = \hat{\mathbf{s}} + \mathbf{q}_0 + \mathbf{L}_\tau \hat{\mathbf{g}} \quad (64)$$

The solution in the time domain is provided by the Bromwich integral³³

$$\underline{\mathbf{q}}(t) = \frac{1}{2\pi i} \int_{\gamma-i\infty}^{\gamma+i\infty} \mathbf{N}^{-1}(\sigma) (\hat{\mathbf{s}} + \mathbf{q}_0 + \mathbf{L}_\tau \hat{\mathbf{g}}) \exp(\sigma t) d\sigma \quad (65)$$

$$= \sum_{j=1}^{\infty} \mathbf{A}_j \exp(\sigma_j t) \quad (66)$$

where $\mathbf{N}^{-1}(\sigma)$ is the resolvent. The last equality is a consequence of the theorem of residues, where $\mathbf{A}_j \equiv \text{Res}\{\hat{\mathbf{q}}_j\} \equiv \lim_{\sigma \rightarrow \sigma_j} (\sigma - \sigma_j) \hat{\mathbf{q}}_j$ for simple eigenvalues, σ_j . On substituting the inverse operator (61) in Eq. (65), the modal amplitudes of the solution in time are calculated as

$$\mathbf{A}_j = \frac{\left\langle \hat{\mathbf{q}}_j^+, \hat{\mathbf{s}}(\sigma_j) + \mathbf{q}_0 + \mathbf{L}_\tau \hat{\mathbf{g}}(\sigma_j) \right\rangle}{\left\langle \hat{\mathbf{q}}_j^+, \frac{\partial \mathbf{N}}{\partial s} \Big|_{\sigma_j} \hat{\mathbf{q}}_j \right\rangle} \quad (67)$$

Physically, the response of the j th component of $\underline{\mathbf{q}}$ in the long-time limit increases (i) as the forcing frequency is close to the j th eigenvalue, σ_j (resonance); (ii) as the forcing, $\hat{\mathbf{s}}$, approaches the adjoint eigenfunction, $\hat{\mathbf{q}}_j^+$; and (iii) as the initial and preshape conditions, \mathbf{q}_0 and $\mathbf{L}_\tau \hat{\mathbf{g}}$, overlap, respectively, the adjoint eigenfunction. Therefore, to observe the maximum amplification of $\hat{\mathbf{q}}_j$, the thermoacoustic system should be either forced with a frequency close to σ_j ; or forced with $\hat{\mathbf{s}} = \hat{\mathbf{q}}_j^+ \exp(i\omega_j t)$, where $\omega_j \equiv \text{Im}(\sigma_j)$; or initialized with $\mathbf{q}_0 = \hat{\mathbf{q}}_j^+$ and $\mathbf{L}_\tau \hat{\mathbf{g}} = \hat{\mathbf{q}}_j^+$; or a combination of the above. For example, the adjoint eigenfunction of the acoustic momentum equation reveals the locations where the thermoacoustic system is most receptive to forces, such as acoustic dampers and drag devices (Secs. 6.1.1 and 6.3).

³³In spatially continuous problems, the continuous spectrum should be considered as well [260,261]. More details for thermoacoustic systems can be found in Ref. [154].

3.3 Eigenvalue Sensitivity. The objective is to calculate the change of a thermoacoustic eigenvalue due to an infinitesimally small change to the problem. Such a calculation is enabled by perturbation methods. Perturbation theory of eigenvalues was pioneered in self-adjoint problems, i.e., acoustic problems by Rayleigh [203] and quantum mechanics³⁴ by Schrödinger [262]. However, in general, thermoacoustic systems are not self-adjoint [35–37,39,40], which is a property calling for adjoint eigenvectors. The philosophy of adjoint perturbation theory can be summarized as follows: First, the thermoacoustic stability problem (55) is solved for a set of parameters \mathbf{p}_0 . The eigenvalue σ_0 and eigenfunction $\hat{\mathbf{q}}_0$, with their multiplicities, are called the unperturbed solutions, which are subject to

$$\mathbf{N}(\sigma_0, \mathbf{p}_0)\hat{\mathbf{q}}_{0,j} = 0, \quad j = 1, \dots, g \quad (68)$$

with the corresponding adjoint problem

$$\mathbf{N}^H(\sigma_0, \mathbf{p}_0)\hat{\mathbf{q}}_{0,j}^+ = 0, \quad j = 1, \dots, g \quad (69)$$

where $\mathbf{N}^H(\sigma_0, \mathbf{p}_0)$ is a shorthand for $[\mathbf{N}(\sigma_0, \mathbf{p}_0)]^H$. It is recalled that the thermoacoustic matrix is assumed analytic in σ and \mathbf{p} . Second, the matrix \mathbf{N} is perturbed by small changes to the parameters, \mathbf{p}_0 , or by small changes to the operator, $\delta\mathbf{P}$ (Sec. 3.3.4). Third, the eigenvalues and eigenvectors are expanded in asymptotic series centered around \mathbf{p}_0 or $\mathbf{N}(\sigma_0, \mathbf{p}_0)$ (Sec. 3.3.4). Finally, the different orders of the eigenvalue and eigenvector drifts (also known as corrections) are governed by linear inhomogeneous systems. These are solved by using the adjoint eigenvectors, which provide solvability conditions (see also Appendix B.2).

3.3.1 Multi-Index Expansion. In multi-index notation up to order k , the expansion of the thermoacoustic matrix \mathbf{N} around the eigenvalue σ_0 and the set of M parameters cast in a vector \mathbf{p}_0 , reads [165,171,172]

$$\mathbf{N}(\sigma, \mathbf{p}) = \sum_{|(i, \mu)| \leq k} \mathbf{N}_{i, \mu} (\sigma - \sigma_0)^i (\mathbf{p} - \mathbf{p}_0)^\mu + \text{h.o.t.} \quad (70)$$

where $(i, \mu) \equiv (i, \mu_1, \dots, \mu_M)$ is an $(M+1)$ -tuple of non-negative integers, h.o.t. are the higher order terms, and

$$\mathbf{N}_{i, \mu} \equiv \frac{1}{(i, \mu)!} \frac{\partial^{|(i, \mu)|} \mathbf{N}}{\partial \sigma^i \partial \mathbf{p}^\mu} \quad (71)$$

where

$$|(i, \mu)| \equiv i + \mu_1 + \dots + \mu_M \quad (72)$$

$$(\mathbf{p} - \mathbf{p}_0)^\mu \equiv (p_1 - p_{0,1})^{\mu_1} \dots (p_M - p_{0,M})^{\mu_M} \quad (73)$$

$$(i, \mu)! \equiv i! \mu_1! \dots \mu_M! \quad (74)$$

$$\frac{\partial^{|(i, \mu)|} \mathbf{N}}{\partial \sigma^i \partial \mathbf{p}^\mu} \equiv \frac{\partial^{|(i, \mu)|} \mathbf{N}}{\partial \sigma^i \partial p_1^{\mu_1} \dots \partial p_M^{\mu_M}} \quad (75)$$

The Taylor series (70) converges providing that a singularity is not encountered. For example, the first-order truncation of Eq. (70) yields

³⁴Quantum mechanics offers a large “repository” of mathematical techniques, some of which can be adapted to tackle acoustic/thermoacoustic problems. For example, some aeroacoustic problems can be cast in a Schrödinger equation and solved by Dyson expansion [195]. There are other examples, which will be the subject of another study.

$$\begin{aligned} \mathbf{N}(\sigma, \mathbf{p}) &\approx \\ &\approx \mathbf{N}(\sigma_0, \mathbf{p}_0) + \mathbf{N}_{1,0}(\sigma - \sigma_0) + \mathbf{N}_{0,1}(\mathbf{p} - \mathbf{p}_0) \\ &= \mathbf{N}(\sigma_0, \mathbf{p}_0) + \frac{\partial \mathbf{N}}{\partial \sigma}(\sigma - \sigma_0) + \sum_{j=1}^M \frac{\partial \mathbf{N}}{\partial p_j}(p_j - p_{0,j}) \end{aligned} \quad (76)$$

3.3.2 Sensitivity to One Parameter. The case of a perturbation applied to one parameter is first analyzed. The parameter is assumed analytic with power series up to order Q

$$\mathbf{p} = \sum_{j=0}^Q \varepsilon^j \mathbf{p}_j + \text{h.o.t.} \quad (77)$$

where ε is the perturbation parameter. Simple and semi-simple thermoacoustic eigenpairs can be expanded as power series³⁵

$$\sigma = \sigma_0 + \sum_{j=1}^Q \sigma_j \varepsilon^j + \text{h.o.t.} \quad (78)$$

$$\hat{\mathbf{q}} = \hat{\mathbf{q}}_0 + \sum_{j=1}^Q \hat{\mathbf{q}}_j \varepsilon^j + \text{h.o.t.} \quad (79)$$

To calculate the coefficients of Eqs. (78) and (79), which are the eigenvalue and eigenvector drifts, respectively, the decompositions (78) and (79) are substituted into the eigenvalue problem (55). Each order of ε defines the equation for the eigenpair drift, which, at k th order, reads in compact notation [172]

$$[\mathbf{N}_{0,0}\hat{\mathbf{q}}_k = -\mathbf{r}_k - \sigma_k \mathbf{N}_{1,0}\hat{\mathbf{q}}_0] \quad (80)$$

where $\mathbf{N}_{0,0} \equiv \mathbf{N}(\sigma_0, \mathbf{p}_0)$ and³⁶

$$\mathbf{r}_k = \sum_{n=1}^k \mathbf{N}_{0,n} \hat{\mathbf{q}}_{k-n} + \sum_{0 < |\nu\mu| \leq k} \sum_{n=0}^{k-|\nu\mu|} \binom{|\mu|}{\mu} \sigma_\nu^\mu \mathbf{N}_{|\mu|, n} \hat{\mathbf{q}}_{k-n-|\nu\mu|} \quad (81)$$

where

$$\nu \equiv (1, 2, \dots, M) \quad (82)$$

$$\binom{|\mu|}{\mu} \equiv \frac{|\mu|}{\mu!} \quad (83)$$

$$\sigma_\nu^\mu \equiv \prod_{n=1}^M \sigma_1^{\mu_1} \dots \sigma_M^{\mu_M} \quad (84)$$

$$\mu\nu \equiv \mu_1\nu_1 \dots \mu_M\nu_M \quad (85)$$

and $\mathbb{1}_k$ is a multi-index of zeros except for the position k , where it is 1. For example, the first three orders of \mathbf{r}_k read

$$\mathbf{r}_1 = \mathbf{N}_{0,1}\hat{\mathbf{q}}_0 \quad (86a)$$

³⁵In contrast, if the eigenvalue is defective and a branch-point solution of the characteristic function, a fractional power series (also known as Newton–Puiseux series or Puiseux series) has to be employed, $\sigma = \sigma_0 + \sum_{j=1}^Q \sigma_j \varepsilon^j + \text{h.o.t.}$ and $\hat{\mathbf{q}} = \hat{\mathbf{q}}_0 + \sum_{j=1}^Q \hat{\mathbf{q}}_j \varepsilon^j + \text{h.o.t.}$, where a is the algebraic multiplicity (Appendix I of Ref. [263], pp. 65–66 of Ref. [261] and [248], [264–269]). Although beyond the scope of this review paper, it is interesting to characterize the sensitivity of defective branch-point eigenvalues because their rate of change is infinitely larger than the rate of change of the parameters. In other words, the thermoacoustic stability at an exceptional point is infinitely more sensitive to perturbations than the thermoacoustic stability of a nondefective system [165, 247].

³⁶Private communication with G. Mensah and A. Orchini.

$$\mathbf{r}_2 = \mathbf{N}_{0,1}\hat{\mathbf{q}}_1 + \mathbf{N}_{0,2}\hat{\mathbf{q}}_0 + \sigma_1(\mathbf{N}_{1,0}\hat{\mathbf{q}}_1 + \mathbf{N}_{1,1}\hat{\mathbf{q}}_0) + \sigma_1^2\mathbf{N}_{2,0}\hat{\mathbf{q}}_0 \quad (86b)$$

$$\begin{aligned} \mathbf{r}_3 = & \mathbf{N}_{0,1}\hat{\mathbf{q}}_2 + \mathbf{N}_{0,2}\hat{\mathbf{q}}_1 + \mathbf{N}_{0,3}\hat{\mathbf{q}}_0 \\ & + \sigma_1(\mathbf{N}_{1,0}\hat{\mathbf{q}}_2 + \mathbf{N}_{1,1}\hat{\mathbf{q}}_1 + \mathbf{N}_{1,2}\hat{\mathbf{q}}_0) \\ & + \sigma_1^2(\mathbf{N}_{2,0}\hat{\mathbf{q}}_1 + \mathbf{N}_{2,1}\hat{\mathbf{q}}_0) + \sigma_2(\mathbf{N}_{1,0}\hat{\mathbf{q}}_1 + \mathbf{N}_{1,1}\hat{\mathbf{q}}_0) \\ & + 2\sigma_1\sigma_2\mathbf{N}_{2,0}\hat{\mathbf{q}}_0 + \sigma_1^3\mathbf{N}_{3,0}\hat{\mathbf{q}}_0 \end{aligned} \quad (86c)$$

Equation (80) is a linear inhomogeneous system, which is not invertible because matrix $\mathbf{N}_{0,0}$ is singular. For the linear system (80) to have solutions, a solvability condition has to be fulfilled at each order. This is where the adjoint eigenfunctions are called upon. Equation (80) is projected onto the corresponding adjoint eigenvector to yield

$$\langle \hat{\mathbf{q}}^+, -\mathbf{r}_k - \sigma_k \mathbf{N}_{1,0}\hat{\mathbf{q}}_0 \rangle = 0 \quad (87)$$

On one hand, if the eigenvalue is simple (nondegeneracy), Eq. (87) can be solved for the eigenvalue drifts, σ_k , which can be subsequently substituted back into Eq. (80) to obtain the eigenvector drift, $\hat{\mathbf{q}}_k$. Numerical strategies to compute $\hat{\mathbf{q}}_k$ can be found in Ref. [165]. On the other hand, if the eigenvalue is semisimple, g solvability conditions have to be fulfilled simultaneously, which give rise to an auxiliary eigenvalue problem

$$\mathbf{X}_k z - \sigma_k \mathbf{Y} z = 0 \quad (88)$$

where \mathbf{X}_k and \mathbf{Y} are matrices whose components are

$$[\mathbf{X}_k]_{i,j} = \langle \hat{\mathbf{q}}_{0,i}^+, -\mathbf{r}_{k,j} \rangle \quad (89)$$

$$[\mathbf{Y}]_{i,j} = \langle \hat{\mathbf{q}}_{0,i}^+, \mathbf{N}_{1,0}\hat{\mathbf{q}}_{0,j} \rangle \quad (90)$$

$$i, j = 1, 2, \dots, g \quad (91)$$

If the $\partial\mathbf{N}/\partial\sigma$ -orthogonality normalization (60) is imposed, then $\mathbf{Y} = \mathbf{I}$. By solving Eq. (88) for problems with double geometric multiplicity, $g=2$, such as rotationally symmetric annular combustors, the first-order eigenvalue drift reads

$$\sigma_{1,\pm} = -\frac{\text{tr}(\mathbf{X})}{2} \pm \sqrt{\frac{\text{tr}(\mathbf{X})^2}{4} - \det(\mathbf{X})} \quad (92)$$

with the corresponding eigenvectors

$$z_\pm = \begin{pmatrix} -[\mathbf{X}]_{12} \\ [\mathbf{X}]_{11} - \sigma_{1,\pm} \end{pmatrix} \quad (93)$$

Two scenarios are considered. First, the perturbation to the system may be such that the auxiliary problem is still degenerate up to k th order, i.e., $\sigma_{k,+} = \sigma_{k,-}$. Geometrically, the degenerate eigenspace does not unfold because $z_+ = z_-$. Second, the perturbation to the system may be such that the auxiliary problem is not degenerate at k th order, i.e., $\sigma_+ \neq \sigma_-$. The directions along which the degenerate eigenspace unfolds are provided by the two different eigendirections z_\pm , along which the perturbation analysis becomes nondegenerate (Sec. 9). Mode degeneracy with semisimple eigenvalues is a problem relevant to annular and can-annular combustors because of their rotationally symmetric geometry (see, among others, [163,165,166,171,221,270–279]). The multiplicity of the degeneracy induced by the symmetry is typically $g=2$, which physically corresponds to two eigenfunctions that are rotating in opposite azimuthal directions with the same frequency.

3.3.3 Sensitivity to Multiple Parameters. If the eigenvalue is simple, the extension to multiparameter expansion simply

involves a multivariate expansion of the eigenvalue with respect to the parameters' vector

$$\sigma = \sigma_0 + \sum_{|\mu| \leq k} \frac{1}{\mu!} \frac{\partial^{|\mu|} \sigma}{\partial \mathbf{p}^\mu} (\mathbf{p} - \mathbf{p}_0)^\mu + \text{h.o.t.} \quad (94)$$

The eigenvalue drifts can be found by applying the method of Sec. 3.3.2. If the eigenvalue is semisimple, Eq. (94) is not totally differentiable because of the auxiliary eigenvalue problem in Eq. (88) [171,261]. To circumvent the lack of total differentiability, the problem can be turned to a single-parameter problem:

- A perturbation direction in the parameter space is chosen, $\Delta\mathbf{p} = \mathbf{p} - \mathbf{p}_0$;
- The perturbation direction is normalized as

$$\tilde{\Delta\mathbf{p}} \equiv \frac{\Delta\mathbf{p}}{\|\Delta\mathbf{p}\|} \quad (95)$$

- The parameters' vector is perturbed as

$$\mathbf{p} \equiv \mathbf{p}_0 + \varepsilon \tilde{\Delta\mathbf{p}} \quad (96)$$

such that

$$\begin{aligned} \mathbf{N}(\sigma, \mathbf{p}) &= \mathbf{N}(\sigma, \mathbf{p}_0 + \varepsilon \tilde{\Delta\mathbf{p}}) \\ &\equiv \mathbf{H}_{\tilde{\Delta\mathbf{p}}}(\sigma, \varepsilon) \end{aligned} \quad (97)$$

where $\mathbf{H}_{\tilde{\Delta\mathbf{p}}}(\sigma, \varepsilon)$ is the thermoacoustic matrix perturbed along the parameters' direction $\tilde{\Delta\mathbf{p}}$ by a single parameter ε ;

- The eigenvalue drifts can be calculated with the formulation of Sec. 3.3.2 by using

$$\mathbf{H}_{\tilde{\Delta\mathbf{p}},m,n} = \frac{1}{m!n!} \frac{\partial^{m+n}}{\partial \sigma^m \partial \varepsilon^n} \mathbf{H}_{\tilde{\Delta\mathbf{p}}} \Big|_{(\sigma=\sigma_0, \varepsilon=0)} \quad (98)$$

3.3.4 Sensitivity to the Thermoacoustic Matrix. Another approach is to directly perturb the operator by another operator

$$\mathbf{N}(\sigma) = \mathbf{N}_0(\sigma) + \varepsilon \delta\mathbf{P}(\sigma) \quad (99)$$

where \mathbf{N}_0 is the unperturbed matrix. This is the usual approach used in hydrodynamic stability [134], which was used in thermoacoustics for the calculation of linearly optimal passive control devices [153,154], base-state sensitivities [158,160,165], uncertainty quantification both in annular [163] and longitudinal combustors [164,167], and optimal acoustic damper placements in annular combustors [172].

Base-flow perturbations: To design control strategies, the effect that a controller has on the base flow has to be considered. When an external controller, such as a Helmholtz resonator, is placed into the thermoacoustic system, it induces a perturbation to the matrix as

$$\delta\mathbf{P} = \frac{\partial \mathbf{N}}{\partial \mathbf{p}} + \frac{\partial \mathbf{N}}{\partial \bar{\mathbf{q}}} \frac{d\bar{\mathbf{q}}}{d\mathbf{p}} \quad (100)$$

where \mathbf{p} are the parameters that the object changes, i.e., a feedback forcing, drag coefficient, etc., and $\bar{\mathbf{q}}$ is the base flow upon which the thermoacoustics evolve. In hydrodynamic stability, the sensitivity $\partial\mathbf{N}/\partial\mathbf{p}$ is customarily called structural sensitivity,³⁷ which estimates the wavemaker regions in the flow. The sensitivity $\partial\mathbf{N}/\partial\bar{\mathbf{q}} d\bar{\mathbf{q}}/d\mathbf{p}$ is called base-flow sensitivity [72,73]. In order to calculate the change of the base flow, another set of adjoint

³⁷More precisely, a norm of such a sensitivity was originally called structural sensitivity in Ref. [67].

equations can be imposed to constrain the base-flow equations when a small steady forcing term is added. The adjoint base flow is the solution of an inhomogeneous linear system, where the inhomogeneous term depends on the direct and adjoint eigenfunctions [73]. Base-flow sensitivity was applied in thermoacoustics in Ref. [158] in a ducted diffusion flame to find the optimal changes to stabilize a thermoacoustic instability. Recently, the effect of shape modifications on annular and longitudinal combustors was calculated in Refs. [173] and [174] to stabilize all the thermoacoustic eigenvalues with adjoint-based optimization. The calculation of the eigenvalue and eigenvector drift closely follows the philosophy presented in Secs. 3.3.2–3.3.3. For example, the eigenvalue drift at first-order reads [165]

$$\sigma_1 = \frac{\langle \hat{\mathbf{q}}^+, \delta \mathbf{P} \hat{\mathbf{q}} \rangle}{\left\langle \hat{\mathbf{q}}^+, \frac{\partial \mathbf{N}}{\partial \sigma} \Big|_{\sigma_0} \hat{\mathbf{q}} \right\rangle} \quad (101)$$

which is a formula that is used in a number of studies in flow instability, some references of which are discussed in Sec. 1.2.1.

3.3.5 Intrinsic Sensitivity. The intrinsic sensitivity is defined as the eigenvalue sensitivity to intrinsic physical mechanisms [49,161], i.e., the perturbation operator of the eigenvalue sensitivity formula (101) is the Jacobian itself (Eq. (53a)), i.e., $\delta \mathbf{P} = \mathbf{L}$ for nontime-delayed systems. This enables us to identify the regions of the flow where the hydrodynamic and acoustic subsystems are active and quantify how they affect the overall thermoacoustic stability. When the mean flow is a fixed point of the equations, the real part of Eq. (101) provides a map showing the regions to which the thermoacoustic stability is most sensitive to the j th variable through the i th equation. Likewise, the imaginary part of Eq. (101) shows the regions to which the thermoacoustic angular frequency is most sensitive.

3.4 Adjoint Methods Versus Finite Difference. On one hand, to calculate the first-order eigenvalue drift, σ_1 , with a traditional finite difference approach, the eigenproblem is solved for each parameter's perturbation, which is computationally costly if the number of parameters is larger than the number of quantities of interest, in this case being the eigenvalues. On the other hand, with adjoint sensitivity analysis, only the unperturbed eigenproblem and its adjoint are solved to obtain σ_1 , regardless of the number of parameters being perturbed. Therefore, if one is interested in the first-order sensitivity of one eigenvalue to, say, one million parameters, finite difference methods would require solving one million eigenproblems, whereas adjoint methods would require solving only one eigenproblem and its adjoint.

3.5 Example of Continuous Adjoint Equations of a Thermoacoustic Network. The adjoint of a thermoacoustic network solved with a wave approach is derived by a continuous adjoint (CA) approach, whereas the adjoint of the multiple-scale model is derived by a discrete adjoint (DA) approach (Sec. 4.4).

The adjoint variables for the governing equations (19) are defined as $\hat{\rho}^+(x)$, $\hat{u}^+(x)$, $\hat{p}^+(x)$, whereas the adjoint variables for the jump conditions (28) are defined as \hat{f}^+ , \hat{g}^+ , \hat{h} . More details can be found in Ref. [162]. Integration by parts of Green's identity (62) yields the continuous adjoint equations

$$-\sigma^* \hat{\rho}^+ + \bar{u} \frac{d\hat{\rho}^+}{dx} = 0 \quad (102a)$$

$$-\sigma^* \bar{\rho} \hat{u}^+ + \bar{\rho} \bar{u} \frac{d\hat{u}^+}{dx} + \bar{\rho} \frac{d\hat{\rho}^+}{dx} + \gamma \bar{p} \frac{d\hat{p}^+}{dx} = 0 \quad (102b)$$

$$-\sigma^* \hat{p}^+ + \bar{u} \frac{d\hat{p}^+}{dx} + \frac{d\hat{u}^+}{dx} = 0 \quad (102c)$$

the relationships between adjoint variables

$$\hat{f}^+ = \hat{\rho}^+(x_f^+) - \bar{u}_d \hat{u}^+(x_f^+) + \frac{1}{2}(\gamma - 1) \bar{u}_d^2 \hat{p}^+(x_f^+) \quad (103a)$$

$$\hat{g}^+ = \hat{u}^+(x_f^+) - (\gamma - 1) \bar{u}_d \hat{p}^+(x_f^+) \quad (103b)$$

$$\hat{h}^+ = (\gamma - 1) \hat{p}^+(x_f^+) \quad (103c)$$

and the adjoint jump conditions

$$\begin{aligned} & \left[\hat{\rho}^+ - \bar{u} \hat{u}^+ + \frac{1}{2}(\gamma - 1) \bar{u}^2 \hat{p}^+ \right]_{x_f^-}^{x_f^+} \\ &= -(\bar{c}_u^2 - \bar{u}_u^2) \hat{u}_s^+ - \frac{1}{2}(\gamma + 1) \bar{u}_u^2 \hat{q}_s^+ \end{aligned} \quad (104a)$$

$$[\hat{u}^+ - (\gamma - 1) \bar{u} \hat{p}^+]_{x_f^-}^{x_f^+} = \gamma \bar{u} \hat{q}_s^+ \quad (104b)$$

$$[\hat{p}^+]_{x_f^-}^{x_f^+} = -\hat{q}_s^+ \quad (104c)$$

where

$$\hat{u}_s^+ = \hat{a}_u^+ + \left(\frac{\bar{\rho}_d - \bar{\rho}_u}{\gamma - 1} + \frac{1}{2} \bar{\rho}_u \bar{u}_u (\bar{u}_d - \bar{u}_u) \right) \hat{a}_2^+ \quad (104d)$$

$$\hat{q}_s^+ = (\bar{q} \hat{a}_1^+ - \hat{u}_s^+) n e^{-\sigma^* \tau} \quad (104e)$$

$$\begin{aligned} \hat{a}_1^+ &= \frac{(\bar{\rho}_d - \bar{\rho}_u)}{\bar{\rho}_u (\bar{c}_u^2 - \bar{u}_u^2)} \\ &\times \left(\hat{\rho}^+(x_f^+) - \bar{u}_d \hat{u}^+(x_f^+) + \frac{1}{2}(\gamma - 1) \bar{u}_d^2 \hat{p}^+(x_f^+) \right) \end{aligned} \quad (104f)$$

$$\hat{a}_2^+ = \frac{(\gamma - 1) \hat{p}^+(x_f^+)}{\bar{\rho}_u (\bar{c}_u^2 - \bar{u}_u^2)} \quad (104g)$$

where \hat{q}' was modeled with an $n - \tau$ model (Eq. (51)). The term \hat{u}_s^+ is the adjoint flame speed in the lab frame of reference. Physically, it provides the response of the thermoacoustic mode to harmonic forcing of the flame speed. The adjoint boundary conditions are defined such that the boundary terms are zero

$$\hat{\rho}^{+\ast} \bar{u} \hat{p} + \hat{p}^{+\ast} \bar{\rho} \hat{u} + \hat{u}^{+\ast} \bar{\rho} \bar{u} \hat{u} + \hat{u}^{+\ast} \hat{p} + \hat{p}^{+\ast} \bar{u} \hat{p} + \hat{p}^{+\ast} \gamma \bar{p} \hat{u} = 0 \quad (105)$$

As shown by Aguilar et al. [162], the set of adjoint partial differential equations is hyperbolic: Two adjoint acoustic waves propagate at speeds $\bar{c} + \bar{u}$ and $\bar{c} - \bar{u}$ and an adjoint entropy wave convects at the mean speed \bar{u} . The flame and frequency-dependent boundary conditions make the system nonself-adjoint. Equation (105) provides the upstream adjoint reflection coefficient relationship at the inlet

$$R_u^+ = \frac{1}{R_u^*} \frac{1 - M_u}{1 + M_u} \quad (106)$$

Therefore, the upstream adjoint boundary condition reads

$$G_u^+ = R_u^{+\ast -1} F_u^+ e^{-\sigma^* \tau_u} \quad (107)$$

Owing to the acceleration through the choked end, the entropy wave generates an acoustic disturbance, whereas the downstream acoustic wave does not generate an entropy wave. In the adjoint problem, however, the outgoing adjoint acoustic wave at the

choked end creates both a backward adjoint acoustic wave and a backward adjoint entropy wave. This is because the direct equations propagate quantities forward in time, while the adjoint equations propagate receptivities backward in time. Equation (105) provides the reflection coefficient relationships at the outlet

$$R_d^+ = \frac{1}{R_d} \frac{1 + M_d}{1 - M_d} \quad (108)$$

$$R_e^+ = \frac{1}{R_e} \frac{M_d}{2(M_d - 1)} \quad (109)$$

Finally, with these expressions, the downstream adjoint boundary conditions are obtained

$$F_d^+ = R_d^{+-1} G_d^+ e^{-s^* \tau_d} \quad (110)$$

$$A_d^+ = R_e^{+-1} G_d^+ e^{-s^* \tau_e} \quad (111)$$

As explained in Ref. [162], the receptivity to the mass equation, used to compute the corresponding feedback mechanisms, is given by $\hat{\rho}^+(x) + \bar{c}^2 \hat{p}^+(x)$. In the same reference, the discrete adjoint equations can be found.

4 Thermoacoustic Models With Multiple Scales

A more general thermoacoustic stability model was proposed by multiple-scale analysis [161]. By multiple-scale analysis, it is possible to simulate the hydrodynamic field and consistently calculate the heat release rate from the chemistry equations. The main assumption of this approach is that the flame is smaller (but not compact) with respect to the acoustic spatial scale. The reacting low-Mach number equations, which govern hydrodynamic phenomena, are coupled with the acoustic equations in a mathematically consistent manner by combining an asymptotic approach with a multiple-scale method. The two perturbation parameters are the hydrodynamic Mach number, $\bar{M} \sim O(\varepsilon)$ and the flame compactness, $\tilde{h}/\tilde{L} \sim O(\varepsilon^m)$, where $0 < \varepsilon \ll 1$, where \tilde{h} is the flame length or shear-layer thickness and \tilde{L} is the combustor longitudinal dimension. The Mach number is the smallest perturbation parameter; hence, $0 \leq m \leq 1$. In most gas turbine chambers, acoustic phenomena evolve at scales that are different from those of hydrodynamic phenomena. This is because low-frequency thermoacoustic instabilities are expected to scale with the longitudinal length, \tilde{L} , whereas hydrodynamic instabilities are expected to scale with the flame length or shear-layer thickness, \tilde{h} . Observing that (i) hydrodynamic phenomena scale with the convective time, \tilde{h}/\tilde{u} , and the flame length, \tilde{h} ; (ii) acoustic phenomena scale with the acoustic time, \tilde{L}/\tilde{c} , and combustor's length, \tilde{L} , it follows that $t_{\text{hyd}}/t_{\text{ac}} = \bar{M}\tilde{L}/\tilde{h} = \varepsilon^{1-m}$ and $x_{\text{hyd},i}/x_{\text{ac},i} = \tilde{L}/\tilde{h} = \varepsilon^{-m}$. t_{hyd} is the hydrodynamic time, t_{ac} is the acoustic time, x_{hyd} are the hydrodynamic spatial coordinates, and x_{ac} are acoustic spatial coordinates. High-frequency transverse instabilities are not considered in this multiple-scale analysis.

To reduce the complexity and separate out hydrodynamic and acoustic phenomena from the original equations (3), the following procedure is carried out:

- (i) Asymptotic expansion: The variables are expanded assuming a low-Mach number decomposition of the form $\phi = \sum_i \varepsilon^i \phi_i$, where ϕ denotes a generic variable.
- (ii) Differential operator's decomposition: In the double-time-double-space approach (2T-2S), $\phi(\mathbf{x}, t) \rightarrow \phi(\mathbf{x}_{\text{hyd}}, \mathbf{x}_{\text{ac}}, t_{\text{hyd}}, t_{\text{ac}})$. By applying the chain rule, both the temporal and spatial derivatives are decomposed as $\partial/\partial t \rightarrow \partial/\partial t_{\text{ac}} + \varepsilon^{1-m} \partial/\partial t_{\text{hyd}}$, and $\nabla \rightarrow \nabla_{\text{hyd}} + \varepsilon^m \nabla_{\text{ac}}$. In the double-time-single-space approach (2T-1S), $\phi(\mathbf{x}, t) \rightarrow \phi(\mathbf{x}, t_{\text{hyd}}, t_{\text{ac}})$ and only the temporal derivative is decomposed as $\partial/\partial t \rightarrow \partial/\partial t_{\text{ac}} + \varepsilon^{1-m} \partial/\partial t_{\text{hyd}}$. In the single-time-double-space approach (1T-2S), $\phi(\mathbf{x}, t) \rightarrow$

$\phi(\mathbf{x}_{\text{hyd}}, \mathbf{x}_{\text{ac}}, t)$ and only the spatial derivative is decomposed as $\nabla \rightarrow \nabla_{\text{hyd}} + \varepsilon^m \nabla_{\text{ac}}$.

- (iii) Order-by-order matching: New equations are defined by collecting terms in order of ε .
- (iv) Average-plus-fluctuation decomposition and equation averaging: In 2T-2S, the time decomposition $\phi = \langle \phi \rangle_{\text{ac}} + \phi'_{\text{ac}}$ is substituted into the operator presented in (ii) and the equations are time averaged over the slow hydrodynamic time scale t_{hyd} . The angle brackets $\langle \cdot \rangle_{\text{ac}}$ represent the time average of the fast variable, t_{ac} , the superscript ' represents the small fluctuation. Then, the variables are split as $\phi = \langle \phi \rangle_{\text{hyd}} + \phi'_{\text{hyd}}$, and the equations are spatially averaged over the long acoustic spatial scale \mathbf{x}_{ac} . The angle brackets $\langle \cdot \rangle_{\text{hyd}}$ represent the spatial average of the short spatial variable \mathbf{x}_{hyd} . In 2T-1S, only the time decomposition and averaging is applied. In 1T-2S, only the spatial decomposition and averaging is applied.

Regardless of the limit used, the above four steps lead to a nonlinearly coupled set of low-Mach number and acoustic equations, which are explained in Secs. 4.1 and 4.2.

4.1 Low-Mach Number Equations. Hydrodynamic phenomena are governed by the continuity, momentum, energy, and mixture-fraction low-Mach number equations for constant pressure flames [192]

$$\frac{\partial \rho}{\partial t_{\text{hyd}}} + \nabla_{\text{hyd}} \cdot (\rho \mathbf{u}) = 0 \quad (112)$$

$$\frac{\partial \mathbf{u}}{\partial t_{\text{hyd}}} + \mathbf{u} \cdot \nabla_{\text{hyd}} \mathbf{u} + \frac{1}{\gamma \rho} \nabla_{\text{hyd}} p - \frac{1}{S_1 \text{Re} \rho} \nabla_{\text{hyd}} \cdot \boldsymbol{\tau} = F_{\text{ac} \rightarrow \text{hyd}} \quad (113)$$

$$\frac{\partial T}{\partial t_{\text{hyd}}} + \mathbf{u} \cdot \nabla_{\text{hyd}} T - \frac{1}{S_1 \text{Re} \text{Pr} \rho} \Delta_{\text{hyd}} T - \text{Da} Q_R = 0 \quad (114)$$

$$\frac{\partial Z}{\partial t_{\text{hyd}}} + \mathbf{u} \cdot \nabla_{\text{hyd}} Z - \frac{1}{S_1 \text{Re} \text{Sc} \rho} \Delta_{\text{hyd}} Z = 0 \quad (115)$$

where the spatial gradient ∇_{hyd} acts on the hydrodynamic spatial scale, \mathbf{x}_{hyd} . Da is the Damköhler number, Sc is the Schmidt number, S_1 is the oxidizer-to-fuel density ratio of the jet, Pr is the Prandtl number, and Q_R is the rate of heat released by reaction as nondimensionalized in Ref. [161]. The state equation is $\rho [(S_1 - 1)Z + 1][(S_2 - 1)T + 1] = 1$, where S_2 is the ratio between the adiabatic flame temperature and the ambient temperature. The state equation shows that the thermodynamic pressure is constant and equal to unity when nondimensionalized. This nonlinear problem can be conveniently expressed in matrix form as $\dot{\mathbf{q}}_{\text{hyd}} - \mathbf{H}(\mathbf{q}_{\text{hyd}}) = \mathbf{F}(\mathbf{q})_{\text{ac} \rightarrow \text{hyd}}$, where $\mathbf{q}_{\text{hyd}} = (\rho, \mathbf{u}, T, Z)^T$ is the vector of the hydrodynamic variables; $\dot{\mathbf{q}}_{\text{hyd}} = \partial \mathbf{q}_{\text{hyd}} / \partial t_{\text{hyd}}$; $\mathbf{q} = (\mathbf{q}_{\text{hyd}}, \mathbf{q}_{\text{ac}})^T$, with \mathbf{q}_{ac} being the vector of the acoustic variables (Sec. 4.2); and $\mathbf{F}_{\text{ac} \rightarrow \text{hyd}} = (0, F_{\text{ac} \rightarrow \text{hyd}}, 0, 0)^T$ is the vector of forcing terms (Table 2). The hydrodynamic operator, \mathbf{H} , is nonlinear because of the convective derivatives and reaction term.

4.2 Acoustics. The acoustic variables are governed by the continuity, momentum, and energy equations

$$\frac{\partial \rho'_{\text{ac}}}{\partial t_{\text{ac}}} + \nabla_{\text{ac}} \cdot (\langle \rho \rangle_{\text{hyd}} \mathbf{u}'_{\text{ac}}) = F_{\text{hyd} \rightarrow \text{ac}_{\text{con}}} \quad (116)$$

$$\frac{\partial \mathbf{u}'_{\text{ac}}}{\partial t_{\text{ac}}} + \frac{1}{\gamma \langle \rho \rangle_{\text{hyd}}} \nabla_{\text{ac}} P'_{\text{ac}} = F_{\text{hyd} \rightarrow \text{ac}_{\text{mom}}} \quad (117)$$

$$\frac{\partial p'_{\text{ac}}}{\partial t_{\text{ac}}} + \gamma \nabla_{\text{ac}} \cdot \mathbf{u}'_{\text{ac}} = F_{\text{hyd} \rightarrow \text{ac}_{\text{en}}} \quad (118)$$

Table 2 Terms coupling hydrodynamics to acoustics, hyd → ac, and acoustics to hydrodynamics, ac → hyd

	2T-2S	2T-1S	1T-2S
$F_{\text{hyd} \rightarrow \text{ac}_{\text{con}}}$	$-\nabla_{\text{ac}} \cdot (\langle \rho \rangle_{\text{hyd}} \langle \mathbf{u}'_{\text{ac}} \rangle_{\text{hyd}} + \langle \rho'_{\text{hyd}} \mathbf{u}'_{\text{hyd}} \rangle_{\text{hyd}})$	0	$-\nabla_{\text{ac}} \cdot (\langle \rho'_{\text{hyd}} \mathbf{u}'_{\text{hyd}} \rangle_{\text{hyd}})$
$F_{\text{hyd} \rightarrow \text{ac}_{\text{mom}}}$	0	0	$-1/\langle \rho \rangle_{\text{hyd}} \partial / \partial t_{\text{hyd}} \langle \rho'_{\text{hyd}} \mathbf{u}'_{\text{hyd}} \rangle_{\text{hyd}}$
$F_{\text{hyd} \rightarrow \text{ac}_{\text{en}}}$	$-\gamma \langle \nabla_{\text{ac}} \cdot \mathbf{u} \rangle_{\text{hyd}}$	$Da Q'_{R0,\text{ac}}$	$Da \langle Q_{R1} \rangle_{\text{hyd}}$
$F_{\text{ac} \rightarrow \text{hyd}}$	$-1/\rho \nabla_{\text{hyd}} \cdot \langle \rho \mathbf{u}'_{\text{ac}} \otimes \mathbf{u}'_{\text{ac}} \rangle_{\text{ac}}$	$-1/\rho \nabla_{\text{hyd}} \cdot \langle \rho \mathbf{u}'_{\text{ac}} \otimes \mathbf{u}'_{\text{ac}} \rangle_{\text{ac}}$	$-1/(\gamma \rho) \nabla_{\text{ac}} p'_{\text{ac}}$

Note: These terms depend on the multiple-scale limit: Double-time-double-space (2T-2S), double-time-single-space (2T-1S) and single-time-double-space (1T-2S). In 2T-1S $\mathbf{x}_{\text{hyd}} = \mathbf{x}_{\text{ac}}$, in 1T-2S $t_{\text{hyd}} = t_{\text{ac}}$. The numbers in the subscripts of Q_{R0} and Q_{R1} refer to the orders of the heat-release asymptotic expansion. Adapted from Ref. [161].

where the spatial gradient ∇_{ac} acts on the acoustic spatial scale, \mathbf{x}_{ac} . The variables are nondimensionalized as in Ref. [161]. This problem can be expressed as $\dot{\mathbf{q}}_{\text{ac}} - \mathbf{A}\mathbf{q}_{\text{ac}} = \mathbf{F}(\mathbf{q})_{\text{hyd} \rightarrow \text{ac}}$, where $\mathbf{q}_{\text{ac}} = (\rho'_{\text{ac}}, \mathbf{u}'_{\text{ac}}, p'_{\text{ac}})^T$ is the vector of the acoustic variables; $\dot{\mathbf{q}}_{\text{ac}} = \partial \mathbf{q}_{\text{ac}} / \partial t_{\text{ac}}$; and $\mathbf{F}_{\text{hyd} \rightarrow \text{ac}} = (F_{\text{hyd} \rightarrow \text{ac}_{\text{con}}}, F_{\text{hyd} \rightarrow \text{ac}_{\text{mom}}}, F_{\text{hyd} \rightarrow \text{ac}_{\text{en}}})^T$ is the vector of forcing terms. The acoustic operator, \mathbf{A} , is linear. The nonlinearities are contained in the forcing term. State and mixture fraction equations (not shown) are required for the calculation of the heat-release terms in 2T-1S and 1T-2S (Sec. 4.3).

The acoustics dissipates mainly by radiation from the combustor's open boundaries and slightly in the viscous-thermal boundary layer. Nonlinear damping effects, such as vortex roll-up at sharp changes to the cross-sectional area, are not included in the current study because this study focuses on the stability of infinitesimal perturbations. In this asymptotic analysis, acoustic dissipation in the viscous-thermal boundary layer is neglected because of its being of higher order. Physically, the acoustic viscous terms are negligible because (i) when the acoustic time is faster than the hydrodynamic time, the acoustic Reynolds number is very large and (ii) when the acoustic scale is longer than the hydrodynamics, the boundary layer scale is negligible. However, near the wall, these terms may be important and need modeling. Therefore, the viscous-thermal acoustic dissipation is modeled as a sink term in the acoustic energy equation proportional to p'_{ac} , in a similar manner to Ref. [280]. The acoustic radiation should be modeled by impedance boundary conditions, which makes the final eigenproblem nonlinear in the eigenvalue (Sec. 3.1.2).

4.3 Two-Way Coupling Terms. The terms coupling the hydrodynamics to the acoustics depend on the multiple-scale limit considered (Table 2). Here, comments are made on the terms that are most relevant to thermoacoustics. On one hand, the hydrodynamics is an acoustic energy source through the spatially averaged dilation of the flow in the 2T-2S limit, which acts as a dipole-like source. This tends to the classic unsteady heat release in the 2T-1S and 1T-2S limits, which acts as a monopole-like source (second to last row in Table 2). Physically, the unsteady heat release only partly contributes to the acoustic energy input in the 2T-2S limit. (The unsteady heat release is calculated by using the acoustic density, temperature, and mixture-fraction equations.) On the other hand, the acoustics forces the hydrodynamic momentum via the nonlinear term $-1/\rho \nabla_{\text{hyd}} \cdot \langle \rho \mathbf{u}'_{\text{ac}} \otimes \mathbf{u}'_{\text{ac}} \rangle_{\text{ac}}$ in the double space limits (2T-2S and 1T-2S, last row in Table 2). This term is known as the acoustic Reynolds stress [281], which, as opposed to the turbulent Reynolds stress, does not require closure because it is obtained from the acoustic solver. In the 1T-2S limit, the hydrodynamic momentum is forced through the acoustic pressure gradient that imposes a global acceleration.

In compact form, the coupled thermoacoustic problem (Fig. 6), governed by Eqs. (112)–(118), reads

$$\dot{\mathbf{q}} - \mathbf{T}(\mathbf{q}) = \mathbf{F} \quad (119)$$

where $\mathbf{T}(\mathbf{q})$ is the nonlinear thermoacoustic operator, and $\mathbf{F} = (\mathbf{F}_{\text{ac} \rightarrow \text{hyd}}, \mathbf{F}_{\text{hyd} \rightarrow \text{ac}})^T$.

4.3.1 Linearization. The linearization of the multiple-scale thermoacoustic model requires extra comments [161]. The hydrodynamic variables are assumed $\sim O(1)$ and the acoustic variables $\sim O(\varepsilon)$. Physically, the acoustics is regarded as a perturbation field on top of the hydrodynamic flow. Different multiple-scale limits spawn different linear behaviors. The hydrodynamic variables are split as $\mathbf{q}_{\text{hyd}} = \bar{\mathbf{q}}_{\text{hyd}} + \varepsilon \mathbf{q}_{\text{hyd},1}$, where $\bar{\mathbf{q}}_{\text{hyd}} \sim O(1)$ is the steady mean flow calculated from numerical simulations or experiments and $\varepsilon \mathbf{q}_{\text{hyd},1}$ is the low-frequency large-scale coherent hydrodynamic structure. Therefore, the perturbation hydrodynamic vector, $\mathbf{q}_{\text{hyd},1}$, and acoustic vector, \mathbf{q}_{ac} , are of the same order ε but act at different scales. When linearized, the thermoacoustic problem can be expressed in compact form as $\dot{\mathbf{q}} = \mathbf{L}\mathbf{q}$, where

$$\mathbf{L} = \begin{bmatrix} \left(\frac{\delta \mathbf{H}}{\delta \mathbf{q}_{\text{hyd}}} + \frac{\delta \mathbf{F}_{\text{ac} \rightarrow \text{hyd}}}{\delta \mathbf{q}_{\text{hyd}}} \right) & \frac{\delta \mathbf{F}_{\text{ac} \rightarrow \text{hyd}}}{\delta \mathbf{q}_{\text{ac}}} \\ \frac{\delta \mathbf{F}_{\text{hyd} \rightarrow \text{ac}}}{\delta \mathbf{q}_{\text{hyd}}} & \left(\mathbf{A} + \frac{\delta \mathbf{F}_{\text{hyd} \rightarrow \text{ac}}}{\delta \mathbf{q}_{\text{ac}}} \right) \end{bmatrix} \quad (120)$$

The Jacobian operator is the functional derivative of the thermoacoustic operator that is evaluated at the base flow $\bar{\mathbf{q}}_{\text{hyd}}$. In the double-time limits, 2T-2S and 2T-1S, the linearized acoustic Reynolds stress, which is the term coupling the acoustics to the hydrodynamics, is neglected because of higher order. The linear dynamics are only one-way coupled because the coupling term $\delta \mathbf{F}_{\text{ac} \rightarrow \text{hyd}} = O(\varepsilon^2)$ is negligible in Eq. (120). This is because, when there are two time scales (the acoustic time being faster than the convective time), the acoustics are driven by the hydrodynamics but do not affect it. Physically, the influence of the acoustics averages to zero over the long time scale of the hydrodynamics. This is equivalent to one of the mechanisms described by Lieuwen [187] in which, if one considers perturbations convecting at uniform speed along a long flame such that there are many oscillations along the flame, most of the heat release perturbations cancel out, causing the flame to behave as a low pass filter. From this two-scale argument, a thermoacoustic instability is more likely to exist when the time scales are the same. In a classic picture of a thermoacoustic instability, the two time scales are indeed the same [282]. In fact, when only one time scale is modeled, as in 1T-2S, the thermoacoustic system is two-way linearly coupled because $\delta \mathbf{F}_{\text{ac} \rightarrow \text{hyd}} = O(\varepsilon)$, i.e., there is a nontrivial interaction between hydrodynamic and thermoacoustic stability. By using modal transformations, the resulting direct thermoacoustic eigenproblem is linear and reads

$$\sigma \hat{\mathbf{q}} = \mathbf{L} \hat{\mathbf{q}} \quad (121)$$

4.4 Discrete Adjoint. The numerical discretization of Eq. (121) was performed by a finite element method [161], which is particularly convenient to calculate the adjoint system because the Jacobian is numerically available. The adjoint problem is obtained by taking the complex-conjugate transpose of Eq. (121)

$$\sigma^* \hat{\mathbf{q}}^+ = \mathbf{L}^H \hat{\mathbf{q}}^+ \quad (122)$$

Intrinsic sensitivity. The intrinsic sensitivity framework introduced in Sec. 3.3.5 is able to calculate the effect that a perturbation onto a subsystem has on the stability of the coupled system. The eigenvalue drift for an intrinsic perturbation $\varepsilon \mathbf{J}$ reads

$$\sigma_1 = \varepsilon \frac{\begin{bmatrix} \hat{\mathbf{q}}_{\text{hyd}}^{++}, \hat{\mathbf{q}}_{\text{ac}}^{++} \end{bmatrix} \begin{bmatrix} \text{Hyd.} & \text{Ac.} \rightarrow \text{Hyd.} \\ \text{Hyd.} \rightarrow \text{Ac.} & \text{Ac.} \end{bmatrix} \begin{bmatrix} \hat{\mathbf{q}}_{\text{hyd}} \\ \hat{\mathbf{q}}_{\text{ac}} \end{bmatrix}}{\langle \hat{\mathbf{q}}^+, \hat{\mathbf{q}} \rangle} \quad (123)$$

where the mathematical expressions of the boxed subsystems are provided in Eq. (120). For example, the exact first-order change of the thermoacoustic stability due to a perturbation applied to the acoustic subsystem that affects the hydrodynamic subsystem is $\sigma_1 = \varepsilon \hat{\mathbf{q}}_{\text{hyd}}^{++} \cdot \boxed{\text{Ac.} \rightarrow \text{Hyd.}} \hat{\mathbf{q}}_{\text{ac}} / \langle \hat{\mathbf{q}}^+, \hat{\mathbf{q}} \rangle$. As shown in Ref. [49], the physical cause of an intrinsic perturbation originates from weakly nonlinear interactions, which are listed in Ref. [283]. The small change induced by the nonlinear interactions is regarded as a local change in the underlying operator, which, at first approximation, is assumed proportional to the operator itself.

5 The Thermoacoustic Spectrum

The calculation of how eigenvalues change due to perturbations is the main subject of this review. It is, thus, important to gain insight on how the thermoacoustic spectrum changes with respect to the two key thermoacoustic parameters: The flame gain and time delay.

The configuration under investigation is a ducted flame [9] with a closed end at the inlet ($\partial \hat{p} / \partial x = 0$) and an open end at the outlet ($\hat{p} = 0$). The flame is placed at $x_f = 0.6$. As reported in Ref. [175], and rigorously shown in Ref. [284] with nondimensional analysis, the physical, qualitative behavior of the spectrum (Fig. 7) is general for longitudinal configurations. The computations were performed with a quasi-one-dimensional Helmholtz solver. For the operating point and other parameters, the reader may refer to Table 3 of Silva et al. [175].

The first acoustic mode is a quarter-wave mode of the duct with nondimensional angular frequency $\omega_{n,\tau=0} = 1$. Figure 7 shows the results of the parametric study by varying the flame gain as $n = [0 \rightarrow 1]$, and nondimensional time delay as $\tau = [0 \rightarrow 1]$. A spiral-like structure and curvilinear trajectories are observed. The center of the star is the acoustic mode. Once n is increased from zero, the eigenvalues depart from the acoustic mode. These trajectories rotate counter clockwise for increments of τ . Some trajectories protrude to the unstable semiplane when the flame gain is greater than a critical value.

Extreme sensitivity. The marginal trajectories connected to the acoustic mode and defined by $0.32 < \tau < 0.33$ change directions suddenly (from left to right when increasing τ) after a critical value $\tau \approx 0.325$. Such a behavior is a signature of extreme sensitivity of thermoacoustics: Physically, a small increment in the time delay may drastically change the stability of the combustor.

Intrinsic thermoacoustic modes. Figure 7 shows quasi-vertical trajectories, whose growth rate for small values of n is very negative and increases with n . The resonance angular frequency tends to $2\pi \cdot j/(2\tau)$ (with $j = 1, 3, 5, \dots$) and the growth rate to $-\infty$ when n approaches zero [193]. The angular frequency corresponds to ITA resonance frequencies [9,10]; therefore, these trajectories are labeled as ITA trajectories (in agreement with [285]). As shown in Ref. [175], the crossing from the unstable to the stable semiplane of the trajectories is a function of only the time delay.

Exceptional points. As thoroughly explained in Ref. [246], the set of parameters and the relevant eigenvalue at which intrinsic and acoustic modes cross each other are an *exceptional point*: The eigenvalue is a branch-point solution of the characteristic

function. The eigenvalue at this exceptional point is twofold defective, has *infinite sensitivity* to first-order perturbations, and the behavior in its neighborhood can be described by a Puiseux series.³⁵

6 Applications of Stability, Receptivity, and Sensitivity Analysis Without Uncertainty

The philosophy of SRS analysis of eigenvalues is summarized in Fig. 8. In Fig. 8(a), the large black circles represent the unperturbed eigenvalues. The flame modes are stable, whereas the acoustic modes protrude toward the unstable semiplane because of the thermoacoustic coupling. Together with the calculation of the corresponding eigenfunctions, this is the outcome of stability analysis. The smaller red circles represent the adjoint eigenvalues, which are the complex conjugate of the direct problem. The calculation of the corresponding adjoint eigenfunctions is the outcome of receptivity analysis. In Fig. 8(b), the eigenvalues slightly change due to a small perturbation to the system. The calculation of this change, in particular of the dominant eigenvalue(s) (Fig. 8(c)), is the outcome of sensitivity analysis. Stability, receptivity, and sensitivity analyses are presented and interpreted in this paper for different thermoacoustic problems and different perturbations. The exact calculation of the sensitivities to design parameters, external passive devices, and intrinsic perturbations, are presented in Secs. 6.2–6.4, respectively.

6.1 Direct and Adjoint Eigenfunctions. This section explains the physical meaning of the direct and adjoint eigenfunctions of open-ended duct acoustics with the heat release modeled by (i) an n - τ response model, (ii) a diffusion flame, and (iii) a premixed flame. The mean-flow Mach number is zero. The direct and adjoint mode shapes are shown in Fig. 9. The eigenfunction is the natural shape with which the system oscillates around the perturbed base state. To maximize observability, a sensor should be placed where the amplitude of the direct mode shape is larger. The adjoint eigenfunction is the receptivity to initial conditions or forcing to excite the corresponding eigenfunction. To maximize controllability, an actuator should be placed where the amplitude of the adjoint mode shape is larger.

First, the top row of Fig. 9 shows the acoustic velocity and pressure eigenfunctions, \hat{u} and \hat{p} , respectively, which are modeled with an n - τ model for the flame. The pressure is continuous, yet not smooth, at the flame's location, whereas the velocity undergoes a discontinuity (Fig. 9(a)). This is because of the jump conditions (28), which physically represent the volume dilation due to the heat released by the flame. Moreover, open ends are modeled as Dirichlet boundary conditions for \hat{p} , which become Neumann boundary conditions for \hat{u} , as seen from the momentum equation (19c) for a zero mean flow. The adjoint pressure, \hat{p}^+ , is the Lagrange multiplier of the energy equation; therefore, it is the receptivity to energy sources, such as heat inputs. It inherits the discontinuity at the heat source location from \hat{u} and the boundary conditions from \hat{p} . The adjoint velocity, \hat{u}^+ , is the Lagrange multiplier of the momentum equation; therefore, it is the receptivity to momentum sources, such as forces. The adjoint velocity is continuous, yet not smooth, at the flame's location.

In Figure 9(b), the eigenfunctions of the mixture fraction of a ducted diffusion flame are shown. The corresponding acoustic variables are similar to Fig. 9(a); therefore, they are not shown. The mixture fraction eigenfunction has a wavy pattern, which is typical of fluid dynamic phenomena that are governed by convection-diffusion processes. The white line is the steady-flame position that corresponds to the stoichiometric line. The adjoint mixture fraction has high magnitude around the flame. This is because species injection affects the heat release only if it changes the gradient of \hat{Z} at the flame itself, which is achieved by injecting species around the flame. Its magnitude increases toward the tip of the flame, where $\nabla \hat{Z}$ is weakest. From a practical point of

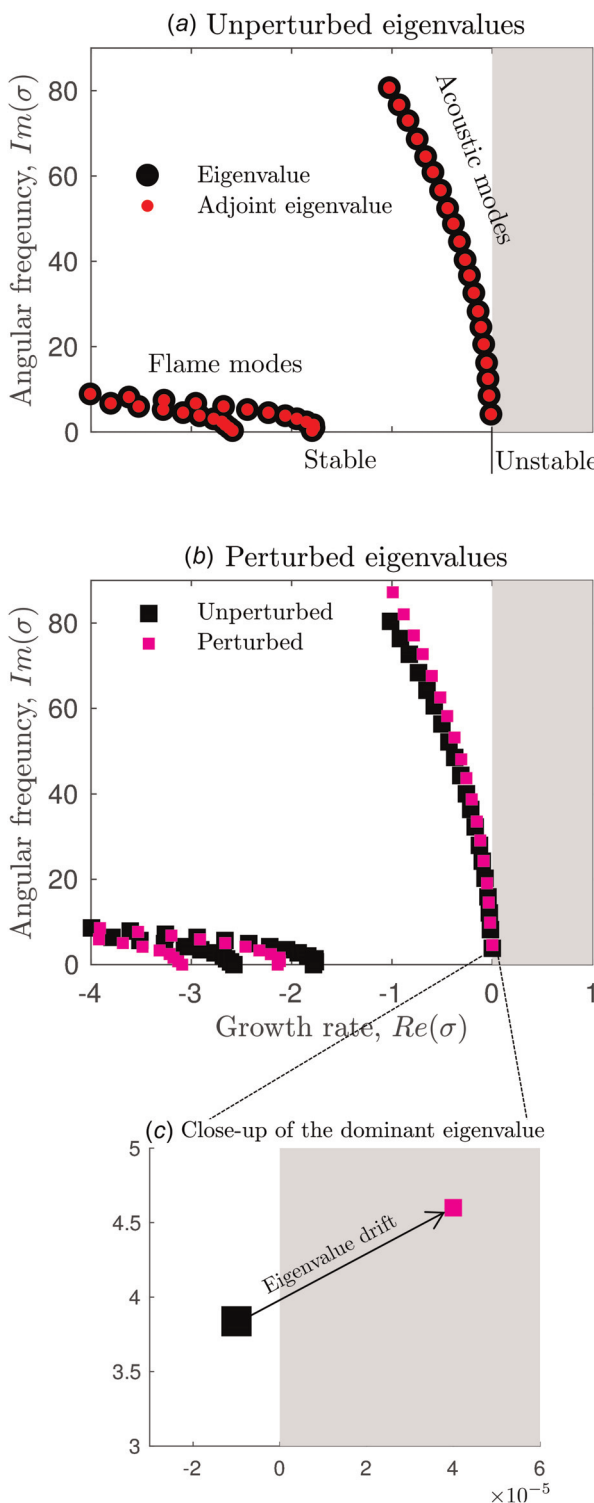


Fig. 8 (a) Spectrum and complex conjugate adjoint spectrum of a ducted flame (here a diffusion flame as an example). (b) Perturbed eigenvalues (small magenta squares) due to a small perturbation to the system. (c) The calculation of the eigenvalue shift is provided by sensitivity analysis.

view, this shows that open-loop control of the mixture fraction has little influence at the injection plane but great influence at the flame tip. In this case, this could be achieved by injecting species at the wall [158].

Finally, a ducted premixed case is considered in Fig. 9(c) [160]. The flame wrinkling is provided by the flame front eigenfunction,

\hat{f} , where the dashed line is the steady conical solution. The adjoint flame front can be used to calculate the sensitivities, as explained in Sec. 6.2. However, the physical interpretation of the adjoint flame front in terms of receptivity is difficult because the flame front is a kinematic quantity with the G-equation model.

6.1.1 Helmholtz Resonators. When the unsteady heat released by the flame is zero, the direct pressure is identical to the adjoint pressure, and the velocity is identical to the adjoint velocity (not shown), i.e., the acoustic system is self-adjoint. When the heat released by the flame is not zero, the direct and adjoint eigenfunctions are different from each other, i.e., the thermoacoustic system is non-self-adjoint. Nonself-adjointness may have an important consequence on the optimal placement of Helmholtz resonators, which are passive devices used in industry to suppress thermoacoustic instabilities [286–292]. Importantly, Helmholtz resonators are typically placed where $\hat{p}\hat{p}^*$ is maximal (see half-wave resonators, e.g., see Refs. [289] and [293]). For an open-ended tube, this condition occurs at the center of the tube. However, in a system that is not self-adjoint, this is not exactly the linearly optimal location because, albeit the pressure is maximum around the center of the tube, the system is more receptive before the flame's location. Therefore, the best location to place the Helmholtz resonator is where the amplitude of $\hat{p}\hat{p}^{+*}$ is maximum, which, in this case, is slightly upstream of the center of the tube (Fig. 9(a)).

6.2 Sensitivity to Design Parameters. The direct and adjoint eigenfunctions of the open-ended duct of Sec. 6.1 are combined to obtain the sensitivity of the most unstable eigenvalue to small changes to some design parameters (Sec. 3.3), where the heat release is modeled by (i) an $n\tau$ flame response, (ii) a diffusion flame, and (iii) a premixed flame.

First, the case of the $n\tau$ model is considered. The sensitivities are depicted in Fig. 10(a) as functions of the flame position. Any small increase from -1 in the reflection coefficients, R_u and R_d , makes the system more stable because less acoustic energy is reflected back into the tube. The sensitivity to the interaction index, n , has the smallest amplitude and shows that a second heat source in the second half of the duct will stabilize the system. However, the sensitivity to the time delay, τ , has a great impact on the eigenvalue drift. An increase in the time delay destabilizes the system if the flame is located in the first half of the duct before ≈ 0.4 [162].

Second, in Fig. 10(b), the sensitivities of a ducted diffusion flame are shown as functions of the stoichiometric mixture fraction, Z_{sto} , and the ratio between the fuel slot and the diameter of the duct, α . When Z_{sto} and α are perturbed, \bar{Z} changes, which, in turn, changes the steady flame shape; hence, the phase between the acoustic pressure and the heat release. The flame length increases as Z_{sto} increases and as α decreases [158]. The sensitivities depend strongly on Z_{sto} and α but are similar at similar values of the flame length.

Third, the eigenvalue sensitivities to the aspect ratio and acoustic location of a ducted premixed flame are shown in Fig. 10(c). For fixed mean-flow velocity and disturbance phase velocity, the time delay in a premixed flame is proportional to the flame length. In this case, the sensitivity is discontinuous across the white lines, where, as shown by Orchini and Juniper [160], the second eigenvalue becomes unstable (or vice versa).

These maps accurately quantify the first-order change in the thermoacoustic stability due to changes of the design parameters. This information can be used for the design of stable combustors to prevent instabilities from occurring. If the technologist wishes to suppress an existing instability, Sec. 6.3 shows how to implement adjoint techniques for passive control with external devices.

6.2.1 Experimental Validation. Rigas et al. [155] carried out experiments to validate some of the sensitivities obtained by adjoint-based analysis. They set up an open-ended vertical Rijke tube with a main electrical heater, which consisted of a gauze of

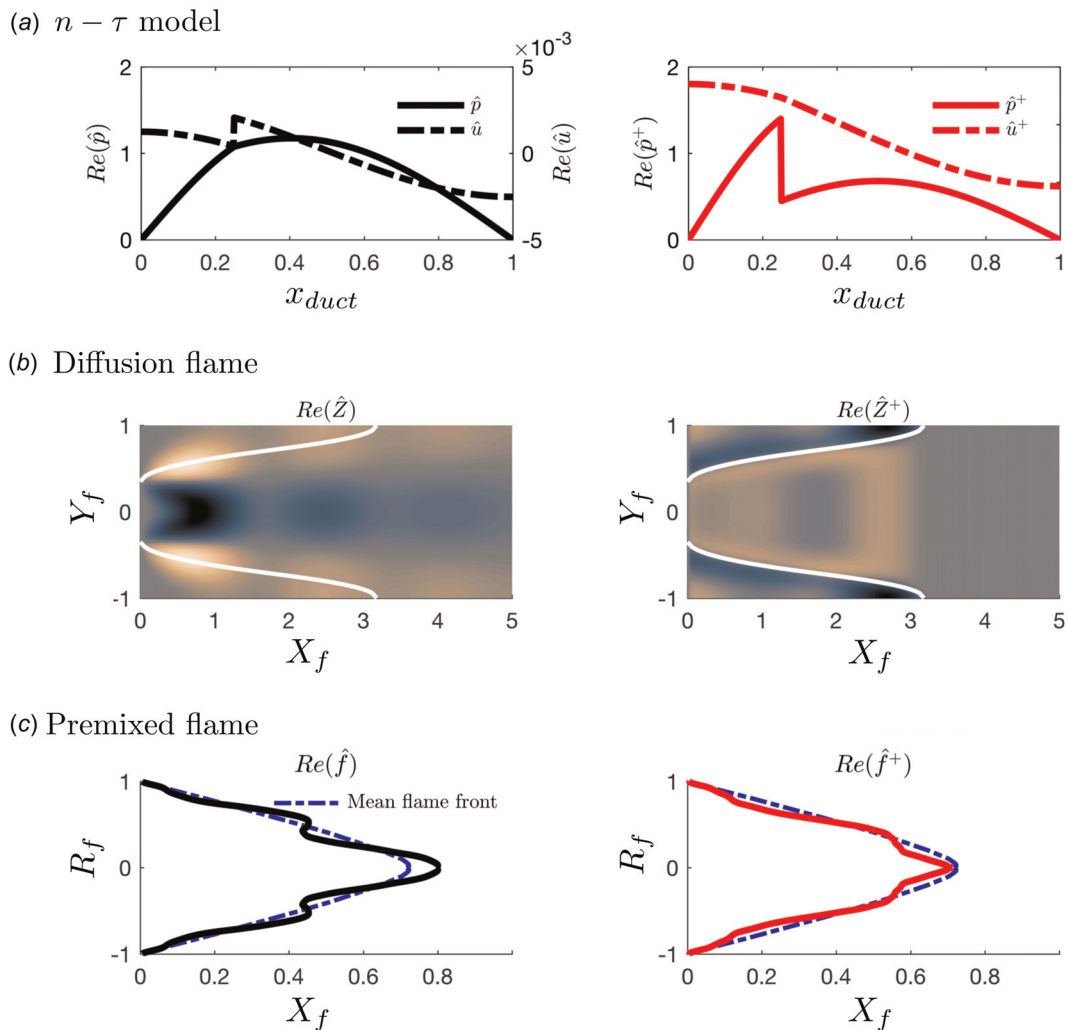


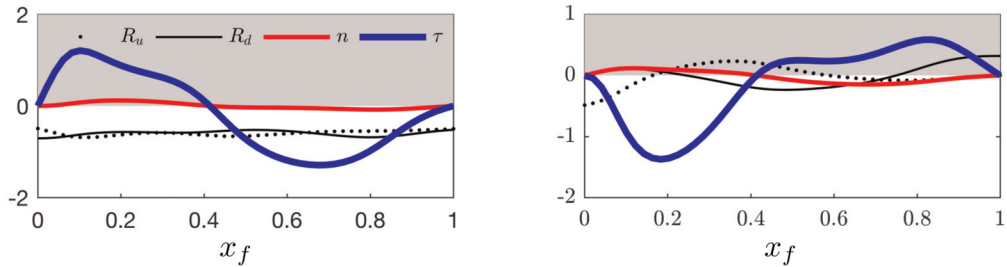
Fig. 9 Direct eigenfunctions (left columns) and adjoint eigenfunctions (right column) for acoustic variables (top row, adapted from Ref. [162] with permission from Elsevier, x_{duct} is the nondimensional axial coordinate of the duct), a diffusion flame (middle row, adapted from Ref. [158] with permission, light/dark colors correspond to positive/negative values), and a premixed flame (bottom row, data are courtesy of Orchini and Juniper [160]) in an open-ended duct with no mean flow. The direct eigenfunctions are the thermoacoustic modes with which the system linearly vibrates. The adjoint eigenfunctions are the receptivity of the system to open-loop sources in the equations. The nondimensional factors of the flame coordinates can be found in Refs. [158] and [160].

wires placed at a quarter from the inlet. When the electrical power was larger than the damping, the first acoustic mode became unstable. The system exhibited hysteresis as the main power was increased/decreased (subcritical bifurcation). A second mesh of wires was used as a passive drag device with no power input. This device was attached to an automated height gauge at the top of the tube, which enabled it to be transversed with high accuracy. The raw pressure signal was sampled at high frequency with a condenser-type microphone. To obtain the growth rates and frequencies after the insertion of the drag device, the main heater power was set just below that of the Hopf point, i.e., where the system is linearly marginally stable. The system was then increased to the critical power with a step function. On one hand, the growth rate was calculated as the slope of the logarithmic linear region of the absolute value of the Hilbert-transformed signal. On the other hand, the frequency was calculated as the mean of the time derivative of the phase in the logarithmic linear region of the Hilbert-transformed signal. To measure the decay rate, the main heater power was initially set just above the fold point, i.e., the first operating point in the hysteresis region at which the system has both a fixed point and a limit-cycle solution. The power

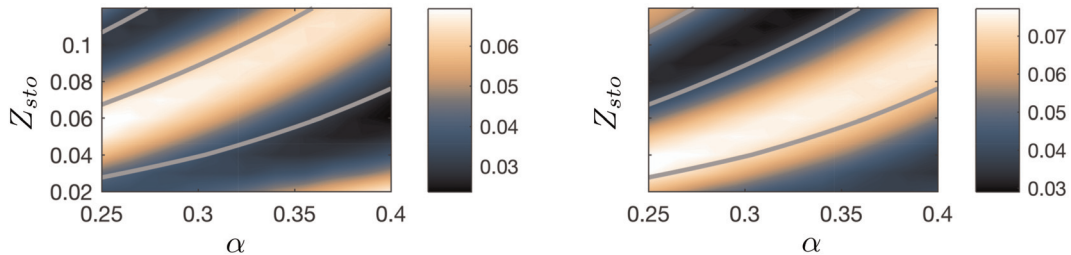
was then decreased as a step function; the growth rate and frequency were measured as before. The sensitivity was calculated by finite difference between the experiments with/without drag device.

Figure 11 shows the experimental growth-rate sensitivities (circles) and the corresponding predictions from adjoint-based sensitivity analysis (black line), which are normalized by their inlet value for a better comparison. The prediction is in favorable agreement with the experimental data. The discrepancy toward the outlet is expected to be due to wall heat transfer and boundary conditions, which were not modeled. In general, the predictions from sensitivity analysis are as good as the physical model adopted. Discrepancies with experimental data are due to the working assumptions made for the thermoacoustic model, not adjoint analysis. The experimental frequency drift was compared in Refs. [156] and [294] with the predictions from adjoint sensitivity analysis. They found that adjoint-based frequency sensitivity was not satisfactorily in agreement with the experimental shift. This was due to the fact that the experiment had more complex physics than that captured by the model, for example, strong mean flow temperature gradients were present in the experiment but not

(a) $n - \tau$ model



(b) Diffusion flame



(c) Premixed flame

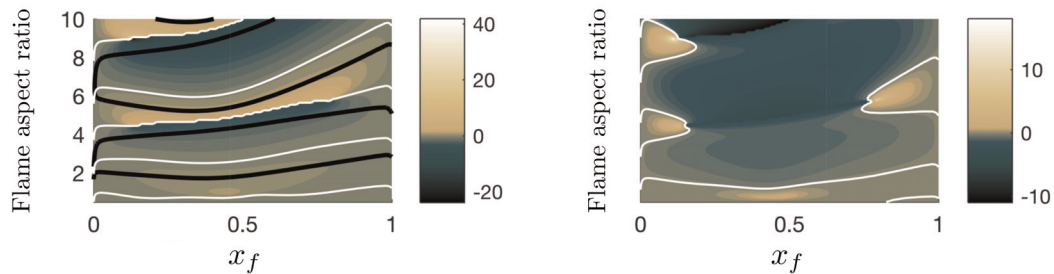


Fig. 10 Growth-rate (left column) and angular-frequency (right column) sensitivity. Top row: Sensitivities to the upstream (downstream) reflection coefficients, R_u (R_d), the flame index, n and time delay, τ , of a ducted flame for different positions of the flame's location (adapted from Ref. [162] with permission from Elsevier). Middle row: Sensitivities to the design parameters α (fuel-to-air port ratio) and Z_{sto} of a ducted diffusion flame with the steady-flame length contours superimposed (values from 4 to 2 from bottom to top) (adapted from Ref. [158] with permission). Bottom row: Sensitivities to the flame aspect ratio and flame location of a ducted premixed flame. The maxima are marked by white lines, the minima are marked by black lines (Left: Reprinted with permission from Elsevier [160], Right: Data are courtesy of A. Orchini).

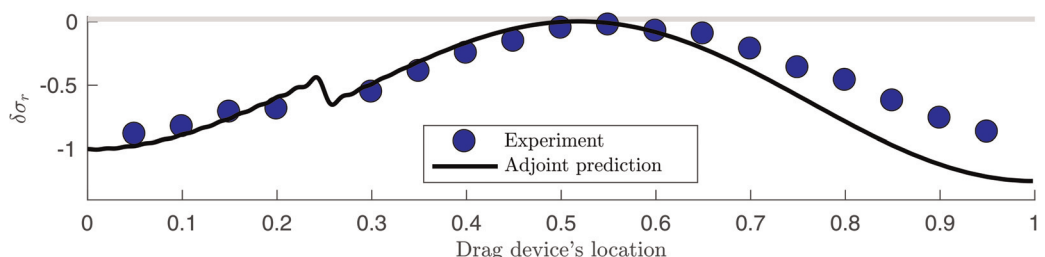


Fig. 11 Growth-rate drift due to the insertion of a drag device. The heat source is located at $x_f = 0.25$. Adjoint predictions (solid line) against experimental results (circles, data are courtesy of Ref. [155]) normalized for comparison.

in the model. This can be explained by observing that the eigenvalue is, at a first approximation, a function of the main-heater power, P , the velocity at the drag device location, x_c , and the mean-flow temperature, i.e.,

$$\sigma = \sigma(P, \bar{U}(x_c), \bar{T}(x_c)) \quad (124)$$

Interestingly, the mean-flow temperature is a function of the position of the drag device, x_c , because after insertion of it the flow

slows down and the heat transfer decreases, accordingly. Therefore, the temperature and the velocity are dependent variables, i.e., $\bar{T} = \bar{T}(\bar{U}(x_c))$. The total derivative of the eigenvalue with respect to a variation of the velocity caused by the drag device reads

$$\frac{d\sigma}{d\bar{U}} = \frac{\partial\sigma}{\partial\bar{U}} + \frac{\partial\sigma}{\partial\bar{T}} \frac{d\bar{T}}{d\bar{U}} \quad (125)$$

Jamieson et al. [156,157,294] experimentally measured the total derivative (left-hand side of Eq. (125)) and compared it with the sensitivity ($\partial\sigma/\partial\bar{U}$) from adjoint-based sensitivity analysis [153] (the analysis of Ref. [153] was improved to include base-flow velocity perturbations by Aguilar [295]). The remaining term, $(\partial\sigma/\partial\bar{T})(d\bar{T}/d\bar{U})$, is a leading-order cause of the discrepancy, which is large because differences in the mean-flow temperature markedly affect the acoustic natural frequency but not the growth rate [158,197].

6.3 Sensitivity to Passive Devices. The case of a choked duct with a premixed flame modeled by an $n-\tau$ model, is considered. This case is particularly relevant to aero-engines, where the nozzle guide vane downstream of the combustor's exit is (nearly) sonic [296]. The inlet is an ideal open end, and the outlet choked condition is provided by Marble and Candel [213].

In a choked combustor, the mean flow cannot be neglected because the outlet is sonic; therefore, the acoustic density is one of the state variables (Fig. 12(c)). In the region upstream of the flame, the density (Fig. 12(c)) shows a similar behavior to the pressure, which is scaled by $1/\bar{c}_u^2$. However, downstream of the flame, the density contains the influence of both acoustic and entropy waves through Gibbs' relation (26). Small entropy inhomogeneities appear in the downstream region because the acoustic fluctuations change the temperature upstream, while the mean heat release is constant in this model [211]. The entropy spots are accelerated through the nozzle and converted into indirect acoustic waves. With a moving flame front, the indirect acoustic wave is only $\lesssim 0.6\%$ the incoming acoustic wave, but with the flame front at rest ($\hat{u}_s = 0$), the indirect acoustic wave is $\approx 21\%$ the incoming acoustic wave. Therefore, the flame at rest produces louder indirect noise than the moving flame front.

As for the system's receptivity, there exist adjoint entropy waves upstream and downstream of the flame in the Lagrange multipliers of both the energy equation (\hat{p}^+ in Fig. 12(b)) and the continuity equation ($\hat{\rho}^+$ in Fig. 12(c)). To produce a change in the generation of entropy waves through the unsteady flame speed, the energy equation should be forced upstream of the flame, as intuitively expected. Forcing the energy equation after the flame changes the intensity with which the entropy waves interact with the choked end.

By combining the direct and adjoint eigenfunctions, the sensitivities to external passive control devices are calculated. First, a mechanism that adds mass proportionally to the state variables is shown in the top row of Fig. 13. As shown by the growth-rate sensitivities, if mass is added in phase with \hat{p} , \hat{u} , or $\hat{\rho}$, the device will destabilize the system. Of particular interest is a feedback proportional to the pressure (first panel, top row). This is a simplified model for a Helmholtz resonator. In a system with a choked end, a Helmholtz resonator optimally stabilizes the eigenvalue at an axial location ≈ 0.96 , which is not exactly the antinode of the resonant mode (see also Sec. 6.1.1 for a discussion of Helmholtz resonators in open-ended ducts). Second, a mechanism that adds momentum proportionally to the state variables is shown in the middle row of Fig. 13. Physically, a drag device, which forces the flow in the opposite direction to the velocity, is an example of these feedback mechanisms. A drag device is strongly stabilizing. Third, a mechanism that adds heat proportionally to the state variables is shown in the bottom row of Fig. 13. Any mechanism that causes increased heat input in phase with the pressure will

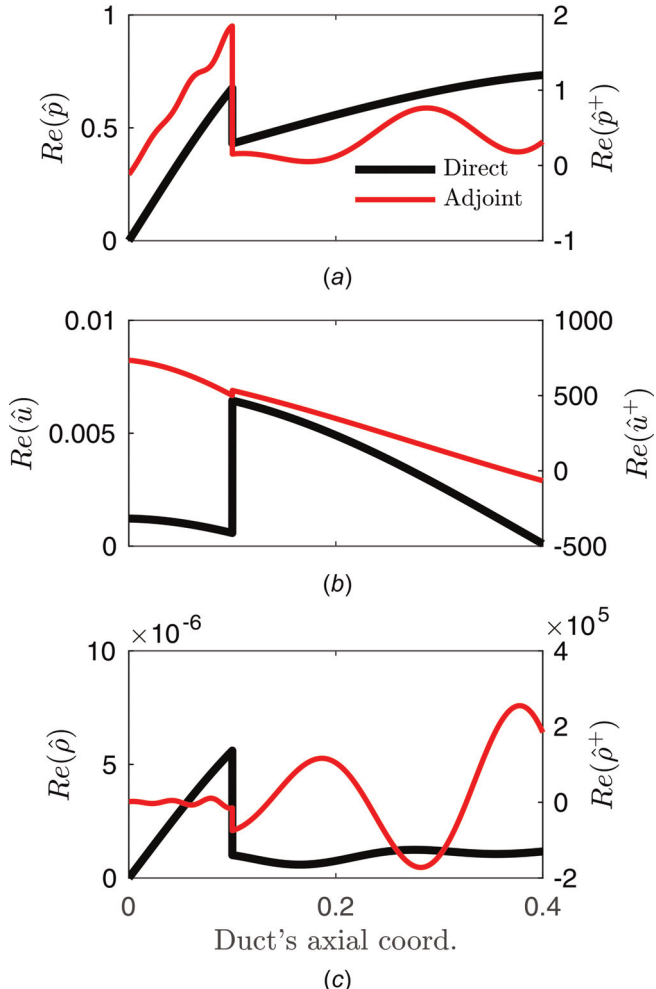


Fig. 12 Direct (left axis, thick-black lines) and adjoint (right axis, thin-red lines) eigenfunctions of a choked combustor with an $n-\tau$ model (adapted from Ref. [161] with permission from Elsevier). The mean flow is not neglected; therefore, the acoustic density belongs in the state vector.

destabilize the system according to the Rayleigh criterion (2) (see Appendix C for an adjoint interpretation of this thermoacoustic stability criterion), as is the case for solid rocket propellants [297]. As explained in Ref. [162], there are oscillations in the sensitivities upstream and downstream of the flame. These are caused by the passage of entropy waves and the indirect generation of acoustic waves at the choked end. Whether the interference between acoustic waves and entropy-induced acoustic waves is constructive or destructive is problem-dependent (it varies with the spatial scales).

This methodology is useful to select an appropriate passive device to stabilize an existing thermoacoustic instability.

6.4 Sensitivity to Intrinsic Physical Mechanisms. A three-dimensional diffusion-flame dump combustor is modeled with the multiple-scale method of Sec. 4. The discretization is performed by a finite element method with Taylor–Hood elements on an unstructured grid [161]. The nondimensional mean-flow temperature is shown in Fig. 14(a). The intrinsic sensitivity (Sec. 3.3.5) is calculated. This enables the identification of the regions of the flow where the hydrodynamic and acoustic subsystems are active and quantify how they affect the overall thermoacoustic stability.

When two-way coupled, the low-Mach number flow and acoustics become unstable. The angular frequency is close to the acoustic frequency; the instability is driven by acoustic effects because

Sensitivity to feedback

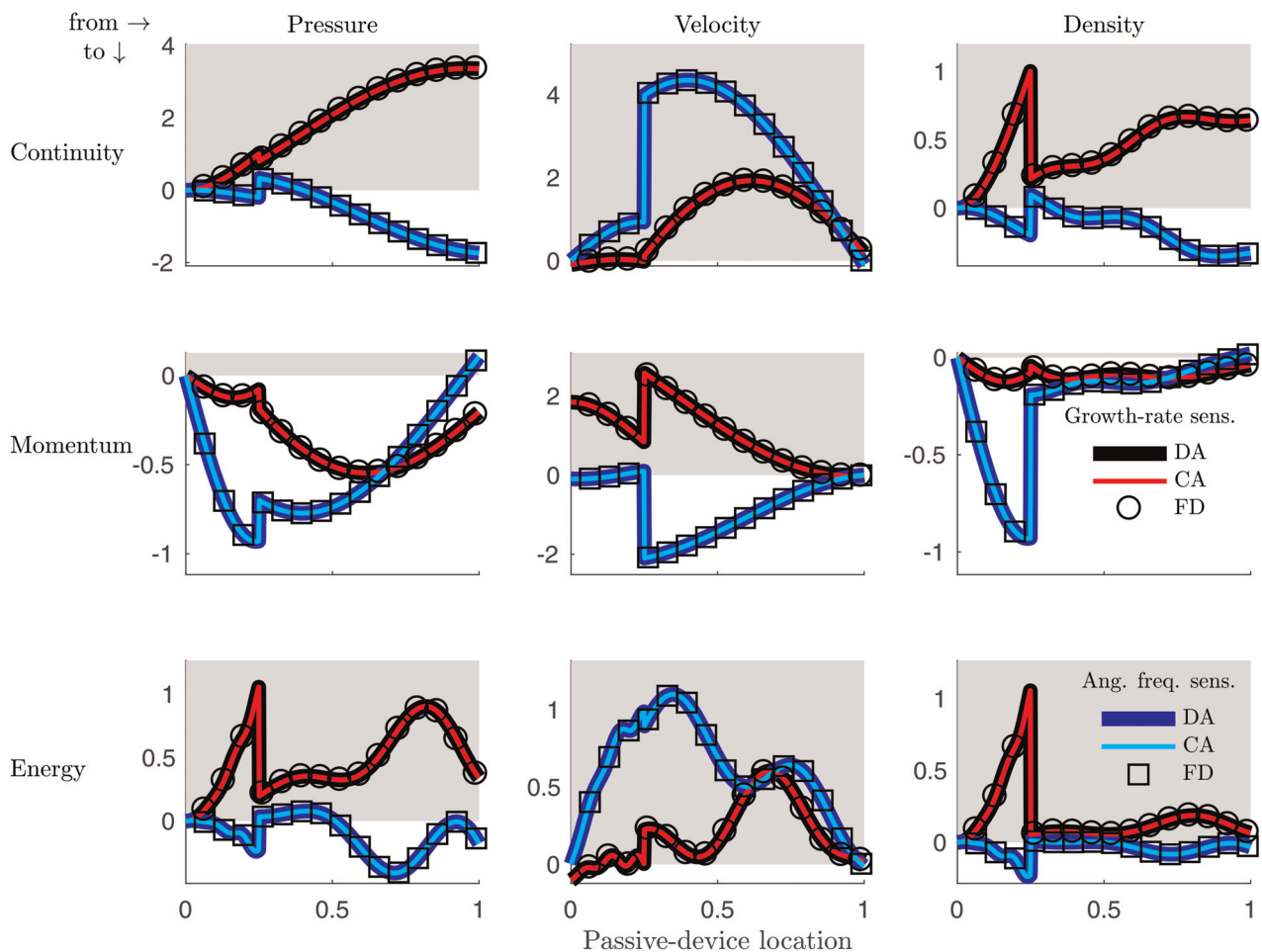


Fig. 13 Sensitivity to passive devices in a choked combustor that generate feedback from pressure, velocity, and density to the continuity, momentum, and energy equation. Thick lines from discrete adjoint calculations, thin lines from continuous adjoint calculations, symbols from finite difference (benchmark solution). Dark (black and red) lines and circles for growth-rate sensitivity, light (blue and cyan) lines and squares for angular-frequency sensitivity. Adapted from Ref. [162] with permission from Elsevier.

the unstable mode is primarily acoustic. In this stability framework, the hydrodynamics is simulated and two-way interacts with the acoustics (Sects. 3.3.5).

First, the spatial function

$$\text{Re}(\sigma_1) = \text{Re}(\hat{\mathbf{q}}_{\text{hyd}}^{+H} \mathbf{L}_{12} \hat{\mathbf{q}}_{\text{ac}}) \quad (126)$$

is analyzed in the top panel of Fig. 14(b), where \mathbf{L}_{12} is the coupling operator from the acoustics to the hydrodynamics (top-right component of matrix (120)) through the acoustic pressure gradient (bottom-right term in Table 2). This formula quantifies how much a unit perturbation to the acoustic vector $\mathbf{L}_{12} \hat{\mathbf{q}}_{\text{ac}}$ changes the thermoacoustic eigenvalue of the coupled system through the receptivity of the hydrodynamic physical process, $\hat{\mathbf{q}}_{\text{hyd}}^+$. The highest sensitivity straddles the recirculation region at the top left corner. Physically, the acoustics are acting as extra feedback momentum sources, enhancing the hydrodynamic sensitivity, which is, indeed, often close to the recirculation boundary [133]. Changes in the strength of the coupling from the acoustics to the hydrodynamics here will have the most influence on this mode, i.e., the mode is very sensitive to the coupling in this region. However, this is only one component of the intrinsic sensitivity and the coupling from acoustics to hydrodynamics is not the dominant mechanism. The maximum growth rate drift is $\text{Re}(\sigma_1) \sim O(10^{-4})$.

Second, the spatial function

$$\text{Re}(\sigma_1) = \text{Re}(\hat{\mathbf{q}}_{\text{ac}}^{+H} \mathbf{L}_{21} \hat{\mathbf{q}}_{\text{hyd}}) \quad (127)$$

is analyzed in the bottom panel of Fig. 14(b), where \mathbf{L}_{21} is the coupling term from the hydrodynamics to the acoustics (bottom-left component of matrix (120)). This formula quantifies how much a unit perturbation to the hydrodynamic field $\mathbf{L}_{21} \hat{\mathbf{q}}_{\text{hyd}}$ changes the thermoacoustic eigenvalue of the coupled system through the receptivity of the acoustic physical process, $\hat{\mathbf{q}}_{\text{ac}}^+$. The maximum value is $\text{Re}(\sigma_1) \sim O(10^{-2})$. The region of high sensitivity straddles the stoichiometric line, where most of the heat is released by the flame. This physically shows the most active physical mechanisms of instability: A small change in the coupling from hydrodynamics to acoustics causes a larger stability drift than a small change in the coupling from the acoustics to the hydrodynamics. In other words, small changes of the strength of the hydrodynamic feedback (i.e., coupling) greatly change the flame response to acoustic perturbations which, in turn, have significant influence on the thermoacoustic stability. In the limit of classic one-way coupled thermoacoustic models, this result is consistent with the diffusion-flame structural sensitivity and Rayleigh Index analysis of Ref. [158].

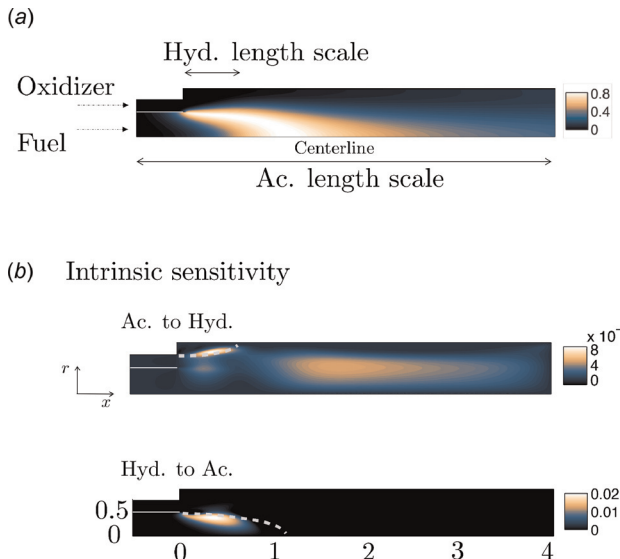


Fig. 14 (a) Nondimensional mean-flow temperature field obtained by large-Eddy simulation [161], (b) Growth-rate sensitivity to intrinsic hydrodynamic feedback feeding the momentum equation, the maximum straddles the recirculation-boundary (upper dashed line), and (c) Sensitivity to the hydrodynamics through acoustic mechanisms, the maximum straddles the stoichiometric line (lower dashed line). Adapted from Ref. [161] with permission from Elsevier.

7 Applications of Stability, Receptivity, and Sensitivity Analysis Under Uncertainty

In Sec. 6, SRS analysis was performed by assuming that the operating condition was exactly known. However, practical systems are affected by uncertainties in the operating conditions and parameters. It is paramount to quickly and accurately calculate the probability that a thermoacoustic system is unstable given uncertainties in the model parameters. The methods presented in this section enable the calculation of how uncertain values of the flame parameters, n and τ , affect the dominant eigenvalue. Adjoint methods will be exploited to calculate the eigenvalue drift with respect to random perturbations.

7.1 Forward Uncertainty Quantification. The input of the forward uncertainty quantification problem³⁸ is the probability density function (PDF) of the model parameters (prior). The least biased PDF should be chosen,³⁹ i.e., the PDF that maximizes the information entropy. Jaynes [300] provides practical criteria for choosing the appropriate PDF. For example, when min/max values of the uncertain parameters are assumed to be known, the uniform distribution is the least biased PDF. Two different approaches are described. In the first approach (Sec. 7.2), the PDF of the growth rate is estimated by Markov-Chain-Monte Carlo (MCMC) sampling (or simply, Monte Carlo sampling) [278]. The probability that the mode is unstable is therefore provided by the measure of the portion of the growth-rate PDF in the unstable semiplane. This is pictorially shown by the intersection of the shaded unstable semiplane and the PDF of the eigenvalue in Fig. 15(b), which mathematically reads⁴⁰

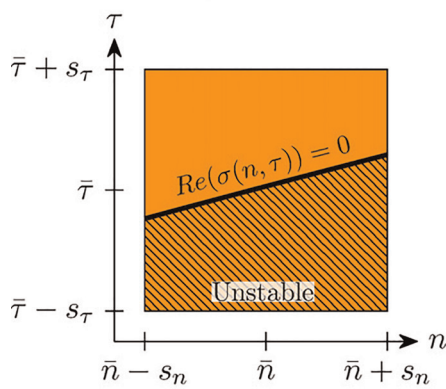
$$\mathcal{P}(\text{Re}(\sigma) > 0) = \int_0^\infty \text{PDF}\{\text{Re}(\sigma)\} d\text{Re}(\sigma) \quad (128)$$

³⁸For inverse uncertainty quantification and data assimilation, the reader may refer to recent works in thermoacoustics and reacting flows [298,299].

³⁹However, the PDF is often practically imposed by an educated guess originating from past experience.

⁴⁰This quantity is sometimes referred to as the risk factor [278].

(a) Uncertain parameters' distribution



(b) Eigenvalues' distribution

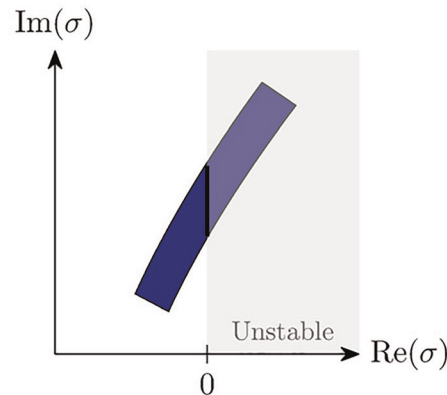


Fig. 15 (a) Uniform distribution of the flame parameters centered around the mean interaction index, \bar{n} , and mean time delay, $\bar{\tau}$. The standard deviations are s_n and s_τ , respectively. The black solid line is the stability margin, i.e., the locus of points that corresponds to a zero growth rate. The ratio between the shaded area and the total area is the probability that the mode is unstable. (b) Corresponding distribution of the eigenvalues. The integration of the PDF of the growth rate in the unstable semiplane is the probability that the mode is unstable.

The second approach (Sec. 7.3) is based on the calculation of the stability margin in the parameters' space, i.e., the locus of parameters such that the system is marginally stable, i.e., $\text{Re}(\sigma(n, \tau)) = 0$, which is calculated by expanding the eigenvalue using adjoint perturbation theory (Sec. 3.3). The probability that the mode is unstable is the measure of the intersection between the PDF of the parameters and the stability margin. The side to choose is the unstable one. This corresponds to the shaded area in Fig. 15(a), labeled E_u in the following definition:

$$\mathcal{P}(\text{Re}(\sigma) > 0) = \int_{E_u} \text{PDF}\{\mathbf{p}\} d\mathbf{p} \quad (129)$$

where \mathbf{p} is the vector of parameters, which, here, are n and τ . If another PDF of the parameters is chosen, the probability that the mode is unstable can be straightforwardly calculated from Eq. (129), which makes this method versatile and computationally cheap.

7.2 Adjoint-Based Monte Carlo Methods. This method is applied to the 19-burner annular combustor described in Refs. [163] and [221]. First, different standard deviations to the uniform distributions of the flame parameters are imposed to calculate the probabilities that the mode is unstable. The results are shown in

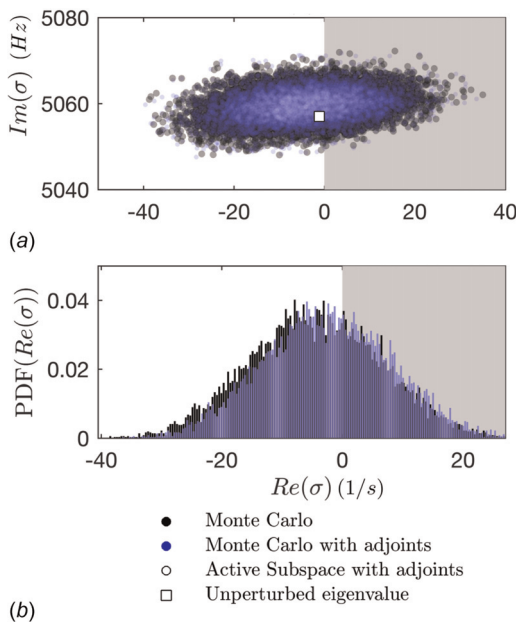


Fig. 16 (a) Scattering of the eigenvalues calculated by standard Monte Carlo method (dark-black circles), Monte Carlo method with adjoint equations (light-blue circles), and Monte Carlo method with a surrogate algebraic model with adjoint equations (white circles). The unperturbed eigenvalue is denoted by a white square. (b) Estimates of the PDFs as histograms of the growth rates of panel (a). Units are dimensional as in the original paper [163], to which the reader is referred for more details.

Table 3 Probabilities that the mode is unstable calculated by the Monte Carlo method as a function of the standard deviation of the flame index and time delay uniform distributions.

Standard deviation	MC	First-order AD	Second-order AD
1%	15.4%	14.7%	15.4%
2.5%	31.3%	33.2%	31.2%
5%	33.25%	40.3%	33%
10%	34.5%	43.2%	34.9%

Note: MC stands for standard Monte Carlo method and AD stands for adjoint. Adapted from [163].

Table 3. When the standard deviations are smaller than 2.5%, the first-order adjoint method provides accurate predictions, although it becomes less accurate for larger deviations. However, the second-order adjoint method provides accurate predictions of the probability up to standard deviations of 10%, matching satisfactorily the benchmark solution by costly finite difference methods (MC). Figure 16(a) shows the scattering of the eigenvalues via Monte Carlo simulations (dark black circles), second-order adjoint method (light blue circles), and surrogate algebraic models obtained by the active subspace method⁴¹ (white-circles) [163,278,301]. The scatterings are obtained by imposing a uniform probability distribution between $\pm 0.1n$, $\pm 0.1\tau$, which represents the uncertainties of the flame parameters (last row of Table 3). The PDFs of the perturbed growth rates are depicted in

⁴¹This method, as applied to uncertainty quantification with adjoints, is explained in Ref. [163]. The directions in the parameters space along which the eigenvalue changes the most are calculated by singular value decomposition of the covariance matrix, which is calculated by MCMC integration. These directions are used to algebraically approximate the response surface, i.e., how the eigenvalue changes with the parameters, with nonlinear regression.

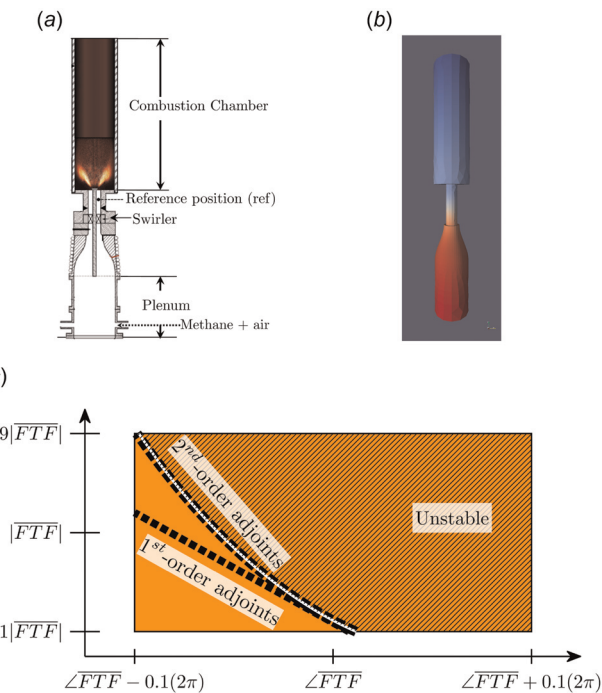


Fig. 17 (a) Turbulent swirled combustor under investigation [302], (b) thermoacoustic eigenfunction calculated with a Helmholtz solver, (c) stability margins calculated by first-order and second-order adjoint methods with no Monte Carlo sampling. The white line is calculated by Monte Carlo sampling for reference. The rectangular represents the uniform PDF of the flame transfer functions parameters. The shaded area is the set of parameters corresponding to positive growth rates. Adapted from Refs. [164] and [167].

Fig. 16(b). The PDF shape is satisfactorily estimated by the second-order adjoint method.

7.3 Monte Carlo Free Methods. This method is demonstrated for the turbulent swirled combustor designed and built at EM2C laboratory [302,303]. A three-dimensional Helmholtz solver is employed [167]. This axisymmetric combustor (Fig. 17(a)) consists of a cylindrical plenum, a convergent duct with a swirl, and a cylindrical combustion chamber. A mixture of methane and air is injected upstream of the plenum. The operating condition “B” of Ref. [303] is considered in this study. More details can be found in Ref. [304] (configuration C03), who estimated the acoustic damping for accurate stability calculations. The flame transfer function gain, $|FTF|$, and phase, $\phi \equiv \angle FTF$, (see Sec. 2.3), are affected by experimental uncertainties, $\Delta|FTF|$ and $\Delta\phi$. The uncertain flame transfer function thus reads

$$FTF(\sigma, \Delta|FTF|, \Delta\phi) = \underbrace{[FTF](\sigma) \exp(i\phi(\sigma))}_{FTF_{\text{measured}}(\sigma)} (1 + \Delta|FTF|) \exp(i\Delta\phi) \quad (130)$$

Note that $\Delta|FTF|$ is defined as a relative measurement error while $\Delta\phi$ is considered an absolute measurement error. The flame gain and phase are extracted from the measured flame describing function of flame B in Ref. [304] with the smallest forcing amplitude. For the eigenvalue to be expanded in power series, the flame transfer function has to be differentiable with respect to its parameters. Therefore, the data have been fit by a rational function [167]. The thermoacoustic system is unstable with the corresponding eigenfunction shown in Fig. 17(b). A relative error for the gain of $\Delta|FTF| = \pm 10\%$ and an absolute error for the phase of $\Delta\phi = 0.1 \cdot 2\pi$ are imposed. Figure 17(c) shows the stability margins calculated from interpolations of 10,000 uniform Monte

Carlo samples and the first- and second-order adjoint algebraic expressions. Because the first-order theory approximates the stability margin as a straight line, it only gives a rough estimate. However, the curvature obtained with second-order theory nearly exactly coincides with the benchmark stability margin calculated by the Monte Carlo method. Second-order methods are particularly suitable for longitudinal thermoacoustic problems because the eigenvalue trajectories have a spiral shape with respect to variations of the flame parameters (Fig. 7), whose local curvature is well approximated by second-order expansion. The probability that the mode is unstable is 76.8% by Monte Carlo sampling (10,000 nonlinear eigenproblems to be solved), 83.78% with the first-order adjoint method (zero eigenproblems solved other than the original one), and 76.8% with the second-order adjoint method (zero eigenproblems solved other than the original one).

8 Applications of Stability, Receptivity, and Sensitivity Analysis to Optimization

Adjoint-based sensitivity analysis (Sec. 3.3) provides the gradient of the eigenvalue with respect to all the thermoacoustic parameters. The gradient information can be embedded in an optimization routine to find the local extremum of a cost functional. Two examples of stabilization of thermoacoustic instabilities via optimization are presented. In the first example, the instability is suppressed by passive devices (Helmholtz resonators, which are acoustic dampers), which are optimally placed and tuned in the combustor [172]. In the second example, the instability is suppressed by modifying the shape of the combustor [173]. Both examples are applied to annular combustors.

8.1 Optimal Placement and Tuning of Acoustic Dampers. A two-step optimization algorithm for the optimal placement and tuning of dampers in annular combustion chambers was proposed by Mensah and Moeck [172]. The optimization algorithm was applied to a simplified two-dimensional rotationally symmetric annular combustor with twelve burner-flame sectors (a simplified model of the annular combustor of Ref. [200]). The optimization algorithm has two steps:

- *Placement of the acoustic dampers.* The effect that the placement of several dampers has on the stability is accurately calculated for different possible configurations by using multiparameter perturbation theory (Sec. 3.3). As summarized in Fig. 18, the placement of dampers in sectors 1, 5, and 9 provides strongest stabilization considering both the first- and second-order azimuthal modes. This is in agreement with the positioning rule [305], i.e., the optimal arrangement of dampers is achieved by evenly distributing them within a sector spanning half the circumferential wavelength of the considered mode (and rotating any of these dampers by half of this wavelength has no effect);
- *Tuning of acoustic damper coefficients.* This is achieved by an iterative gradient-based method. In each iteration step, first, the optimal direction in parameter space to tune the dampers is estimated by the multiparameter perturbation theory. Once the direction is found, the problem is reduced to a single-parameter perturbation to compute the step size to be taken in that direction with second-order perturbations. The stabilization of the annular combustor was achieved after 45 iterations.

8.2 Shape Optimization. Aguilar and Juniper [173] stabilized a thermoacoustic annular configuration by optimizing the geometry of the sectors of the combustor by a wave approach (Sec. 2.2.3) combined with a flame response model (Sec. 2.3). First, they calculated the adjoint-based sensitivity of the unstable modes to small changes in the geometry, whose shape was parametrized. Second, the gradient information was embedded in an optimization routine based on a steepest descent method. The cost

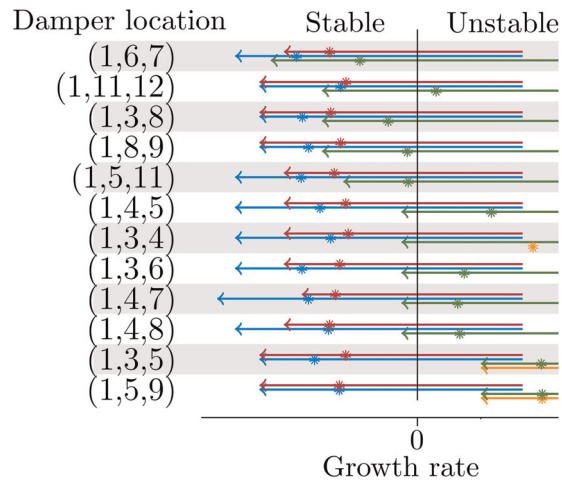


Fig. 18 Placement of the acoustic dampers in an annular combustor with 12 burners (first step of the optimization algorithm). Green and orange arrows indicate the predicted shift in growth rate for the first azimuthal mode, while red and blue arrows correspond to the second azimuthal mode. Both modes are degenerate; symmetry breaking damper placements split the degenerate eigenvalues, e.g., (1,6,7), whereas rotationally symmetric damper placements do not split the eigenvalues, e.g., (1,5,9). The asterisk denotes the growth rate that is actually computed. The triplets denote the annular sectors where acoustic dampers are applied (only a set of three dampers is considered). The most stabilizing pattern is (1,5,9). Adapted from Ref. [172].

functional to minimize was defined as the sum of the growth rates in a given frequency range. Figure 19 shows the application of shape optimization to a sector of annular combustor. It was found that only small changes in the areas are required to stabilize the longitudinal mode, with wave number $n=0$, and the azimuthal unstable modes, with wave number $n \neq 0$. Physically, the optimization procedure modifies the configuration such that the pressure fluctuations are sufficiently out of phase with respect to the heat released by the flame so that the Rayleigh criterion (Eq. (2)) becomes negative.

9 Combining Bloch Theory With Adjoints: The Inclination Rule in Annular Combustors

In annular combustors with discrete rotational symmetry, the eigenfunctions can be represented as Bloch waves [168,169], for example, the acoustic pressure eigenfunctions read

$$\hat{p} = \exp(ib\varphi)\psi_b(\varphi) \quad (131)$$

where φ is the azimuthal coordinate, b is the Bloch wavenumber, and $\psi_b(\varphi)$ is a periodic function of the azimuthal coordinate, i.e., $\psi_b(\varphi) = \psi_b(\varphi + (2\pi/N))$, where N denotes the degree of rotational symmetry of the unperturbed annular combustor. In the MICCA combustor, $N=16$. By using a basis of Bloch waves, it can be shown that the auxiliary matrix \mathbf{Y} in Eq. (88) is equal to the identity matrix. When the same perturbation, ε , is applied to any number of burners, the operator derivative in sector n is either identical in all perturbed burners, or $N_{0,1}=0$ in the unperturbed burners. It can be shown that due to Bloch periodicity, the matrix that defines the auxiliary eigenproblem of the semisimple eigenvalue in Eq. (88) reads [171]

$$\mathbf{X}_1 = \langle \hat{p}^+(0), N_{0,1}\hat{p}(0) \rangle_{(0)} \sum_{n \in \text{per.}} \underbrace{\begin{bmatrix} 1 & \exp\left(i2bn\frac{2\pi}{N}\right) \\ \exp\left(-i2bn\frac{2\pi}{N}\right) & 1 \end{bmatrix}}_{\chi} \quad (132)$$

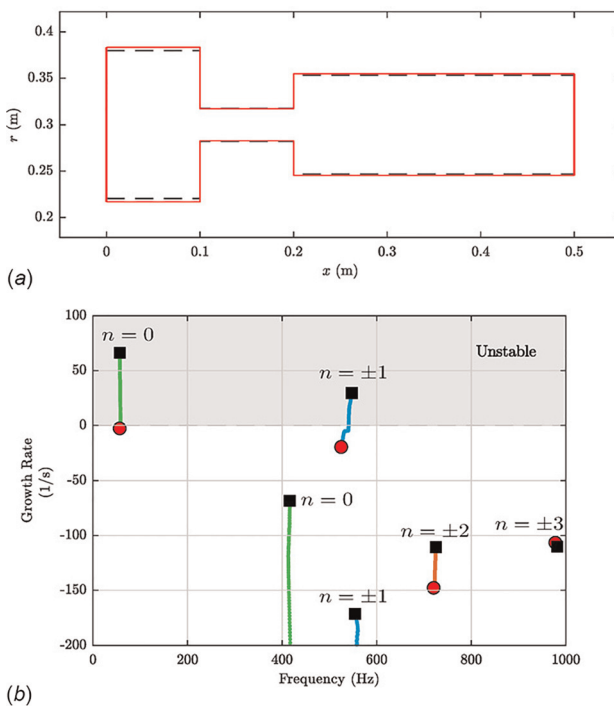


Fig. 19 (a) The black (dashed) line denotes the original unstable annular combustor (a cross section of a sector is shown). The red (solid) line shows the optimized combustor. (b) Eigenvalue trajectories from the original unstable configuration (black squares) to the stabilized configuration (red circles). n indicates the wave number of the mode. Adapted from Ref. [173]. Units are dimensional as in the original paper, to which the reader may refer for details.

where (0) represents a reference sector. Matrix χ is Hermitian; therefore, its eigenvalues are real. Therefore, regardless the number of the perturbed burners, the phase of $\langle \hat{p}^+(0), N_{0,1}\hat{p}(0) \rangle_{(0)}$ is the same as that of the eigenvalues of X_1 (modulo phase shift of π if the eigenvalues of χ are negative). The matrix χ depends on the distribution pattern of the perturbed burners only, and it can be argued that the Bloch wavenumber b is equivalent to the azimuthal mode order. Hence, $\sum_{n \in \text{per}} \exp(i2bn(2\pi/N))$ is the second coefficient of the Fourier transform of the burner arrangement pattern. Such a first-order splitting theory has analogies with the C_{2n} -criterion of Refs. [273] and [274] and the weakly nonlinear analysis of Ref. [277].

The above rationale can be generalized to predict the first-order eigenvalue drift for different perturbations of the burners. An interesting case is obtained when two separate sets of burners are perturbed in different ways such that the average FTF perturbation is zero. For these perturbations, it can be proven that the eigenvalue splits in opposite directions, which is numerically demonstrated in the MICCA combustor [202,219] solved by a Helmholtz solver (Sec. 2.2.3). The eigenvalue trajectories are shown in Fig. 20 for increasing values of the perturbation parameter. Despite the variation of the eigenvalues being nonlinear, the first-order theory predicts the two degenerate eigenvalues to split precisely in opposite directions. It is, therefore, impossible to make a combustor more stable by applying this type of perturbation: If the growth rate of one of the split eigenvalues is decreased, as a consequence, the growth rate of the other split eigenvalue is increased.

10 Weakly Nonlinear Analysis

Just after the Hopf bifurcation, in the linearly unstable region, oscillations grow in amplitude and saturate at low (large)

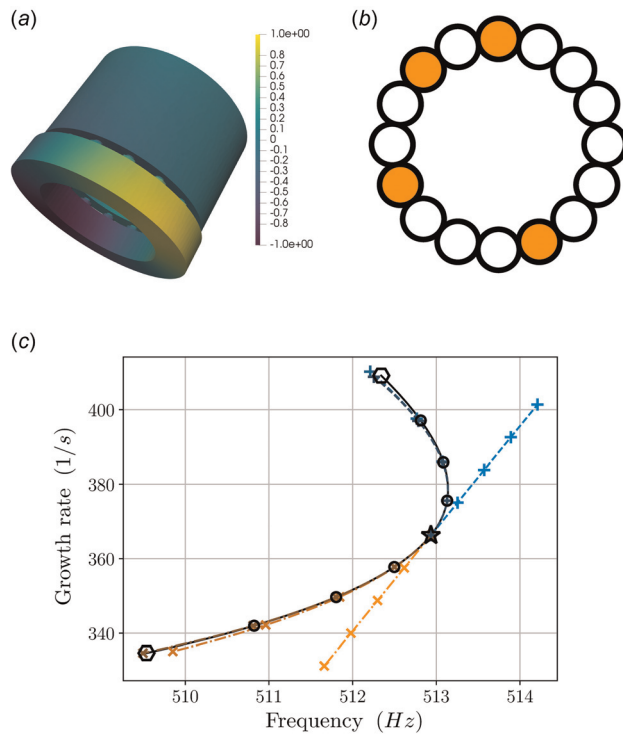


Fig. 20 (a) Pressure eigenfunction of the first plenum-dominant azimuthal mode of the MICCA combustor computed with a Helmholtz solver. (b) symmetry breaking perturbation pattern under consideration. The FTF of the burners with the same colors is perturbed by the same amount. The orange color represents positive perturbations, whereas the white color represents negative perturbations. The average perturbation to the FTF is zero. (c) Eigenvalue trajectories due to the symmetry breaking perturbation pattern (b). The star denotes the twofold semi-simple (degenerate) eigenvalue; different colors indicate the eigenvalue splitting due to the symmetry breaking perturbation; cross and plus symbols denote calculations from adjoint analysis; and black lines/symbols denote the exact solution. Third-order adjoint analysis favorably captures the actual eigenvalue splitting. For the inclination rule, it is not possible to stabilize an annular combustor (at first-order) by applying an azimuthal perturbation with zero average. The units are physical for a better comparison with the experimental data of Refs. [202] and [219]. Adapted from Ref. [171].

amplitudes in super-(sub-)critical bifurcations. Generally, it is of interest to (i) identify if the Hopf bifurcation is super- or subcritical; and (ii) estimate the amplitude of the oscillations in the vicinity of the Hopf bifurcation. Weakly nonlinear analysis is a method to achieve objectives (i) and (ii) without performing fully nonlinear simulations. (Eigenvalue analysis of a fixed point can only identify when the Hopf bifurcation occurs.) Weakly nonlinear analysis is a method based on an asymptotic expansion of the governing equations with respect to a perturbation parameter in the vicinity of a marginally stable point. The weakly nonlinear analysis of fluid systems of Ref. [106] was applied and extended by Orchini et al. [181] in thermoacoustics to analyze the subcritical bifurcation of a ducted heat source. By weakly nonlinear analysis, the dynamics of the perturbed states are calculated by (i) applying a slow-manifold reduction with the method of multiple scale (or, equivalently, the method of averaging); (ii) expanding the equations at the desired order; (iii) projecting the equations onto the marginally stable adjoint eigenfunction. The temporal evolution of the amplitude and frequency of the oscillation, which are generally obtained by solving a nonlinear PDE, are reduced to the Stuart–Landau equation [182,183], which is a first-order ODE. Adjoint methods play a crucial role at step (iii) of the above

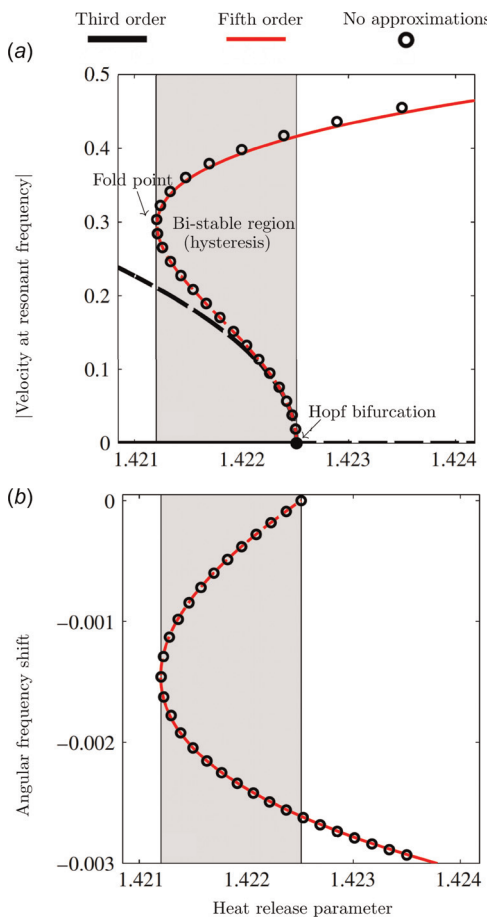


Fig. 21 Weakly nonlinear analysis at third-order (black thick line), fifth-order (red line) and numerical continuation of the fully nonlinear equations (circles). Solid and dashed lines indicate stable and unstable solutions, respectively. (a) Bifurcation diagram of the amplitude of the oscillations at the resonant frequency. (b) Frequency shift of the oscillations with respect to the marginally stable frequency. Adapted from Ref. [181] with permission.

procedure, where the set of inhomogeneous linear equations that stem from the perturbation expansion is solved by solvability conditions. This way, the Landau coefficients, which govern the amplitude evolution, are uniquely determined. In a ducted heat source, Orchini et al. [181] showed that at least a fifth-order expansion is necessary to satisfactorily predict the amplitude in the bistable region of a subcritical thermoacoustic bifurcation up to the fold point, as shown in Fig. 21. (Although not shown, in the supercritical bifurcation, only a third-order expansion is sufficient [106].) The effect that stochastic perturbations have on thermoacoustic oscillations in subcritical bifurcations was investigated in Refs. [43,44,306].

11 Sensitivity of Limit Cycles: Adjoint Floquet Analysis

The calculation of the stability of limit cycles is provided by Floquet analysis, which is a form of eigenvalue analysis on the linearized Poincaré map. An adjoint-based method to calculate the first-order sensitivity of the stability and the period of a limit cycle is proposed.

11.1 Floquet Analysis. Upon spatial discretization, the nonlinear thermoacoustic problem is cast in compact form as a dynamical system

$$\frac{d\mathbf{q}}{dt} = \mathbf{L}\mathbf{q} + \mathcal{N}(\mathbf{q}) \quad (133)$$

where \mathbf{q} is the state vector, \mathbf{L} is the linear part of the equations, and $\mathcal{N}(\mathbf{q})$ is the nonlinearity. Let $\bar{\mathbf{Q}}$ be a \bar{T} -periodic solution of Eq. (133) such that $\bar{\mathbf{Q}}(t + \bar{T}) = \bar{\mathbf{Q}}(t)$. Robust numerical procedures to compute limit cycles in high dimensional systems can be found in Refs. [307–309], among others. The objective is to investigate the stability of the periodic solution, $\bar{\mathbf{Q}}(t)$, by calculating the evolution of small perturbations on the periodic attractor. The state vector is expanded as $\mathbf{q}(t) = \bar{\mathbf{Q}}(t) + \varepsilon\mathbf{y}(t)$, where $\varepsilon \ll 1$ is the arbitrary perturbation parameter and $\mathbf{y}(t)$ is the time-dependent perturbation. From Floquet theorem [168], the time-dependent perturbation can be expressed as

$$\mathbf{y}(t) = \hat{\mathbf{y}}(t)\exp(\bar{\sigma}_F t) \quad (134)$$

where $\hat{\mathbf{y}}(t + \bar{T}) = \hat{\mathbf{y}}(t)$, and $\bar{\sigma}_F \in \mathbb{C}$ is the Floquet exponent.⁴² On introducing the normalized temporal variable $\tilde{t} = t/\bar{T}$ to avoid secular effects, the linearized problem around the periodic solution, $\bar{\mathbf{Q}}$, reads

$$\frac{1}{\bar{T}} \frac{d\hat{\mathbf{y}}}{d\tilde{t}} + \bar{\sigma}_F \hat{\mathbf{y}} = \mathbf{L}\hat{\mathbf{y}} + \mathbf{J}\hat{\mathbf{y}} \quad (135)$$

where $\mathbf{J} \equiv \partial\mathbf{N}/\partial\mathbf{Q}$ calculated at $\bar{\mathbf{Q}}$ is the (now time-dependent, periodic) Jacobian. To define the discrete adjoint operator, a temporal inner product is defined

$$\langle \mathbf{a}, \mathbf{b} \rangle \equiv \int_0^1 \mathbf{a}^H \mathbf{b} d\tilde{t} \quad (136)$$

where \mathbf{a} and \mathbf{b} are generic vectors. By applying a similar procedure as described in Sec. 3.3, the adjoint Floquet problem, which is denoted by $^+$, is derived and reads

$$\frac{1}{\bar{T}} \frac{d\hat{\mathbf{y}}^+}{d\tilde{t}} - \bar{\sigma}_F^* \hat{\mathbf{y}}^+ = \mathbf{L}^H \hat{\mathbf{y}}^+ + \mathbf{J}^H \hat{\mathbf{y}}^+ \quad (137)$$

where * denotes the complex conjugate.

11.2 Floquet-Exponent Sensitivity. A generic perturbation, $\varepsilon\delta\mathbf{H}$, is imposed to the unperturbed equations (133) such that the perturbed periodic solution⁴³ is governed by

$$\frac{1}{\bar{T}} \frac{d\delta\mathbf{Q}}{d\tilde{t}} = \mathbf{L}\delta\mathbf{Q} + \mathcal{N}(\mathbf{Q}) + \varepsilon\delta\mathbf{H} \quad (138)$$

By considering a sufficiently small perturbation, $\varepsilon\delta\mathbf{H}$, the periodic variables are linearized as $\mathbf{Q} = \bar{\mathbf{Q}} + \varepsilon\delta\mathbf{Q}$ and the period as $T = \bar{T} + \varepsilon\delta T$. The evolution of the first-order perturbation of the base flow is governed by

$$\frac{1}{\bar{T}} \frac{d\delta\mathbf{Q}}{d\tilde{t}} - \mathbf{L}\delta\mathbf{Q} - \mathbf{J}\delta\mathbf{Q} = \frac{\delta T}{T^2} \frac{d\bar{\mathbf{Q}}}{d\tilde{t}} + \delta\mathbf{H} \quad (139)$$

The Floquet pair is linearized as $\hat{\mathbf{y}} = \hat{\mathbf{y}} + \varepsilon\delta\hat{\mathbf{y}}$ and $\sigma_F = \bar{\sigma}_F + \varepsilon\delta\sigma_F$. The perturbed Floquet equation becomes

$$\begin{aligned} \frac{1}{\bar{T}} \frac{d\delta\hat{\mathbf{y}}}{d\tilde{t}} - \frac{\delta T}{T^2} \frac{d\bar{\mathbf{Q}}}{d\tilde{t}} + \bar{\sigma}_F \delta\hat{\mathbf{y}} + \delta\sigma_F \hat{\mathbf{y}} &= \mathbf{L}\delta\hat{\mathbf{y}} + \mathbf{J}\delta\hat{\mathbf{y}} + \left(\frac{\partial \mathbf{J}}{\partial \mathbf{Q}} \delta\mathbf{Q} \right) \hat{\mathbf{y}} \\ &+ \delta\hat{\mathbf{H}} \end{aligned} \quad (140)$$

⁴² $\bar{\mu} = \exp(\bar{\sigma}_F \bar{T})$ is the Floquet multiplier. The Floquet exponents are nonunique because $\exp(\bar{\sigma}_F \bar{T}) = \exp(\bar{\sigma}_F \bar{T} + 2\pi i n)$, where n is an integer, whereas the Floquet multipliers $\bar{\mu}$ are unique.

⁴³It is assumed the perturbed periodic solution is still periodic, i.e., it does not bifurcate to another solution.

where $\delta\hat{\mathbf{H}}$ is a generic small perturbation that acts only on the Floquet dynamics. To isolate $\delta\sigma_F$, which is the quantity that needs to be determined in sensitivity analysis, the adjoint base-flow is invoked. Its governing equation reads⁴⁴

$$\frac{1}{\bar{T}} \frac{d\mathbf{Q}^{+H}}{dt} + \mathbf{Q}^{+H}\mathbf{L} + \mathbf{Q}^{+H}\mathbf{J} + \mathbf{f}^H(\hat{\mathbf{y}}^+, \hat{\mathbf{y}}) = 0 \quad (141)$$

where $\mathbf{f}(\hat{\mathbf{y}}^+, \hat{\mathbf{y}})$ is a sesquilinear operator defined such that $\langle \hat{\mathbf{y}}^+, ((\partial\mathbf{J}/\partial\mathbf{Q})\delta\mathbf{Q})\hat{\mathbf{y}} \rangle = \langle \mathbf{f}(\hat{\mathbf{y}}^+, \hat{\mathbf{y}}), \delta\mathbf{Q} \rangle$. The adjoint initial conditions are defined as $\hat{\mathbf{y}}^+(0) = 0$ and $\mathbf{Q}^+(0) = 0$. (Both adjoint variables are one-periodic with respect to the normalized time \tilde{t} .) Finally, the first-order drift of the Floquet exponent is expressed as

$$\delta\sigma_F = \frac{\left\langle \mathbf{Q}^+, \frac{\delta T}{\bar{T}^2} \frac{d\bar{\mathbf{Q}}}{dt} + \delta\mathbf{H} \right\rangle + \left\langle \hat{\mathbf{y}}^+, \frac{\delta T}{\bar{T}^2} \frac{d\hat{\mathbf{y}}}{dt} + \delta\hat{\mathbf{H}} \right\rangle}{\langle \hat{\mathbf{y}}^+, \hat{\mathbf{y}} \rangle} \quad (142)$$

where the terms with δT are related to the base-flow sensitivity, whereas the term with $\delta\hat{\mathbf{H}}$ is related to the sensitivity of the Floquet exponents for a frozen base flow. δT can be calculated by the Fredholm alternative, which provides a solvability condition as explained in Sec. 11.3.

11.3 Period Sensitivity. The governing equation of the base-flow perturbation (139) is a linear inhomogeneous differential equation, which has a solution if the Fredholm alternative is satisfied, i.e., the right-hand side must be orthogonal to the kernel of the homogeneous adjoint equation. The homogeneous adjoint equation is provided by Eq. (141) by setting $\mathbf{f}(\hat{\mathbf{y}}^+, \hat{\mathbf{y}}) = 0$. The adjoint base-flow solution therefore is a linear combination of a particular solution, p , and the homogeneous solution, h , $\mathbf{Q}^+ = \mathbf{Q}_p^+ + \mathbf{Q}_h^+$. The Fredholm alternative provides the first-order drift in the period due to a small perturbation $\delta\mathbf{H}$ such that Eq. (139) is fulfilled. This is mathematically achieved by projecting Eq. (140) onto \mathbf{Q}_h^+ , i.e., $\langle \mathbf{Q}_h^+, (\delta T/\bar{T}^2)(d\bar{\mathbf{Q}}/d\tilde{t}) + \delta\mathbf{H} \rangle = 0$, which implies

$$\frac{\delta T}{\bar{T}^2} = -\frac{\langle \mathbf{Q}_h^+, \delta\mathbf{H} \rangle}{\langle \mathbf{Q}_h^+, \frac{d\bar{\mathbf{Q}}}{dt} \rangle} \quad (143)$$

When δT is substituted back into Eq. (142), the Floquet-exponent drift is calculated with respect to any linear perturbation $\delta\mathbf{H}$ and $\delta\hat{\mathbf{H}}$. Note that if the base flow is unperturbed, i.e., $\delta\mathbf{H} = 0$, then $\delta T = 0$. Equation (142) is the general equation for the first-order (nondegenerate) Floquet-exponent drift due to linear perturbations acting on a periodic attractor both at base flow and linearized levels.

12 Conclusions

One of the objectives of gas turbine manufacturers is to design linearly stable thermoacoustic systems and make them operate in safe operating conditions. Thermoacoustic systems have many parameters but the quantities of interest, for example the unstable modes, are usually only very few. Calculating how the stability changes because of perturbations or modifications to the system is one of the central problems in thermoacoustics. First, it is shown that adjoint methods are accurate and versatile design tools for thermoacoustics and, in general, multiphysical problems. The appeal of adjoint techniques applied to thermoacoustics is that, in very few calculations, one can predict accurately how the growth rate and frequency of thermoacoustic oscillations are affected

⁴⁴The equation can be derived by defining a Lagrangian that constrains the base flow equations and perturbation Floquet equations. The derivation is left out for brevity.

either by all possible passive control elements in the system, or by all possible changes to its design parameters. The versatility of adjoint methods is shown by tackling a variety of problems, which are often encountered in industrial applications, such as longitudinal and annular combustors modeled with flame responses and reduced-order models for the flame dynamics. Adjoint methods can be applied to most of the solution methodologies in thermoacoustics: Helmholtz solvers, wave approaches, Galerkin methods, and multiple-scale methods.

Second, the concept of intrinsic sensitivity is shown to reveal physical insight in the active physical mechanism in thermoacoustics. The method was applied to a dump combustor, the mean flow of which was calculated by large eddy simulation. The intrinsic sensitivity shows that the hydrodynamics greatly influences the overall thermoacoustic stability's sensitivity straddling the flame, which means that the active physical mechanism is due to the Rayleigh criterion. Intrinsic sensitivity is a general framework, which can be applied to problems where different physical phenomena are at play.

Third, it is shown that model and parameter uncertainties can greatly affect the stability calculations. This review recommends evaluating the uncertainty of stability calculations to estimate the confidence, or degree of belief, in our calculations. The probability that combustors are unstable given uncertainties in the flame transfer functions are calculated by two adjoint methods. The first is an adjoint Monte Carlo method, which is applied to an annular combustor and a turbulent swirl dump combustor. By implementing the adjoint code, the number of nonlinear eigenproblems solved is reduced by a factor equal to the number of Monte Carlo samples which, in this case, is 10,000. The second method is Monte Carlo free, which is applied to a longitudinal combustor. Adjoint methods enable the calculation of the stability margin, with which it is possible to evaluate the uncertainty on the stability for free.

Fourthly, Bloch wave theory can reduce the number of computations in rotationally symmetric annular combustors by a factor equal to the number of sectors. An application of adjoint methods combined with Bloch wave theory is reviewed to determine the effect of symmetry-breaking perturbations in an annular combustor (in this case, the MICCA combustor). Because of the inclination rule, which is analytically derived, it is not possible to stabilize an annular combustor (at first-order) by applying a perturbation to the annulus with zero mean.

Fifth, the gradient information is embedded in optimization routines to find (i) the optimal placement of acoustic dampers to stabilize an unstable annular combustor, and (ii) the optimal area and length dimensions to design a stable sector of an annular combustor. Key to the gradient-based optimization process is the implementation of the adjoint code, which provides the gradient of the quantity of interest, i.e., the eigenvalue, with respect to the quantities that the technologist wishes to change.

Finally, moving onward from linear analysis, adjoint equations are deployed to predict the amplitude of a limit cycle by weakly nonlinear analysis. An adjoint Floquet method is proposed to calculate the sensitivity of nonlinear periodic solutions.

The application of adjoint methods to industrial configurations can make a step change in the way that design is performed. The tools are ready for eigenvalue and linear analysis; however, adjoint equations have great potential in other applications in thermoacoustics and reacting flows (Sec. 12.1).

12.1 Current and Future Directions

- *Modeling:* To fully take advantage of the versatility and robustness of adjoint methods, it is important to remind that the results from adjoint analysis are as good as the physical model. Indeed, the accuracy of the eigenvalue drifts predicted by the adjoint-based sensitivity framework depends strongly on the accuracy of the thermoacoustic models

adopted. Effort to develop accurate thermoacoustic models should, of course, be continued, for example, to include sprays, evaporation, and imperfectly premixed flames of real aero-engines.

- *Nonlinearity and unsteadiness:* Thermoacoustic systems can be highly nonlinear and display periodic, quasi-periodic, and chaotic oscillations. Most, but not all, techniques reviewed in this paper are applied to eigenvalue sensitivity of fixed points. The proposed theoretical framework (adjoint Floquet analysis) can be used to calculate the sensitivity of periodic orbits to predict the effect of external passive devices or design parameters, accordingly. Floquet analysis will be necessary in subcritical bifurcations, where the thermoacoustic system may have self-sustained large oscillations despite the eigenvalue being stable. When oscillations become chaotic, adjoint methods become notoriously unstable because of the butterfly effect. Methods to stabilize the calculation of adjoint systems in chaotic oscillations are in constant development. Covariant Lyapunov analysis [310] and shadowing methods with automatic differentiation [253] offer potential ways to tackle chaotic thermoacoustic systems.
- *Physics-informed data-driven methods:* Because thermoacoustic systems are extremely sensitive to perturbations, the time accurate prediction of their nonlinear evolution is challenging. To improve the accuracy of design tools, such as reduced-order models, algorithms from Bayesian inference and machine learning [298] can be used to (i) optimally calibrate an uncertain model on the fly, given data from sensors or flame images; (ii) identify deficiencies in the model; (iii) assimilate data from experiments to improve the state estimation to capture extreme events, such as sudden bifurcations or the occurrence of instabilities. Adjoint methods enable the calculation of the above by statistically constrained optimization [299]. In particular, ad hoc experimental campaigns should be run to provide machine learning and data assimilation algorithms with training data, such as flame images and pressure from sensors.
- *Industrial applications:* Because adjoint-based techniques are versatile, they can be implemented in industrial design tools by creating the adjoint of a thermoacoustic code. The effort of implementing the adjoint code pays off because manufacturers will be able, among others, to (i) compute the optimal passive change of the system's parameters and boundary conditions given an operating condition; (ii) find the optimal set of operating conditions to make the system work in the stable regime given some constraints, such as the geometry (constrained optimization); or calculate the optimal passive feedback mechanism in an elaborate thermoacoustic network and position to suppress a thermoacoustic oscillation; and (iii) evaluate the uncertainty of design tools to better inform the design decision process. Furthermore, adjoint methods can help identify the optimal location where to place a sensor and actuator in active feedback control [205,210,311]. The sensor should be placed where the direct eigenfunction has largest magnitude, the actuator should be placed where the adjoint eigenfunction is greatest. New strategies through fuel injection can be devised utilizing the adjoint flame field.

Adjoint methods help design safer, quieter, and cleaner combustors both for power generation and propulsion.

Acknowledgment

The author wholeheartedly thanks J. P. Moeck, J. Aguilar, A. Orchini, G. Mensah, A. Bottaro, G. Ghirardo, V. Citro, C. F. Silva, and A. Giusti for painstakingly reading, and commenting on, a draft of this manuscript. Comments from G. Rigas and discussions with M. P. Juniper are gratefully acknowledged. The

author is thankful to J. M. Foale for proofreading a draft of this manuscript. The author gratefully acknowledges support from the Royal Academy of Engineering Research Fellowships and the visiting fellowship of the Technical University of Munich—Institute for Advanced Study, funded by the German Excellence Initiative and the European Union Seventh Framework Programme under grant agreement n. 291763. Part of the results shown in this review was sponsored by the European Research Council through project ALORS 2590620. Data kindly provided by colleagues are acknowledged in the relevant figure captions.

Funding Data

- Royal Academy of Engineering (Research Fellowships) (Funder ID: 10.13039/501100000287).

Nomenclature

Mathematical

\mathcal{A}_e	= Laplace transform of \mathcal{S}_e
D	= diffusion coefficient
$\text{Im}(\cdot)$	= imaginary part
\mathcal{L}	= Markstein length, or generic continuous linear operator, or Lagrangian
\mathcal{N}	= a nonlinear operator of the governing equations
Q	= external-source heat release rate
R	= specific gas constant
R_u	= universal gas constant
$\text{Re}(\cdot)$	= real part
S_e	= advected entropy disturbance
Z	= acoustic impedance
\sim	= dimensional quantity
\angle	= phase
$\bar{\cdot}$	= base- or mean-flow quantity
\cdot	= scalar product
\equiv	= definition
$\hat{\cdot}$	= Laplace transformed quantity
$\langle \cdot, \cdot \rangle$	= bilinear, or sesquilinear form
$\ \cdot\ $	= Euclidean norm ($p = 2$)
$\ \cdot\ _p$	= p -norm
\mathbb{C}^N	= field of N -tuple of complex numbers
\mathbb{R}^N	= field of N -tuple of real numbers

Roman

a	= algebraic multiplicity of an eigenvalue
b	= Bloch wave number
c	= speed of sound
$c_{p,i}$	= heat capacity at constant pressure of species i
$c_{v,i}$	= heat capacity at constant volume of species i
\det	= determinant
\dim	= dimension of a vector space
Da	= Damköhler number
f	= acoustic wave traveling in the direction of the mean flow
F	= Laplace transform of f
\mathbf{f}_i	= volume force on species i
F_G	= coordinates of the flame front of a premixed flame
g	= acoustic wave traveling in the opposite direction of the mean flow, or geometric multiplicity of an eigenvalue
G	= flame gain, or G field in the level-set method for premixed flames, or Laplace transform of g
h	= enthalpy
$h_{s,i}$	= sensible enthalpy of species i
He	= Helmholtz number
$\mathbf{H}_{\Delta p}$	= thermoacoustic matrix perturbed along the multi-parameter direction Δp
i	= eigenvalue's index in multi-index notation, or imaginary unit
\mathbf{I}	= identity matrix

K = disturbance phase velocity in premixed flames
 L = length scale
 M = Mach number, or number of parameters, i.e. length of \mathbf{p}
 \mathbf{M} = positive-definite matrix
 m_i = partial multiplicity of local Smith form
 n = flame index
 \mathbf{n} = normal vector
 \mathbf{N} = matrix of the nonlinear eigenproblem
 N_s = number of species
null = null space (or kernel)
 p = pressure, or single parameter
Pe = Péclet number
 Q = number of elements in truncated asymptotic expansion
 \mathbf{q} = state vector
 $\bar{\mathbf{q}}$ = base- or mean-flow solution
 $\hat{\mathbf{q}}$ = direct eigenvector
 $\hat{\mathbf{q}}^+$ = adjoint eigenvector
 \mathbf{q} = state in continuous spaces
 Q_R = rate of heat released by reaction with multiple-scales
 R_d = acoustic reflection coefficient at the outlet
 R_e = entropy-to-acoustics reflection coefficient at the outlet
 R_u = acoustic reflection coefficient at the inlet
Re = Reynolds number
rank = rank of a matrix
 s = entropy
 \hat{s} = spatial structure of harmonic forcing
 $s_{s,i}$ = sensible entropy of species i
 s_L^0 = flame speed in premixed flames
 S_1 = density ratio
 S_2 = adiabatic flame temperature to ambient temperature ratio
Sc = Schmidt number
 t = time
 T = temperature
tr = trace
 u = axial velocity
 \mathbf{u} = velocity
 u'_s = flame front speed in a one-dimensional flame
 V = domain
 V_f = flame domain
 \mathbf{V}_i = diffusion velocity of species i
 W_i = molar mass of species i
 \mathbf{x} = spatial coordinates
 \mathbf{X} = matrix of auxiliary eigenproblem
 x_f = flame location
 $\mathbf{X}_f, \mathbf{Y}_f$ = spatial coordinates in the flame domain
 \mathbf{Y} = mass matrix of auxiliary eigenproblem
 Y_i = mass fraction of species i
 Z = mixture fraction
 \mathbf{z}_{\pm} = eigenvectors of auxiliary eigenproblem
 $\tilde{\Delta}\mathbf{p}$ = perturbation unit direction in the multiparameter space
 $\delta\mathbf{P}$ = perturbation matrix
 $\sigma_{k,\pm}$ = k th order eigenvalue drifts in auxiliary eigenproblem

Greek Symbols

α = fuel-to-air port ratio in the diffusion flame
 α_j = acoustic pressure amplitude of the j th Galerkin mode
 γ = heat-capacity ratio, $\gamma = c_p/c_v$
 $\Delta h_{f,i}^\circ$ = formation enthalpy of species i
 $\Delta s_{f,i}^\circ$ = formation entropy of species i
 ε = perturbation parameter
 η_j = acoustic velocity amplitude of the j th Galerkin mode
 κ = flame curvature
 λ = thermal diffusivity
 μ = M-tuple of non-negative integers for multi-index notation
 μ_i = chemical potential of species i
 ν = stoichiometric mass ratio
 ρ = density

σ = eigenvalue, or Laplace variable (context dependent)
 τ = flame time delay
 τ_d = traveling-acoustic-wave time downstream of the flame
 τ_e = advected entropy disturbance time downstream of the flame
 τ_u = traveling-acoustic-wave time upstream of the flame
 $\underline{\tau}$ = stress tensor
 Φ_j = acoustic velocity spatial shape of the j -th Galerkin mode
 ϕ = phase in the flame model, or equivalence ratio
 Ψ_i = chemical potential function of species i
 Ψ_j = acoustic pressure spatial shape of the j -th Galerkin mode
 ω = angular frequency, $\text{Im}(\sigma)$
 ω_i = production rate of species i
 \mathbf{p} = vector of system's parameters
 \mathcal{O} = big O notation
 \mathfrak{N}_i = heat capacity factor of species i

Subscripts

d = downstream of the flame
 f = flame
 F = fuel
fr = flame front of the premixed flame
 h = homogeneous solution
in = inlet
 O = oxidizer
 p = particular solution
ref = reference condition
 u = upstream of the flame
0 = unperturbed variable, or initial condition
1 = first-order perturbation
2 = second-order perturbation

Superscripts

H = conjugate transpose
 $'$ = fluctuation in the time domain
 $*$ = complex conjugate
 $+$ = right limit
 $-$ = left limit
 $^\circ$ = standard condition

Abbreviations

FTF = flame transfer function
h.o.t. = higher order terms
LES = large-eddy simulation
NEP = nonlinear eigenproblem
ODE = ordinary differential equation
PDE = partial differential equation
PDF = probability density function

Appendix A: Local Smith Form of Nonlinear Eigenproblems

Matrix $\mathbf{N}(\sigma)$ can be decomposed around an eigenvalue σ_0 in local Smith form as

$$\mathbf{P}(\sigma)\mathbf{N}(\sigma)\mathbf{Q}(\sigma) = \mathbf{D}(\sigma) \quad (\text{A1})$$

where \mathbf{P} and \mathbf{Q} are invertible analytic matrix functions, and \mathbf{D} is an analytic diagonal matrix of the form

$$\mathbf{D}(\sigma) = \begin{bmatrix} (\sigma - \sigma_0)^{m_1} & & & \\ & \ddots & & \\ & & (\sigma - \sigma_0)^{m_g} & \\ & & & \mathbf{I} \\ & & & 0_{d \times d} \end{bmatrix} \quad (\text{A2})$$

where $d = N - \text{rank}(\mathbf{N}(\sigma))$, with N being the dimension of the vector space. Matrix \mathbf{D} is the local Smith form of \mathbf{N} at σ_0 ; m_1, \dots, m_g are the partial multiplicities; the number of partial multiplicities is the geometric multiplicity, g , and $\sum_{i=1}^g m_i$ is the algebraic multiplicity. An eigenvalue is semisimple if $m_i = 1$ with $i = 1, \dots, g$, which becomes simple if $g = 1$. Otherwise, the eigenvalue is defective. The j th column of \mathbf{Q} is the eigenvector associated with the j th diagonal element of \mathbf{D} , the root of which is the eigenvalue. The local Smith decomposition generalizes the modal decomposition for defective NEPs.

Appendix B: More on Adjoint Equations

Some extra remarks on adjoint equations are presented for the reader who wishes to delve more into the matter.

B.1 Adjoint Equations of Nonlinear Time-Dependent Systems

This review paper is mostly focused on frequency-based approaches. For completeness, the adjoint equations of a generic nonlinear dynamical system are derived and discussed.

Let $\mathbf{x} \in \mathbb{R}^N$ be the state vector (e.g., fluid variables at grid points or nodes, etc.); $\mathbf{p} \in \mathbb{R}^M$ be the parameters' vector (e.g., boundary shape, Reynolds number, flame transfer functions, geometric parameters, etc.); and $\mathcal{J}(\mathbf{x}, \mathbf{p})$ be the cost functional such that $\mathcal{J} : \mathbb{R}^N \times \mathbb{R}^M \rightarrow \mathbb{R}$. The state vector is the solution of a system of partial differential equations with relevant initial and boundary conditions. The spatial derivatives are numerically discretized and encapsulated in the operator \mathbf{F} . The time is continuous. In so doing, the dynamical system is governed by a set of ordinary differential equations, which can be cast as

$$\mathbf{F}(\mathbf{x}, \dot{\mathbf{x}}, \mathbf{p}, t) = 0 \quad (\text{B1})$$

$$\mathbf{g}(\mathbf{x}(0), \mathbf{p}) = 0 \quad (\text{B2})$$

where \mathbf{F} is a nonlinear implicit operator that depends on the parameters \mathbf{p} , and \mathbf{g} is a nonlinear function that sets the initial conditions.

The objective of sensitivity analysis is to calculate the gradient of the quantity of interest, \mathcal{J} , with respect to the parameters

$$\frac{d\mathcal{J}(\mathbf{x}, \mathbf{p})}{d\mathbf{p}} = \frac{\partial \mathcal{J}}{\partial \mathbf{p}} + \frac{\partial \mathcal{J}}{\partial \mathbf{x}} \frac{d\mathbf{x}}{d\mathbf{p}} \quad (\text{B3})$$

A Lagrangian functional is defined

$$\mathcal{L} \equiv \mathcal{J}(\mathbf{x}, \mathbf{p}) - \langle \mathbf{q}^+, \mathbf{F}(\mathbf{x}, \dot{\mathbf{x}}, \mathbf{p}, t) \rangle - \boldsymbol{\mu}^T \mathbf{g}(\mathbf{x}(0), \mathbf{p}) \quad (\text{B4})$$

where $\mathbf{q}^+ \in \mathbb{R}^N$ and $\boldsymbol{\mu} \in \mathbb{R}^N$ are the as-yet-unknown Lagrangian multipliers; $\dot{\mathbf{x}} \equiv d\mathbf{x}/dt$; and

$$\langle \mathbf{a}, \mathbf{b} \rangle \equiv \frac{1}{T} \int_0^T \mathbf{a}^T \mathbf{b} dt \quad (\text{B5})$$

is an inner product, where \mathbf{a} and \mathbf{b} are arbitrary vectors in \mathbb{R}^N . Although not necessary, the cost functional is considered in the form of a time average over $[0, T]$

$$\mathcal{J}(\mathbf{x}, \mathbf{p}) = \frac{1}{T} \int_0^T \tilde{\mathcal{J}}(\mathbf{x}, \mathbf{p}) dt \quad (\text{B6})$$

Because of the constraints (B1) and (B2), it follows that:

$$\frac{d\mathcal{L}}{d\mathbf{p}} = \frac{d\mathcal{J}}{d\mathbf{p}} \quad (\text{B7})$$

Therefore, the total derivative of the Lagrangian reads

$$\begin{aligned} \frac{d\mathcal{L}}{d\mathbf{p}} &= \frac{1}{T} \int_0^T \left(\frac{\partial \tilde{\mathcal{J}}}{\partial \mathbf{p}} + \frac{\partial \tilde{\mathcal{J}}}{\partial \mathbf{x}} \frac{d\mathbf{x}}{d\mathbf{p}} \right) dt \\ &\quad - \frac{1}{T} \int_0^T \mathbf{q}^{+T} \left(\frac{\partial \mathbf{F}}{\partial \mathbf{p}} + \frac{\partial \mathbf{F}}{\partial \mathbf{x}} \frac{d\mathbf{x}}{d\mathbf{p}} + \frac{\partial \mathbf{F}}{\partial \dot{\mathbf{x}}} \frac{d\dot{\mathbf{x}}}{d\mathbf{p}} \right) dt \\ &\quad - \boldsymbol{\mu}^T \left(\frac{\partial \mathbf{g}}{\partial \mathbf{p}} + \frac{\partial \mathbf{g}}{\partial \mathbf{x}(0)} \frac{d\mathbf{x}(0)}{d\mathbf{p}} \right) \end{aligned} \quad (\text{B8})$$

which, after some re-arrangement and integration by parts, reads

$$\begin{aligned} \frac{d\mathcal{L}}{d\mathbf{p}} &= \frac{1}{T} \int_0^T \frac{\partial \tilde{\mathcal{J}}}{\partial \mathbf{p}} dt - \frac{1}{T} \int_0^T \left(-\frac{\partial \tilde{\mathcal{J}}}{\partial \mathbf{x}} + \mathbf{q}^{+T} \frac{\partial \mathbf{F}}{\partial \mathbf{x}} - \mathbf{q}^{+T} \frac{d}{dt} \left(\frac{\partial \mathbf{F}}{\partial \dot{\mathbf{x}}} \right) \right. \\ &\quad \left. - \frac{d\mathbf{q}^{+T} \partial \mathbf{F}}{dt} \frac{d\dot{\mathbf{x}}}{d\mathbf{p}} \right) dt - \frac{1}{T} \int_0^T \mathbf{q}^{+T} \frac{\partial \mathbf{F}}{\partial \mathbf{p}} dt \\ &\quad - \frac{1}{T} \left[\mathbf{q}^{+T} \frac{\partial \mathbf{F}}{\partial \dot{\mathbf{x}}} \frac{d\dot{\mathbf{x}}}{d\mathbf{p}} \right]_0^T - \boldsymbol{\mu}^T \left(\frac{\partial \mathbf{g}}{\partial \mathbf{p}} + \frac{\partial \mathbf{g}}{\partial \mathbf{x}(0)} \frac{d\mathbf{x}(0)}{d\mathbf{p}} \right) \end{aligned} \quad (\text{B9})$$

The objective is to calculate the gradient information $d\mathcal{L}/d\mathbf{p}$ without calculating $d\mathbf{x}/d\mathbf{p}$ for any $t \in [0, T]$. By defining the following conditions:

$$\mathbf{q}^{+T}(T) = 0 \quad (\text{B10})$$

$$\boldsymbol{\mu}^T = \frac{1}{T} \mathbf{q}^{+T}(0) \frac{\partial \mathbf{F}}{\partial \dot{\mathbf{x}}} \Big|_0^T \left(\frac{\partial \mathbf{g}}{\partial \mathbf{x}(0)} \right)^{-1} \quad (\text{B11})$$

$$\frac{\partial \tilde{\mathcal{J}}}{\partial \mathbf{x}} = \mathbf{q}^{+T} \frac{\partial \mathbf{F}}{\partial \mathbf{x}} - \mathbf{q}^{+T} \frac{d}{dt} \left(\frac{\partial \mathbf{F}}{\partial \dot{\mathbf{x}}} \right) - \frac{d\mathbf{q}^{+T} \partial \mathbf{F}}{dt} \frac{d\dot{\mathbf{x}}}{d\mathbf{p}} \quad (\text{B12})$$

the sensitivity of the quantity of interest can be calculated from Eq. (B9) as

$$\begin{aligned} \frac{d\mathcal{L}}{d\mathbf{p}} &= \frac{d\mathcal{J}}{d\mathbf{p}} = \frac{1}{T} \int_0^T \left(\frac{\partial \tilde{\mathcal{J}}}{\partial \mathbf{p}} - \mathbf{q}^{+T} \frac{\partial \mathbf{F}}{\partial \mathbf{p}} \right) dt \\ &\quad - \frac{1}{T} \mathbf{q}^{+T}(0) \frac{\partial \mathbf{F}}{\partial \dot{\mathbf{x}}} \Big|_0^T \left(\frac{\partial \mathbf{g}}{\partial \mathbf{x}(0)} \right)^{-1} \frac{\partial \mathbf{g}}{\partial \mathbf{p}} \end{aligned} \quad (\text{B13})$$

B.1.1 Simplifications. In many cases, the nonlinear dynamical system is explicit

$$\mathbf{F}(\mathbf{x}, \dot{\mathbf{x}}, \mathbf{p}, t) = \dot{\mathbf{x}} - \tilde{\mathbf{F}}(\mathbf{x}, \mathbf{p}, t) \quad (\text{B14})$$

and the initial conditions are

$$\mathbf{g}(\mathbf{x}(0), \mathbf{p}) = \mathbf{x}(0) - \mathbf{x}_0 = 0 \quad (\text{B15})$$

The adjoint system simplifies to

$$\mathbf{q}^{+T}(T) = 0 \quad (\text{B16})$$

$$\boldsymbol{\mu}^T = \frac{1}{T} \mathbf{q}^{+T}(0) \quad (\text{B17})$$

$$\frac{\partial \tilde{\mathcal{J}}}{\partial \mathbf{x}} = -\mathbf{q}^{+T} \frac{\partial \tilde{\mathbf{F}}}{\partial \mathbf{x}} - \frac{d\mathbf{q}^{+T}}{dt} \quad (\text{B18})$$

If the quantity of interest is not an integral quantity but is a functional evaluated only at the end of a time window, T , i.e., $\mathcal{J} = \mathcal{J}(\mathbf{x}(T), \mathbf{p})$, the adjoint system further simplifies to

$$\mathbf{q}^{+T}(T) = \frac{\partial \mathcal{J}}{\partial \mathbf{x}(T)} \quad (\text{B19})$$

$$\boldsymbol{\mu}^T = \frac{1}{T} \mathbf{q}^{+T}(0) \quad (\text{B20})$$

$$0 = \mathbf{q}^{+T} \frac{\partial \tilde{\mathbf{F}}}{\partial \mathbf{x}} + \frac{d\mathbf{q}^{+T}}{dt} \quad (\text{B21})$$

The adjoint equation (B21) becomes homogeneous and the gradient of the quantity of interest becomes the initial condition⁴⁵ (at $t=T$) for the adjoint equations. Finally, if the parameters of interest are the initial conditions $\mathbf{p} = \mathbf{x}_0$, then Eq. (B13) simplifies to

$$\frac{d\mathcal{L}}{dx_0} = \frac{d\mathcal{J}}{dx_0} = \frac{\partial \mathcal{J}(T)}{\partial \mathbf{x}_0} - \frac{1}{T} \mathbf{q}^{+T}(0) \quad (\text{B22})$$

A necessary condition for optimality is that the Lagrangian is stationary with respect to first-order perturbations, i.e., $d\mathcal{L}/dx_0 = 0$.

B.2 More Remarks on Adjoint Equations

- *Labels.* In functional analysis and linear algebra, adjoint operators are also known as dual or back projection operators;
- *Adjoint models are anticausal.* In the time domain, the adjoint system is anticausal because it evolves backward in time. This is because the initial condition is prescribed at the end of the integration, $t=T$ (e.g., Eq. (B19)), i.e., the adjoint variables carry information on the sensitivity of an output to inputs. Adjoint equations are always linear by definition, i.e., they are dual to the tangent equation. They are defined with respect to the Jacobian of the direct system, which, in nonlinear systems, depends on the direct solution (which can be stored or check-pointed to save storage). In the frequency domain, the anticausality of the adjoint equations results in a modal transformation with opposite sign, i.e., $\mathbf{q}(\mathbf{x}, t) = \hat{\mathbf{q}}(\mathbf{x})\exp(\sigma t)$ and $\mathbf{q}^+(\mathbf{x}, t) = \hat{\mathbf{q}}^+(\mathbf{x})\exp(-\sigma^2 t)$.
- *Adjoint codes are reverse differentiation codes.* The adjoint code can be regarded as a differentiation algorithm in reverse mode. Some examples of direct/adjoint algorithms are: Truncation/zero padding, matrix multiplication/conjugate-transpose matrix multiplication, derivative/negative derivative, convolution/cross-correlation;
- *Adjoint solutions are Lagrange multipliers.* In constrained optimization, the adjoint solutions are the Lagrange multipliers of the governing equations in the constrained functional (Eq. (B4)). Thus, the adjoint variables provide the gradient of the quantity of interest, or cost functional, with respect to the variables of the system. The gradient information can be combined with gradient-based optimization algorithms (e.g., steepest descent/ascent, conjugate gradient, etc.);
- *Adjoint models are not physical models per se.* Although adjoint solutions have a physical interpretation as Lagrange multipliers in constrained optimization, adjoint equations can be defined without any cost functional: Only a bilinear form is required (and, of course, the identification of the correct spaces in the continuous approach). When working in complex spaces, instead of a bilinear form, a sesquilinear form that defines an inner product is commonly used.⁴⁶ Therefore, adjoint equations do depend on the definition of the bilinear/

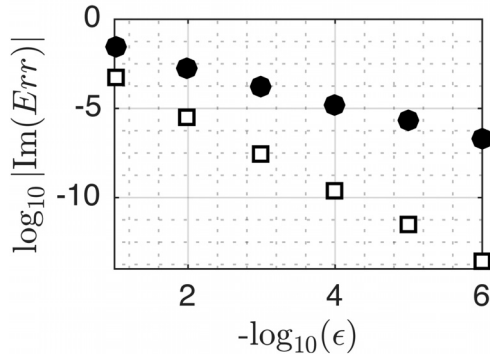
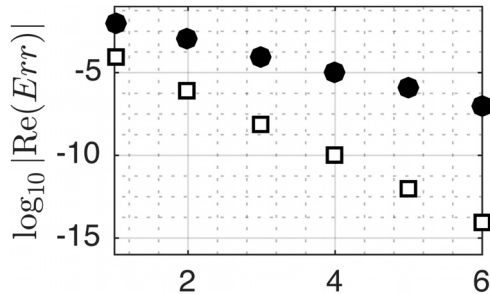


Fig. 22 An example of a successful Taylor test for first- (circles) and second-order (squares) adjoint eigenvalue perturbations in a 19-burner annular combustor. Data are nondimensionalized by the modulus of the unperturbed eigenvalue. Reprinted from Ref. [165] with permission from Elsevier.

sesquilinear form, which means that an adjoint model is not a physical model per se.⁴⁷ See Sec. 3.2 for more details;

- *Adjoint solutions enforce solvability conditions.* In linear algebra, for an inhomogeneous noninvertible linear system to have a solution, the known vector has to be orthogonal to the solution of the homogeneous adjoint system (solvability condition, or compatibility condition, or Fredholm alternative);
- *Adjoint solutions and Green's functions.* The i th component of the adjoint solution is the value of the cost functional when the direct solution is the i th Green's function;
- *Testing an adjoint code.* In the time domain, the adjoint system must pass the dot-product test. This test requires the tangent equation, or a finite difference approximation of it, and checks that at each time step $\mathbf{q}^+(t) \cdot \mathbf{q}(t) = \text{constant} \pm \text{tol}$, where tol is a numerical tolerance, as it ought to be.⁴⁸ In the frequency domain, the first test is to check that the spectrum of the adjoint system is the complex conjugate of the spectrum of the original system. The second test is to check that the $\partial N/\partial \sigma$ -orthogonality conditions, or the biorthogonality conditions of linear eigenproblems, hold. Both in time and frequency domains, the adjoint code must pass the Taylor test. With respect to a parameter, p_0 , that is perturbed as $p_1 = p_0 + \varepsilon$

$$\mathcal{J}(p_1) = \mathcal{J}(p_0) + \varepsilon \frac{d\mathcal{J}}{dp} \Big|_{p_0} + \mathcal{O}(\varepsilon^2) \quad (\text{B23})$$

the test is passed if

⁴⁵This does not imply that no physical information can be extracted from the adjoint model.

⁴⁶By (i) projecting the direct equations onto the adjoint function and the adjoint equations onto the direct function, and (ii) combining these two projections; it follows that $d(\mathbf{q}^+(t) \cdot \mathbf{q}(t))/dt = 0$.

$$\frac{\mathcal{J}(p_1) - \mathcal{J}(p_0) - \varepsilon \frac{d\mathcal{J}}{dp} \Big|_{p_0}}{\varepsilon} \sim \mathcal{O}(\varepsilon) \quad (\text{B24})$$

where $\mathcal{J}(p_1)$ is calculated by rerunning the code, and $d\mathcal{J}/dp|_{p_0}$ is calculated by the adjoint code. In other words, the left-hand side of Eq. (B24), which is the relative error, is a straight line with respect to the perturbation, ε . The same test applies to the eigenvalue, σ , as the quantity of interest. Higher order adjoint codes can be checked by truncating the Taylor expansion (B23) to higher order. An example of a successful Taylor test for first- and second-order adjoint eigenvalue perturbations is shown in Fig. 22.

To delve into the mathematics of adjoint equations, the following readings are suggested: [256,257,312–319].

B.3 Regularity of the Continuous Adjoint Function in Strong and Weak Forms

Given two Banach spaces B_1 and B_2 and the linear mapping $T: B_1 \rightarrow B_2$, the problem is to find $x \in B_1$ such that $T(x) = f$ for a given $f \in B_2$. In particular, the calculation of the sensitivity of the solution x is the goal. An adjoint method can be used to obtain such a sensitivity. Adjoint methods require the introduction of the adjoint of the operator T , which is formally defined as:

Given two Banach spaces B_1, B_2 , and their dual space B_1^+, B_2^+ , the adjoint (also called dual) of the operator $T: B_1 \rightarrow B_2$ is the mapping between the dual spaces $T^+: B_2^+ \rightarrow B_1^+$ satisfying $\forall (x, y^+) \in (B_1, B_2^+): \langle y^+, T(x) \rangle_{B_2^+, B_2} = \langle T^+(y^+), x \rangle_{B_1^+, B_1}$ with $\langle \cdot, \cdot \rangle$ denoting the duality pairing.

This definition is then used to introduce the adjoint equation:

Find $y^+ \in B_2^+$ such that $T^+(y^+) = g$ with g carefully chosen to obtain the desired sensitivity.

Because of the definition of the adjoint of an operator, the adjoint equation is an equality in B_1^+ . This space might lack sufficient regularity to make a numerical estimation very difficult. For example, if $T: H^2(\Omega) \rightarrow L^2(\Omega)$, then $T^+: L^2(\Omega) \rightarrow H^{-2}(\Omega)$ and an adjoint equation has to be interpreted as an equality in $H^{-2}(\Omega)$; where Ω is a bounded open domain in \mathbb{R}^n , $H^k(\Omega)$ is a Sobolev space of degree k equipped with two-norm; and L^2 is the space of square Lebesgue integrable functions. In principle, the adjoint equation must be solved as equality in the distribution sense. However, when the direct problem is studied in weak formulation, its adjoint equations are obtained simply by interchanging the arguments of the sesquilinear form (trial and test functions) that defines the direct equation. The adjoint function is the test function, for example in finite element methods. Consequently, the definition of its adjoint does not require the introduction of an adjoint operator as defined above. Therefore, in problems formulated in weak form, the direct and adjoint solutions have the same degree of regularity, meaning that the adjoint solution does not live in the dual space of the direct solution.

Appendix C: An Adjoint-Based Interpretation of Thermoacoustic Stability Criteria

The same assumptions made in the subsection “Helmholtz equation” (Sec. 2.2.3) are invoked here. The direct and adjoint eigenvectors are decomposed as

$$[u(x, t), p(x, t)] = [\hat{u}, \hat{p}] \exp(\sigma t) \quad (\text{C1})$$

$$[u^+(x, t), p^+(x, t)] = [\hat{u}^+, \hat{p}^+] \exp(-\sigma^* t) \quad (\text{C2})$$

With these modal transformations, in the time domain, the direct and adjoint eigenvectors rotate in the same direction in the complex plane, i.e., their angular frequencies have the same sign (and are equal to each other). The nondimensional momentum and energy equations for one-dimensional acoustics read

$$\sigma \hat{u} + \frac{\partial \hat{p}}{\partial x} = 0 \quad (\text{C3})$$

$$\sigma \hat{p} + \frac{\partial \hat{u}}{\partial x} = \hat{q} \quad (\text{C4})$$

The heat release rate, \hat{q} , is assumed to be in feedback with the state variables so that the problem is closed. For simplicity, $\bar{\rho} = 1$, $\gamma \bar{p} = 1$ and the factor $(\gamma - 1)$ is encapsulated in \hat{q} . The continuous adjoint equations, which are defined with respect to the sesquilinear form $\langle f, g \rangle \equiv \int_0^1 f^* g \, dx$, read

$$-\sigma^* \hat{u}^+ + \frac{\partial \hat{p}^+}{\partial x} = 0 \quad (\text{C5})$$

$$-\sigma^* \hat{p}^+ + \frac{\partial \hat{u}^+}{\partial x} = 0 \quad (\text{C6})$$

The heat release rate is perturbed as $\hat{q} + \delta \hat{q}$, where $|\delta \hat{q}| \sim O(\varepsilon)$. From Eq. (101), the first-order eigenvalue drift reads

$$\sigma_1 = \langle \hat{p}^+, \delta \hat{q} \rangle \quad (\text{C7})$$

where the denominator of Eq. (101) was normalized to unity. If the heat source is localized at $x = x_f$ (with a Dirac delta), then the eigenvalue drift is a function of x_f

$$\sigma_1 = \hat{p}_f^{*+} \delta \hat{q}_f \quad (\text{C8})$$

which in polar representation reads

$$\sigma_1 = |\hat{p}_f^{*+}| |\delta \hat{q}_f| \exp(-i\theta_{\hat{p}_f^+}) \exp(i\theta_{\delta \hat{q}}) \quad (\text{C9})$$

where

$$\theta_{\hat{p}_f^+} \equiv \text{atan2}(\text{Im}(\hat{p}_f^+), \text{Re}(\hat{p}_f^+)) \quad (\text{C10})$$

$$\theta_{\delta \hat{q}} \equiv \text{atan2}(\text{Im}(\delta \hat{q}), \text{Re}(\delta \hat{q})) \quad (\text{C11})$$

are the arguments of the adjoint pressure and heat release rate perturbation, respectively. The real part of σ_1 provides the growth-rate drift, i.e., the change in the linear stability

$$\text{Re}(\sigma_1) = |\hat{p}_f^{*+}| |\delta \hat{q}_f| \cos(\theta_{\delta \hat{q}} - \theta_{\hat{p}_f^+}) \quad (\text{C12})$$

Equation (C12) has a physical interpretation. Assuming that $\delta \hat{q}_f$ is imposed where $\hat{p}_f^+ \neq 0$, first, $\text{Re}(\sigma_1)$ is maximum when $\theta_{\delta \hat{q}} - \theta_{\hat{p}_f^+} = \pm 2(k-1)\pi$, where k is a positive integer. This physically signifies that when a perturbation to the heat release is in phase with the adjoint pressure, the system's stability is maximally destabilized. Second, $\text{Re}(\sigma_1)$ is minimum when $\theta_{\delta \hat{q}} - \theta_{\hat{p}_f^+} = \pm (k+1)\pi$. This physically signifies that when a perturbation to the heat release is in antiphase with the adjoint pressure, the system's stability is maximally stabilized. Third, $\text{Re}(\sigma_1)$ is zero when $\theta_{\delta \hat{q}} - \theta_{\hat{p}_f^+} = \pm (2k+1)\pi/2$. This physically signifies that when a perturbation to the heat release is in quadrature with the adjoint pressure, the system's stability is unaffected.

(Note that we could have used the adjoint modal transformation and sesquilinear form without the complex conjugate (Sec. 3.2) because the complex conjugate is not mandatory in the definition of the adjoint problem for the calculation of the eigenvalue drift. The results discussed would still be valid by taking into account that, without complex conjugate, the adjoint eigenvector rotates in time in the direction opposite to the direct eigenvector.)

References

- [1] Oefelein, J. C., and Yang, V., 1993, “Comprehensive Review of Liquid-Propellant Combustion Instabilities in F-1 Engines,” *J. Propul. Power*, **9**(5), pp. 657–677.

- [2] Natanzon, A. S., 1999, *Combustion Instability*, Vol. 222, American Institute of Aeronautics and Astronautics, Reston, VA.
- [3] Lieuwen, T. C., and Yang, V., 2005, *Combustion Instabilities in Gas Turbine Engines: Operational Experience, Fundamental Mechanisms, and Modeling*, American Institute of Aeronautics and Astronautics, Reston, VA.
- [4] Culick, F. E. C., 2006, "Unsteady Motions in Combustion Chambers for Propulsion Systems," North Atlantic Treaty Organization, Brussels, Belgium, Report No. RTO AG-AVT-039.
- [5] Huang, Y., and Yang, V., 2009, "Dynamics and Stability of Lean-Premixed Swirl-Stabilized Combustion," *Prog. Energy Combust. Sci.*, **35**(4), pp. 293–364.
- [6] Poinsot, T., 2017, "Prediction and Control of Combustion Instabilities in Real Engines," *Proc. Combust. Inst.*, **36**(1), pp. 1–28.
- [7] Juniper, M. P., and Sujith, R. I., 2018, "Sensitivity and Nonlinearity of Thermoacoustic Oscillations," *Annu. Rev. Fluid Mech.*, **50**(1), pp. 661–689.
- [8] Dowling, A. P., and Ffowcs Williams, J. E., 1983, *Sound and Sources of Sound*, Ellis Horwood, Chichester, UK.
- [9] Hoeijmakers, M., Kornilov, V., Lopez Arteaga, I., de Goey, P., and Nijmeijer, H., 2014, "Intrinsic Instability of Flame-Acoustic Coupling," *Combust. Flame*, **161**(11), pp. 2860–2867.
- [10] Emmert, T., Bomberg, S., and Polifke, W., 2015, "Intrinsic Thermoacoustic Instability of Premixed Flames," *Combust. Flame*, **162**(1), pp. 75–85.
- [11] Bomberg, S., Emmert, T., and Polifke, W., 2015, "Thermal Versus Acoustic Response of Velocity Sensitive Premixed Flames," *Proc. Combust. Inst.*, **35**(3), pp. 3185–3192.
- [12] Courtine, E., Selle, L., and Poinsot, T., 2015, "DNS of Intrinsic ThermoAcoustic Modes in Laminar Premixed Flames," *Combust. Flame*, **162**(11), pp. 4331–4341.
- [13] Silva, C. F., Emmert, T., Jaensch, S., and Polifke, W., 2015, "Numerical Study on Intrinsic Thermoacoustic Instability of a Laminar Premixed Flame," *Combust. Flame*, **162**(9), pp. 3370–3378.
- [14] Silva, C. F., Merk, M., Komarek, T., and Polifke, W., 2017, "The Contribution of Intrinsic Thermoacoustic Feedback to Combustion Noise and Resonances of a Confined Turbulent Premixed Flame," *Combust. Flame*, **182**, pp. 269–278.
- [15] Emmert, T., Bomberg, S., Jaensch, S., and Polifke, W., 2017, "Acoustic and Intrinsic Thermoacoustic Modes of a Premixed Combustor," *Proc. Combust. Inst.*, **36**(3), pp. 3835–3842.
- [16] Rayleigh, L., 1878, "The Explanation of Certain Acoustical Phenomena," *Nature*, **18**, pp. 319–321.
- [17] Putnam, A. A., and Dennis, W. R., 1954, "Burner Oscillations of the Gauze-Tone Type," *J. Acoust. Soc. Am.*, **26**(5), pp. 716–725.
- [18] Chu, B. T., 1956, "Stability of Systems Containing a Heat Source: The Rayleigh Criterion," National Advisory Committee for Aeronautics, Washington, DC, Report No. **RM-56D27**.
- [19] Chu, B. T., 1965, "On the Energy Transfer to Small Disturbances in Fluid Flow—Part I," *Acta Mech.*, **1**(3), pp. 215–234.
- [20] Cantrell, R. H., and Hart, R. W., 1964, "Interaction Between Sound and Flow in Acoustic Cavities: Mass, Momentum and Energy Considerations," *J. Acoust. Soc. Am.*, **36**(4), pp. 697–706.
- [21] Candel, S. M., 1975, "Acoustic Conservation Principles and an Application to Plane and Modal Propagation in Nozzles and Diffusers," *J. Sound Vib.*, **41**(2), pp. 207–232.
- [22] Myers, M. K., 1991, "Transport of Energy by Disturbances in Arbitrary Steady Flows," *J. Fluid Mech.*, **226**(1), pp. 383–400.
- [23] Hanifi, A., Schmid, P. J., and Henningson, D. S., 1996, "Transient Growth in Compressible Boundary Layer Flow," *Phys. Fluids*, **8**(3), p. 826.
- [24] Nicoud, F., and Poinsot, T., 2005, "Thermoacoustic Instabilities: Should the Rayleigh Criterion Be Extended to Include Entropy Changes?," *Combust. Flame*, **142**(1–2), pp. 153–159.
- [25] Karimi, N., Brear, M. J., and Moase, W. H., 2008, "Acoustic and Disturbance Energy Analysis of a Flow With Heat Communication," *J. Fluid Mech.*, **597**, pp. 67–89.
- [26] George, K. J., and Sujith, R. I., 2011, "On Chu's Disturbance Energy," *J. Sound Vib.*, **330**(22), pp. 5280–5291.
- [27] George, K. J., and Sujith, R. I., 2012, "Disturbance Energy Norms: A Critical Analysis," *J. Sound Vib.*, **331**(7), pp. 1552–1566.
- [28] Brear, M. J., Nicoud, F., Talei, M., Giauque, A., and Hawkes, E. R., 2012, "Disturbance Energy Transport and Sound Production in Gaseous Combustion," *J. Fluid Mech.*, **707**, pp. 53–73.
- [29] Trefethen, L. N., Trefethen, A. E., Reddy, S. C., and Driscoll, T. A., 1993, "Hydrodynamic Stability Without Eigenvalues," *Science*, **261**(5121), pp. 578–584.
- [30] Schmid, P. J., and Henningson, D. S., 2001, *Stability and Transition of Shear Flows*, Springer, New York.
- [31] Trefethen, L. N., and Embree, M., 2005, *Spectra and Pseudospectra*, Princeton University Press, Princeton, NJ.
- [32] Schmid, P. J., 2007, "Nonmodal Stability Theory," *Ann. Rev. Fluid Mech.*, **39**(1), pp. 129–162.
- [33] Schmid, P. J., and Brandt, L., 2014, "Analysis of Fluid Systems: Stability, Receptivity, Sensitivity," *ASME Appl. Mech. Rev.*, **66**(2), p. 021003.
- [34] Juniper, M. P., 2011, "Transient Growth and Triggering in the Horizontal Rijke Tube," *Int. J. Spray Combust. Dyn.*, **3**(3), pp. 209–224.
- [35] Balasubramanian, K., and Sujith, R. I., 2008, "Non-Normality and Nonlinearity in Combustion-Acoustic Interaction in Diffusion Flames," *J. Fluid Mech.*, **594**, pp. 29–57.
- [36] Balasubramanian, K., and Sujith, R. I., 2008, "Thermoacoustic Instability in a Rijke Tube: Non-Normality and Nonlinearity," *Phys. Fluids*, **20**(4), p. 044103.
- [37] Balasubramanian, K., and Sujith, R. I., 2013, "Non-Normality and Nonlinearity in Combustion-Acoustic Interaction in Diffusion Flames—CORRIGENDUM," *J. Fluid Mech.*, **733**, p. 680.
- [38] Magri, L., Balasubramanian, K., Sujith, R. I., and Juniper, M. P., 2013, "Non-Normality in Combustion-Acoustic Interaction in Diffusion Flames: A Critical Revision," *J. Fluid Mech.*, **733**, pp. 681–684.
- [39] Sujith, R. I., Juniper, M. P., and Schmid, P. J., 2016, "Non-Normality and Nonlinearity in Thermoacoustic Instabilities," *Int. J. Spray Combust. Dyn.*, **8**(2), pp. 119–146.
- [40] Nicoud, F., Benoit, L., Sensiau, C., and Poinsot, T., 2007, "Acoustic Modes in Combustors With Complex Impedances and Multidimensional Active Flames," *AIAA J.*, **45**(2), pp. 426–441.
- [41] Nagaraja, S., Kedia, K., and Sujith, R. I., 2009, "Characterizing Energy Growth During Combustion Instabilities: Singular values or Eigenvalues?," *Proc. Combust. Inst.*, **32**(2), pp. 2933–2940.
- [42] Juniper, M. P., 2011, "Triggering in the Horizontal Rijke Tube: Non-Normality, Transient Growth and Bypass Transition," *J. Fluid Mech.*, **667**, pp. 272–308.
- [43] Waugh, I., Geuß, M., and Juniper, M., 2011, "Triggering, Bypass Transition and the Effect of Noise on a Linearly Stable Thermoacoustic System," *Proc. Combust. Inst.*, **33**(2), pp. 2945–2952.
- [44] Waugh, I. C., and Juniper, M. P., 2011, "Triggering in a Thermoacoustic System With Stochastic Noise," *Int. J. Spray Combust. Dyn.*, **3**(3), pp. 225–242.
- [45] Wieczorek, K., Sensiau, C., Polifke, W., and Nicoud, F., 2011, "Assessing Non-Normal Effects in Thermoacoustic Systems With Mean Flow," *Phys. Fluids*, **23**(10), p. 107103.
- [46] Mariappan, S., and Sujith, R. I., 2010, "Thermoacoustic Instability in a Solid Rocket Motor: Non-Normality and Nonlinear Instabilities," *J. Fluid Mech.*, **653**, pp. 1–33.
- [47] Mariappan, S., 2011, "Theoretical and Experimental Investigation of the Non-Normal Nature of Thermoacoustic Interactions," Ph.D. thesis, IIT Madras, Chennai, India.
- [48] Subramanian, P., and Sujith, R. I., 2011, "Non-Normality and Internal Flame Dynamics in Premixed Flame-Acoustic Interaction," *J. Fluid Mech.*, **679**, pp. 315–342.
- [49] Magri, L., 2015, "Adjoint Methods in Thermo-Acoustic and Combustion Instability," Ph.D. thesis, University of Cambridge, Cambridge, UK.
- [50] Blumenthal, R. S., Tangirala, A. K., Sujith, R., and Polifke, W., 2017, "A Systems Perspective on Non-Normality in Low-Order Thermoacoustic Models: Full Norms, Semi-Norms and Transient Growth," *Int. J. Spray Combust. Dyn.*, **9**(1), pp. 19–43.
- [51] Stow, S. R., and Dowling, A. P., 2008, "A Time-Domain Network Model for Nonlinear Thermoacoustic Oscillations," ASME Paper No. GT2008-50770.
- [52] Pironneau, O., 1973, "On Optimum Profiles in Stokes Flow," *J. Fluid Mech.*, **59**(1), pp. 117–128.
- [53] Pironneau, O., 1974, "On Optimum Design in Fluid Mechanics," *J. Fluid Mech.*, **64**(1), pp. 97–110.
- [54] Jameson, A., 1988, "Aerodynamic Design Via Control Theory," *J. Sci. Comput.*, **3**(3), pp. 233–260.
- [55] Jameson, A., Martinelli, L., and Pierce, N. A., 1998, "Optimum Aerodynamic Design Using the Navier-Stokes Equations," *Theor. Comput. Fluid Dyn.*, **10**(1–4), pp. 213–237.
- [56] Jameson, A., 1999, "Re-Engineering the Design Process Through Computation," *J. Aircr.*, **36**(1), pp. 36–50.
- [57] Liang, C., Fidkowski, K., Persson, P.-O., and Vincent, P., 2014, "Celebrating the 80th Birthday of Professor Antony Jameson," *Comput. Fluids*, **98**, pp. 1–2.
- [58] Tumin, A. M., and Fedorov, A. V., 1984, "Instability Wave Excitation by a Localized Vibrator in the Boundary Layer," *J. Appl. Mech. Tech. Phys.*, **25**(6), pp. 867–873.
- [59] Hill, D. C., 1992, "A Theoretical Approach for Analyzing the Restabilization of Wakes," National Aeronautics and Space Administration, Washington, DC, Memorandum No. 103858.
- [60] Strykowski, P. J., and Sreenivasan, K. R., 1990, "On the Formation and Suppression of Vortex 'Shedding' at Low Reynolds Numbers," *J. Fluid Mech.*, **218**(1), pp. 71–107.
- [61] Grosch, C. E., and Salwen, H., 1978, "The Continuous Spectrum of the Orr-Sommerfeld Equation—Part 1: The Spectrum and the Eigenfunctions," *J. Fluid Mech.*, **87**(1), pp. 33–54.
- [62] Salwen, H., and Grosch, C. E., 1981, "The Continuous Spectrum of the Orr-Sommerfeld Equation—Part 2: Eigenfunction Expansions," *J. Fluid Mech.*, **104**(1), pp. 445–465.
- [63] Hill, D. C., 1995, "Adjoint Systems and Their Role in the Receptivity Problem for Boundary Layers," *J. Fluid Mech.*, **292**(1), pp. 183–204.
- [64] Luchini, P., and Bottaro, A., 1998, "Görtler Vortices: A Backward-In-Time Approach to the Receptivity Problem," *J. Fluid Mech.*, **363**, pp. 1–23.
- [65] Pralits, J. O., Airiau, C., Hanifi, A., and Henningson, D. S., 2000, "Sensitivity Analysis Using Adjoint Parabolized Stability Equations for Compressible Flows," *Flow, Turbul. Combust.*, **65**(3/4), pp. 321–346.
- [66] Giannetti, F., and Luchini, P., 2006, "Leading-Edge Receptivity by Adjoint Methods," *J. Fluid Mech.*, **547**(1), pp. 21–53.
- [67] Giannetti, F., and Luchini, P., 2007, "Structural Sensitivity of the First Instability of the Cylinder Wake," *J. Fluid Mech.*, **581**, pp. 167–197.
- [68] Huerre, P., and Monkewitz, P. A., 1990, "Local and Global Instabilities in Spatially Developing Flows," *Annu. Rev. Fluid Mech.*, **22**(1), pp. 473–537.
- [69] Schmid, P. J., Henningson, D. S., Khorrami, M. R., and Malik, M. R., 1993, "A Study of Eigenvalue Sensitivity for Hydrodynamic Stability Operators," *Theor. Comput. Fluid Dyn.*, **4**(5), pp. 227–240.

- [70] Chomaz, J.-M., 1993, "Linear and Non-Linear, Local and Global Stability Analysis of Open Flows," *Turbulence in Spatially Extended Systems*, Nova Science Publishers, Hauppauge, NY, pp. 245–257.
- [71] Chomaz, J.-M., 2005, "Global Instabilities in Spatially Developing Flows: Non-Normality and Nonlinearity," *Annu. Rev. Fluid Mech.*, **37**(1), pp. 357–392.
- [72] Bottaro, A., Corbett, P., and Luchini, P., 2003, "The Effect of Base Flow Variation on Flow Stability," *J. Fluid Mech.*, **476**, pp. 293–302.
- [73] Marquet, O., Sipp, D., and Jacquin, L., 2008, "Sensitivity Analysis and Passive Control of Cylinder Flow," *J. Fluid Mech.*, **615**, pp. 221–252.
- [74] Luchini, P., Giannetti, F., and Pralits, J. O., 2008, "Structural Sensitivity of Linear and Nonlinear Global Modes," *AIAA Paper No. 2008-4227*.
- [75] Luchini, P., Giannetti, F., and Pralits, J., 2009, "Structural Sensitivity of the Finite-Amplitude Vortex Shedding Behind a Circular Cylinder," *IUTAM Symposium on Unsteady Separated Flows and Their Control* (IUTAM Bookseries, Vol. 14), M. Braza and K. Hourigan, eds., Springer, Dordrecht, The Netherlands, pp. 151–160.
- [76] Marino, L., and Luchini, P., 2009, "Adjoint Analysis of the Flow Over a Forward-Facing Step," *Theor. Comput. Fluid Dyn.*, **23**(1), pp. 37–54.
- [77] Meliga, P., Chomaz, J.-M., and Sipp, D., 2009, "Unsteadiness in the Wake of Disks and Spheres: Instability, Receptivity and Control Using Direct and Adjoint Global Stability Analyses," *J. Fluid Struct.*, **25**(4), pp. 601–616.
- [78] Citro, V., Tchoufag, J., Fabre, D., Giannetti, F., and Luchini, P., 2016, "Linear Stability and Weakly Nonlinear Analysis of the Flow Past Rotating Spheres," *J. Fluid Mech.*, **807**, pp. 62–86.
- [79] Citro, V., Siconolfi, L., Fabre, D., Giannetti, F., and Luchini, P., 2017, "Stability and Sensitivity Analysis of the Secondary Instability in the Sphere Wake," *AIAA J.*, **55**(11), pp. 3661–3668.
- [80] Pralits, J. O., Brandt, L., and Giannetti, F., 2010, "Instability and Sensitivity of the Flow Around a Rotating Circular Cylinder," *J. Fluid Mech.*, **650**, pp. 1–24.
- [81] Tammisola, O., 2012, "Oscillatory Sensitivity Patterns for Global Modes in Wakes," *J. Fluid Mech.*, **701**, pp. 251–277.
- [82] Lashgari, I., Pralits, J. O., Giannetti, F., and Brandt, L., 2012, "First Instability of the Flow of Shear-Thinning and Shear-Thickening Fluids Past a Circular Cylinder," *J. Fluid Mech.*, **701**, pp. 201–227.
- [83] Fani, A., Camarri, S., and Salvetti, M. V., 2012, "Stability Analysis and Control of the Flow in a Symmetric Channel With a Sudden Expansion," *Phys. Fluids*, **24**(8), p. 084102.
- [84] Tchoufag, J., Magnaudet, J., and Fabre, D., 2013, "Linear Stability and Sensitivity of the Flow Past a Fixed Oblate Spheroidal Bubble," *Phys. Fluids*, **25**(5), p. 054108.
- [85] Fani, A., Camarri, S., and Salvetti, M. V., 2013, "Investigation of the Steady Engulfment Regime in a Three-Dimensional T-Mixer," *Phys. Fluids*, **25**(6), p. 064102.
- [86] Fani, A., Camarri, S., and Salvetti, M. V., 2014, "Unsteady Asymmetric Engulfment Regime in a T-Mixer," *Phys. Fluids*, **26**(7), p. 074101.
- [87] Lashgari, I., Tammisola, O., Citro, V., Juniper, M. P., and Brandt, L., 2014, "The Planar X-Junction Flow: Stability Analysis and Control," *J. Fluid Mech.*, **753**, pp. 1–28.
- [88] Carini, M., Giannetti, F., and Auteri, F., 2014, "First Instability and Structural Sensitivity of the Flow Past Two Side-by-Side Cylinders," *J. Fluid Mech.*, **749**, pp. 627–648.
- [89] Boujo, E., and Gallaire, F., 2014, "Controlled Reattachment in Separated Flows: A Variational Approach to Recirculation Length Reduction," *J. Fluid Mech.*, **742**, pp. 618–635.
- [90] Citro, V., Giannetti, F., Brandt, L., and Luchini, P., 2015, "Linear Three-Dimensional Global and Asymptotic Stability Analysis of Incompressible Open Cavity Flow," *J. Fluid Mech.*, **768**, pp. 113–140.
- [91] Citro, V., Giannetti, F., and Pralits, J. O., 2015, "Three-Dimensional Stability, Receptivity and Sensitivity of Non-Newtonian Flows Inside Open Cavities," *Fluid Dyn. Res.*, **47**(1), p. 015503.
- [92] Tammisola, O., Giannetti, F., Citro, V., and Juniper, M. P. P., 2014, "Second-Order Perturbation of Global Modes and Implications for Spanwise Wavy Actuation," *J. Fluid Mech.*, **755**, pp. 314–335.
- [93] Boujo, E., Fani, A., and Gallaire, F., 2015, "Second-Order Sensitivity of Parallel Shear Flows and Optimal Spanwise-Periodic Flow Modifications," *J. Fluid Mech.*, **782**, pp. 491–514.
- [94] Qadri, U. A., Mistri, D., and Juniper, M. P., 2013, "Structural Sensitivity of Spiral Vortex Breakdown," *J. Fluid Mech.*, **720**, pp. 558–581.
- [95] Qadri, U. A., 2014, "Global Stability and Control of Swirling Jets and Flames," *Ph.D. thesis*, University of Cambridge, Cambridge, UK.
- [96] Qadri, U. A., Chandler, G. J., and Juniper, M. P., 2018, "Passive Control of Global Instability in Low-Density Jets," *Eur. J. Mech.-B/Fluids*, **72**, pp. 311–319.
- [97] Meliga, P., Sipp, D., and Chomaz, J.-M., 2010, "Open-Loop Control of Compressible Afterbody Flows Using Adjoint Methods," *Phys. Fluids*, **22**(5), p. 054109.
- [98] Meliga, P., Sipp, D., and Chomaz, J.-M., 2010, "Effect of Compressibility on the Global Stability of Axisymmetric Wake Flows," *J. Fluid Mech.*, **660**, pp. 499–526.
- [99] Fedorov, A. V., 2013, "Receptivity of a Supersonic Boundary Layer to Solid Particulates," *J. Fluid Mech.*, **737**, pp. 105–131.
- [100] Giannetti, F., Camarri, S., and Luchini, P., 2010, "Structural Sensitivity of the Secondary Instability in the Wake of a Circular Cylinder," *J. Fluid Mech.*, **651**, pp. 319–337.
- [101] Pralits, J. O., Giannetti, F., and Brandt, L., 2013, "Three-Dimensional Instability of the Flow Around a Rotating Circular Cylinder," *J. Fluid Mech.*, **730**, pp. 5–18.
- [102] Carini, M., Giannetti, F., and Auteri, F., 2014, "On the Origin of the Flip-Flop Instability of Two Side-By-Side Cylinder Wakes," *J. Fluid Mech.*, **742**, pp. 552–576.
- [103] Giannetti, F., Camarri, V., and Citro, V., 2019, "Sensitivity Analysis and Passive Control of the Secondary Instability in the Cylinder Wake," *J. Fluid Mech.*, **864**, pp. 45–72.
- [104] Crighton, D. G., and Gaster, M., 1976, "Stability of Slowly Diverging Jet Flow," *J. Fluid Mech.*, **77**(2), pp. 397–413.
- [105] Barkley, D., 2006, "Linear Analysis of the Cylinder Wake Mean Flow," *Europhys. Lett.*, **75**(5), pp. 750–756.
- [106] Sipp, D., and Lebedev, A., 2007, "Global Stability of Base and Mean Flows: A General Approach and Its Applications to Cylinder and Open Cavity Flows," *J. Fluid Mech.*, **593**, pp. 333–358.
- [107] Beneddine, S., Sipp, D., Arnault, A., Dandois, J., and Lesshaft, L., 2016, "Conditions for Validity of Mean Flow Stability Analysis," *J. Fluid Mech.*, **798**, pp. 485–504.
- [108] McKeon, B. J., and Sharma, A. S., 2010, "A Critical-Layer Framework for Turbulent Pipe Flow," *J. Fluid Mech.*, **658**, pp. 336–382.
- [109] Turton, S. E., Tuckerman, L. S., and Barkley, D., 2015, "Prediction of Frequencies in Thermosolutal Convection From Mean Flows," *Phys. Rev. E*, **91**(4), p. 043009.
- [110] Crouch, J. D., Garbaruk, A., and Magidov, D., 2007, "Predicting the Onset of Flow Unsteadiness Based on Global Instability," *J. Comput. Phys.*, **224**(2), pp. 924–940.
- [111] Fosas de Pando, M. A., Sipp, D., and Schmid, P. J., 2012, "Efficient Evaluation of the Direct and Adjoint Linearized Dynamics From Compressible Flow Solvers," *J. Comput. Phys.*, **231**(23), pp. 7739–7755.
- [112] Fosas de Pando, M., Schmid, P. J., and Sipp, D., 2014, "A Global Analysis of Tonal Noise in Flows Around Aerofoils," *J. Fluid Mech.*, **754**, pp. 5–38.
- [113] Meliga, P., Pujals, G., and Serre, E., 2012, "Sensitivity of 2-D Turbulent Flow Past a D-Shaped Cylinder Using Global Stability," *Phys. Fluids*, **24**(6), p. 061701.
- [114] Mettot, C., Sipp, D., and Bézard, H., 2014, "Quasi-Laminar Stability and Sensitivity Analyses for Turbulent Flows: Prediction of Low-Frequency Unsteadiness and Passive Control," *Phys. Fluids*, **26**(4), p. 045112.
- [115] Reynolds, W. C., and Hussain, K. M. F., 1972, "The Mechanics of an Organized Wave in Turbulent Shear Flow—Part 3: Theoretical Models and Comparisons With Experiments," *J. Fluid Mech.*, **54**(2), pp. 263–288.
- [116] Tammisola, O., and Juniper, M. P., 2016, "Coherent Structures in a Swirl Injector at $Re = 4800$ by Nonlinear Simulations and Linear Global Modes," *J. Fluid Mech.*, **792**, pp. 620–657.
- [117] Camarri, S., Falleni, B. E. G., and Fransson, J. H. M., 2013, "Stability Analysis of Experimental Flow Fields Behind a Porous Cylinder for the Investigation of the Large-Scale Wake Vortices," *J. Fluid Mech.*, **715**, pp. 499–536.
- [118] Camarri, S., Trip, R., and Fransson, J. H. M., 2017, "Investigation of Passive Control of the Wake Past a Thick Plate by Stability and Sensitivity Analysis of Experimental Data," *J. Fluid Mech.*, **828**, pp. 753–778.
- [119] Wang, Q., and Gao, J., 2012, "The Drag-Adjoint Field of a Circular Cylinder Wake at Reynolds Numbers 20, 100 and 500," *J. Fluid Mech.*, **730**, pp. 145–161.
- [120] Pilyugin, S. Y., 2006, *Shadowing in Dynamical Systems*, Springer, Berlin.
- [121] Palmer, K. J., 2009, "Shadowing Lemma for Flows," *Scholarpedia*, **4**(4), p. 7918.
- [122] Wang, Q., 2013, "Forward and Adjoint Sensitivity Computation of Chaotic Dynamical Systems," *J. Comput. Phys.*, **235**, pp. 1–13.
- [123] Wang, Q., Hu, R., and Blonigan, P., 2014, "Least Squares Shadowing Sensitivity Analysis of Chaotic Limit Cycle Oscillations," *J. Comput. Phys.*, **267**, pp. 210–224.
- [124] Wang, Q., 2014, "Convergence of the Least Squares Shadowing Method for Computing Derivative of Ergodic Averages," *SIAM J. Numer. Anal.*, **52**(1), pp. 156–170.
- [125] Blonigan, P., Gomez, S., and Wang, Q., 2014, "Least Squares Shadowing for Sensitivity Analysis of Turbulent Fluid Flows," *AIAA Paper No. 2014-1426*.
- [126] Blonigan, P. J., and Wang, Q., 2014, "Probability Density Adjoint for Sensitivity Analysis of the Mean of Chaos," *J. Comput. Phys.*, **270**, pp. 660–686.
- [127] Ni, A., and Wang, Q., 2017, "Sensitivity Analysis on Chaotic Dynamical Systems by Non-Intrusive Least Squares Shadowing (NILSS)," *J. Comput. Phys.*, **347**, pp. 56–77.
- [128] Chater, M., Ni, A., and Wang, Q., 2017, "Simplified Least Squares Shadowing Sensitivity Analysis for Chaotic ODEs and PDEs," *J. Comput. Phys.*, **329**, pp. 126–140.
- [129] Blonigan, P. J., 2017, "Adjoint Sensitivity Analysis of Chaotic Dynamical Systems With Non-Intrusive Least Squares Shadowing," *J. Comput. Phys.*, **348**, pp. 803–826.
- [130] Larsson, J., and Wang, Q., 2014, "The Prospect of Using Large Eddy and Detached Eddy Simulations in Engineering Design, and the Research Required to Get There," *Philos. Trans. R. Soc. A*, **372**, p. 20130329.
- [131] Kim, J., Bodony, D. J., and Freund, J. B., 2014, "Adjoint-Based Control of Loud Events in a Turbulent Jet," *J. Fluid Mech.*, **741**, pp. 28–59.
- [132] Caeiro, F., Sovardi, C., Förner, K., and Polifke, W., 2017, "Shape Optimization of a Helmholtz Resonator Using an Adjoint Method," *Int. J. Spray Combust. Dyn.*, **9**(4), pp. 394–408.
- [133] Sipp, D., Marquet, O., Meliga, P., and Barbagallo, A., 2010, "Dynamics and Control of Global Instabilities in Open-Flows: A Linearized Approach," *ASME Appl. Mech. Rev.*, **63**(3), p. 030801.
- [134] Luchini, P., and Bottaro, A., 2014, "Adjoint Equations in Stability Analysis," *Annu. Rev. Fluid Mech.*, **46**(1), pp. 493–517.

- [135] Camarri, S., 2015, "Flow Control Design Inspired by Linear Stability Analysis," *Acta Mech.*, **226**(4), pp. 979–1010.
- [136] Chandler, G. J., Juniper, M. P., Nichols, J. W., and Schmid, P. J., 2012, "Adjoint Algorithms for the Navier-Stokes Equations in the Low Mach Number Limit," *J. Comput. Phys.*, **231**(4), pp. 1900–1916.
- [137] Qadri, U. A., Chandler, G. J., and Juniper, M. P., 2015, "Self-Sustained Hydrodynamic Oscillations in Lifted Jet Diffusion Flames: Origin and Control," *J. Fluid Mech.*, **775**, pp. 201–222.
- [138] Emerson, B., Lieuwen, T., and Juniper, M. P., 2016, "Local Stability Analysis and Eigenvalue Sensitivity of Reacting Bluff-Body Wakes," *J. Fluid Mech.*, **788**, pp. 549–575.
- [139] Sandu, A., Daescu, D. N., and Carmichael, G. R., 2003, "Direct and Adjoint Sensitivity Analysis of Chemical Kinetic Systems With KPP—Part I: Theory and Software Tools," *Atmos. Environ.*, **37**(36), pp. 5083–5096.
- [140] Goodwin, D. G., Moffat, H. K., and Speth, R. L., 2017, "Cantera: An Object-Oriented Software Toolkit for Chemical Kinetics, Thermodynamics, and Transport Processes," accessed Feb. 26, 2019, <http://www.cantera.org>
- [141] Wang, Q., Duraisamy, K., Alonso, J. J., and Iaccarino, G., 2012, "Risk Assessment of Scramjet Unstart Using Adjoint-Based Sampling Methods," *AIAA J.*, **50**(3), pp. 581–592.
- [142] Braman, K., Oliver, T. A., and Raman, V., 2015, "Adjoint-Based Sensitivity Analysis of Flames," *Combust. Theory Modell.*, **19**(1), pp. 29–56.
- [143] Duraisamy, K., and Alonso, J., 2012, "Adjoint Based Techniques for Uncertainty Quantification in Turbulent Flows With Combustion," *AIAA Paper No. 2012-2711*.
- [144] Yumuşak, M., and Eyi, S., 2012, "Design Optimization of Rocket Nozzles in Chemically Reacting Flows," *Comput. Fluids*, **65**, pp. 25–34.
- [145] Copeland, S. R., Palacios, F., and Alonso, J. J., 2014, "Adjoint-Based Aerothermodynamic Shape Design of Hypersonic Vehicles in Non-Equilibrium Flows," *AIAA Paper No. 2014-0513*.
- [146] Lemke, M., Reiss, J., and Sesterhenn, J., 2013, "Adjoint-Based Analysis of Thermoacoustic Coupling," *AIP Conf. Proc.*, **1588**(1), pp. 2163–2166.
- [147] Lemke, M., Reiss, J., and Sesterhenn, J., 2014, "Adjoint Based Optimisation of Reactive Compressible Flows," *Combust. Flame*, **161**(10), pp. 2552–2564.
- [148] Sashittal, P., Sayadi, T., Schmid, P. J., Jang, I., and Magri, L., 2016, "Adjoint-Based Sensitivity Analysis for a Reacting Jet in Crossflow," Center for Turbulence Research, Summer Program, Stanford, CA, June 26–July 22, pp. 375–384.
- [149] Qadri, U. A., Magri, L., Ihme, M., and Schmid, P. J., 2016, "Optimal Ignition Placement in Diffusion Flames by Nonlinear Adjoint Looping," Center for Turbulence Research, Summer Program, Stanford, CA, June 26–July 22, pp. 95–104.
- [150] Blanchard, M., Schmid, P. J., Sipp, D., and Schuller, T., 2016, "Pressure Wave Generation From Perturbed Premixed Flames," *J. Fluid Mech.*, **797**, pp. 231–246.
- [151] Skene, C. S., and Schmid, P. J., 2019, "Adjoint-Based Parametric Sensitivity Analysis for Swirling M-Flames," *J. Fluid Mech.*, **859**, pp. 516–542.
- [152] Capecelatro, J., Bodony, D. J., and Freund, J. B., 2018, "Adjoint-Based Sensitivity and Ignition Threshold Mapping in a Turbulent Mixing Layer," *Combust. Theory Modell.* (epub).
- [153] Magri, L., and Juniper, M. P., 2013, "Sensitivity Analysis of a Time-Delayed Thermo-Acoustic System Via an Adjoint-Based Approach," *J. Fluid Mech.*, **719**, pp. 183–202.
- [154] Magri, L., and Juniper, M. P., 2014, "Adjoint-Based Linear Analysis in Reduced-Order Thermo-Acoustic Models," *Int. J. Spray Combust. Dyn.*, **6**(3), pp. 225–246.
- [155] Rigas, G., Jamieson, N. P., Li, L. K. B., and Juniper, M. P., 2016, "Experimental Sensitivity Analysis and Control of Thermoacoustic Systems," *J. Fluid Mech.*, **787**, p. R1.
- [156] Jamieson, N. P., Rigas, G., and Juniper, M. P., 2017, "Experimental Sensitivity Analysis Via a Secondary Heat Source in an Oscillating Thermoacoustic System," *Int. J. Spray Combust. Dyn.*, **9**(4), pp. 230–240.
- [157] Jamieson, N. P., and Juniper, M. P., 2017, "Experimental Sensitivity Analysis and the Equivalence of Pulsed Forcing and Feedback Control in Thermoacoustic Systems," *ASME Paper No. GT2017-63441*.
- [158] Magri, L., and Juniper, M. P., 2014, "Global Modes, Receptivity, and Sensitivity Analysis of Diffusion Flames Coupled With Duct Acoustics," *J. Fluid Mech.*, **752**, pp. 237–265.
- [159] Magri, L., and Juniper, M. P., 2013, "A Theoretical Approach for Passive Control of Thermoacoustic Oscillations: Application to Ducted Flames," *ASME J. Eng. Gas Turbines Power*, **135**(9), p. 091604.
- [160] Orchini, A., and Juniper, M. P., 2016, "Linear Stability and Adjoint Sensitivity Analysis of Thermoacoustic Networks With Premixed Flames," *Combust. Flame*, **165**, pp. 97–108.
- [161] Magri, L., See, Y.-C., Tammisola, O., Ihme, M., and Juniper, M., 2017, "Multiple-Scale Thermo-Acoustic Stability Analysis of a Coaxial Jet Combustor," *Proc. Combust. Inst.*, **36**(3), pp. 3863–3871.
- [162] Aguilar, J. G., Magri, L., and Juniper, M. P., 2017, "Adjoint-Based Sensitivity Analysis of Low Order Thermoacoustic Networks Using a Wave-Based Approach," *J. Comput. Phys.*, **341**, pp. 163–181.
- [163] Magri, L., Bauerheim, M., Nicoud, F., and Juniper, M. P., 2016, "Stability Analysis of Thermo-Acoustic Nonlinear Eigenproblems in Annular Combustors—Part II: Uncertainty Quantification," *J. Comput. Phys.*, **325**, pp. 411–421.
- [164] Silva, C. F., Magri, L., Runte, T., and Polifke, W., 2016, "Uncertainty Quantification of Growth Rates of Thermoacoustic Instability by an Adjoint Helmholtz Solver," *ASME J. Eng. Gas Turbines Power*, **139**(1), p. 011901.
- [165] Magri, L., Bauerheim, M., Nicoud, F., and Juniper, M. P., 2016, "Stability Analysis of Thermo-Acoustic Nonlinear Eigenproblems in Annular Combustors—Part I: Sensitivity," *J. Comput. Phys.*, **325**, pp. 411–421.
- [166] Mensah, G. A., Campa, G., and Moeck, J. P., 2016, "Efficient Computation of Thermoacoustic Modes in Industrial Annular Combustion Chambers Based on Bloch-Wave Theory," *ASME J. Eng. Gas Turbines Power*, **138**(8), p. 081502.
- [167] Mensah, G. A., Magri, L., and Moeck, J. P., 2018, "Methods for the Calculation of Thermoacoustic Stability Margins and Monte Carlo Free Uncertainty Quantification," *ASME J. Eng. Gas Turbines Power*, **140**(6), p. 061501.
- [168] Floquet, G., 1883, "Sur Les Équations Différentielles Linéaires à coefficients Périodiques," *Ann. Sci. L'École Norm. Supér.*, Série 2, **12**, pp. 47–88.
- [169] Bloch, F., 1929, "Über Die Quantenmechanik Der Elektronen in Kristallgittern," *Z. Für Phys.*, **52**(7–8), pp. 555–600.
- [170] Mensah, G. A., and Moeck, J. P., 2017, "Limit Cycles of Spinning Thermoacoustic Modes in Annular Combustors: A Bloch-Wave and Adjoint-Perturbation Approach," *ASME Paper No. GT2017-64817*.
- [171] Mensah, G. A., Magri, L., Orchini, A., and Moeck, J. P., 2018, "Effects of Asymmetry on Thermoacoustic Modes in Annular Combustors: A Higher-Order Perturbation Study," *ASME Paper No. GT2018-76797*.
- [172] Mensah, G. A., and Moeck, J. P., 2017, "Acoustic Damper Placement and Tuning for Annular Combustors: An Adjoint-Based Optimization Study," *ASME J. Eng. Gas Turbines Power*, **139**(6), p. 061501.
- [173] Aguilar, J., and Juniper, M. P., 2018, "Adjoint Methods for Elimination of Thermoacoustic Oscillations in a Model Annular Combustor Via Small Geometry Modifications," *ASME Paper No. GT2018-75692*.
- [174] Aguilar, J., and Juniper, M. P., 2018, "Shape Optimization in Low-Order Thermoacoustic Networks," *GPPS Forum 18, Global Power and Propulsion Society*, Zurich, Switzerland, Jan. 10–12, Paper No. GPPS-2018-0024.
- [175] Silva, C. F., Yong, K. J., and Magri, L., 2018, "Thermoacoustic Modes of Quasi-One-Dimensional Combustors in the Region of Marginal Stability," *ASME J. Eng. Gas Turbines Power*, **141**(2), p. 021022.
- [176] Juniper, M. P., 2018, "Sensitivity Analysis of Thermoacoustic Instability With Adjoint Helmholtz Solvers," *Phys. Rev. Fluids*, **3**, p. 110509.
- [177] Boujo, E., and Noiray, N., 2017, "Robust Identification of Harmonic Oscillator Parameters Using the Adjoint Fokker-Planck Equation," *Proc. R. Soc. A*, **473**(2200), p. 20160894.
- [178] Noiray, N., and Schuermans, B., 2013, "Deterministic Quantities Characterizing Noise Driven Hopf Bifurcations in Gas Turbine Combustors," *Int. J. Non-Linear Mech.*, **50**, pp. 152–163.
- [179] Noiray, N., 2016, "Linear Growth Rate Estimation From Dynamics and Statistics of Acoustic Signal Envelope in Turbulent Combustors," *ASME J. Eng. Gas Turbines Power*, **139**(4), p. 041503.
- [180] Noiray, N., and Denisov, A., 2017, "A Method to Identify Thermoacoustic Growth Rates in Combustion Chambers From Dynamic Pressure Time Series," *Proc. Combust. Inst.*, **36**(3), pp. 3843–3850.
- [181] Orchini, A., Rigas, G., and Juniper, M. P., 2016, "Weakly Nonlinear Analysis of Thermoacoustic Bifurcations in the Rijke Tube," *J. Fluid Mech.*, **805**, pp. 523–550.
- [182] Landau, L. D., 1944, "On the Problem of Turbulence," *Dokl. Akad. Nauk SSSR*, **44**(8), pp. 339–349.
- [183] Stuart, J. T., 1958, "On the Non-Linear Mechanics of Hydrodynamic Stability," *J. Fluid Mech.*, **4**(1), pp. 1–21.
- [184] Stuart, J. T., 1971, "Nonlinear Stability Theory," *Annu. Rev. Fluid Mech.*, **3**(1), pp. 347–370.
- [185] Provansal, M., Mathis, C., and Boyer, L., 1987, "Bénard-von Kármán Instability: Transient and Forced Regimes," *J. Fluid Mech.*, **182**(1), pp. 1–22.
- [186] Dušek, J., Le Gal, P., and Fraunie, P., 1994, "A Numerical and Theoretical Study of the First Hopf Bifurcation in a Cylinder Wake," *J. Fluid Mech.*, **264**(1), pp. 59–80.
- [187] Lieuwen, T., 2012, *Unsteady Combustor Physics*, Cambridge University Press, Cambridge, UK.
- [188] Eckstein, J., and Sattelmayer, T., 2006, "Low-Order Modeling of Low-Frequency Combustion Instabilities in AeroEngines," *J. Propul. Power*, **22**(2), pp. 425–432.
- [189] Williams, F. A., 1985, *Combustion Theory*, Perseus Books, Reading, MA.
- [190] Kuo, K. K., 1986, *Principles of Combustion*, Wiley, Hoboken, NJ.
- [191] Peters, N., 2000, *Turbulent Combustion*, Cambridge University Press, Cambridge, UK.
- [192] Poinsot, T., and Veynante, D., 2005, *Theoretical and Numerical Combustion*, 2nd ed., R. T. Edwards, Philadelphia, PA.
- [193] Dowling, A. P., and Stow, S. R., 2003, "Acoustic Analysis of Gas Turbine Combustors," *J. Propul. Power*, **19**(5), pp. 751–764.
- [194] Rienstra, S., and Hirschberg, A., 2004, "An Introduction to Acoustics," accessed Feb. 26, 2019, <https://www.win.tue.nl/~sjoerdri/papers/book.pdf>
- [195] Magri, L., 2017, "On Indirect Noise in Multi-Component Nozzle Flows," *J. Fluid Mech.*, **828**, p. R2.
- [196] Magri, L., O'Brien, J., and Ihme, M., 2016, "Compositional Inhomogeneities as a Source of Indirect Combustion Noise," *J. Fluid Mech.*, **799**, p. R4.
- [197] Nicoud, F., and Wieczorek, K., 2009, "About the Zero Mach Number Assumption in the Calculation of Thermoacoustic Instabilities," *Int. J. Spray Combust. Dyn.*, **1**(1), pp. 67–111.
- [198] Dowling, A. P., 1995, "The Calculation of Thermoacoustic Oscillations," *J. Sound Vib.*, **180**(4), pp. 557–581.
- [199] Krebs, W., Walz, G., Flohr, P., and Hoffman, S., 2001, "Modal Analysis of Annular Combustors: Effect of Burner Impedance," *ASME Paper No. 2001-GT-0042*.

- [200] Evesque, S., and Polifke, W., 2002, "Low-Order Acoustic Modelling for Annular Combustors: Validation and Inclusion of Modal Coupling," *ASME Paper No. GT-2002-30064*.
- [201] Camporeale, S. M., Bari, P., David, R., Bottaro, A., Campa, G., Camporeale, S. M., Guaus, A., Favier, J., Bargiacchi, M., Bottaro, A., Cosatto, E., and Mori, M., 2011, "A Quantitative Comparison Between a Low Order Model and a 3D FEM Code for the Study of Thermoacoustic Combustion Instabilities," *ASME Paper No. GT2011-45969*.
- [202] Laera, D., Schuller, T., Prieur, K., Durox, D., Camporeale, S. M., and Candel, S., 2017, "Flame Describing Function Analysis of Spinning and Standing Modes in an Annular Combustor and Comparison With Experiments," *Combust. Flame*, **184**, pp. 136–152.
- [203] Rayleigh, J. W. S. B., 1896, *The Theory of Sound*, Vol. 2, Macmillan, London.
- [204] Carrier, G. F., 1955, "The Mechanics of the Rijke Tube," *Q. Appl. Math.*, **12**(4), pp. 383–395.
- [205] Heckl, M. A., 1988, "Active Control of the Noise From a Rijke Tube," *J. Sound Vib.*, **124**(1), pp. 117–133.
- [206] Dowling, A. P., 1997, "Nonlinear Self-Excited Oscillations of a Ducted Flame," *J. Fluid Mech.*, **346**, pp. 271–290.
- [207] Schuermans, B. B. H., Polifke, W., and Paschereit, C. O., 1999, "Modeling Transfer Matrices of Premixed Flames and Comparison With Experimental Results," *ASME Paper No. 99-GT-132*.
- [208] Polifke, W., Poncet, A., Paschereit, C. O., and Döbbeling, K., 2001, "Reconstruction of Acoustic Transfer Matrices by Instationary Computational Fluid Dynamics," *J. Sound Vib.*, **245**(3), pp. 483–510.
- [209] Stow, S. R., and Dowling, A. P., 2001, "Thermoacoustic Oscillations in an Annular Combustor," *ASME Paper No. 2001-GT-0037*.
- [210] Dowling, A. P., and Morgans, A. S., 2005, "Feedback Control of Combustion Oscillations," *Annu. Rev. Fluid Mech.*, **37**(1), pp. 151–182.
- [211] Morfey, C. L., 1973, "Amplification of Aerodynamic Noise by Convected Flow Inhomogeneities," *J. Sound Vib.*, **31**(4), pp. 391–397.
- [212] Strobl Chen, L., Bomberg, S., and Polifke, W., 2016, "Propagation and Generation of Acoustic and Entropy Waves Across a Moving Flame Front," *Combust. Flame*, **166**, pp. 170–180.
- [213] Bloxsidge, G. J., Dowling, A. P., and Langhorne, P. J., 1988, "Reheat Buzz: An Acoustically Coupled Combustion Instability—Part 2: Theory," *J. Fluid Mech.*, **193**(1), pp. 445–473.
- [214] Marble, F. E., and Candel, S. M., 1977, "Acoustic Disturbance From Gas Non-Uniformities Convected Through a Nozzle," *J. Sound Vib.*, **55**(2), pp. 225–243.
- [215] Boileau, M., Staffelbach, G., Cuenot, B., Poinsot, T., and Berat, C., 2008, "LES of an Ignition Sequence in a Gas Turbine Engine," *Combust. Flame*, **154**(1–2), pp. 2–22.
- [216] O'Connor, J., Acharya, V., and Lieuwen, T., 2015, "Transverse Combustion Instabilities: Acoustic, Fluid Mechanic, and Flame Processes," *Prog. Energy Combust. Sci.*, **49**, pp. 1–39.
- [217] Bourguin, J.-F., Durox, D., Moeck, J. P., Schuller, T., and Candel, S., 2014, "Characterization and Modeling of a Spinning Thermoacoustic Instability in an Annular Combustor Equipped With Multiple Matrix Injectors," *ASME J. Eng. Gas Turbines Power*, **137**(2), p. 021503.
- [218] Prieur, K., Durox, D., Schuller, T., and Candel, S., 2017, "A Hysteresis Phenomenon Leading to Spinning or Standing Azimuthal Instabilities in an Annular Combustor," *Combust. Flame*, **175**, pp. 283–291.
- [219] Laera, D., Prieur, K., Durox, D., Schuller, T., Camporeale, S., and Candel, S., 2017, "Impact of Heat Release Distribution on the Spinning Modes of an Annular Combustor With Multiple Matrix Burners," *ASME J. Eng. Gas Turbines Power*, **139**(5), p. 051505.
- [220] Stow, S. R., and Dowling, A. P., 2004, "Low-Order Modelling of Thermoacoustic Limit Cycles," *ASME Paper No. GT2004-54245*.
- [221] Bauerheim, M., Parmentier, J. F., Salas, P., Nicoud, F., and Poinsot, T., 2014, "An Analytical Model for Azimuthal Thermoacoustic Modes in an Annular Chamber Fed by an Annular Plenum," *Combust. Flame*, **161**(5), pp. 1374–1389.
- [222] Orchini, A., Mensah, G. A., and Moeck, J. P., 2018, "Effects of Nonlinear Modal Interactions on the Thermoacoustic Stability of Annular Combustors," *ASME J. Eng. Gas Turbines Power*, **141**, p. 021002.
- [223] Peters, N., 1992, "Fifteen Lectures on Laminar and Turbulent Combustion," *Ercofac Summer School*, Aachen, Germany, Sept. 14–28.
- [224] Tyagi, M., Chakravarthy, S. R., and Sujith, R. I., 2007, "Unsteady Combustion Response of a Ducted Non-Premixed Flame and Acoustic Coupling," *Combust. Theory Model.*, **11**(2), pp. 205–226.
- [225] Tyagi, M., Jamadar, N., and Chakravarthy, S., 2007, "Oscillatory Response of an Idealized Two-Dimensional Diffusion Flame: Analytical and Numerical Study," *Combust. Flame*, **149**(3), pp. 271–285.
- [226] Magina, N. A., and Lieuwen, T. C., 2016, "Effect of Axial Diffusion on the Response of Diffusion Flames to Axial Flow Perturbations," *Combust. Flame*, **167**, pp. 395–408.
- [227] Dowling, A. P., 1999, "A Kinematic Model of a Ducted Flame," *J. Fluid Mech.*, **394**, pp. 51–72.
- [228] Schuller, T., Duxruix, S., Durox, D., and Candel, S., 2002, "Modeling Tools for the Prediction of Premixed Flame," *Proc. Combust. Inst.*, **29**(1), pp. 107–113.
- [229] Lieuwen, T., 2005, "Nonlinear Kinematic Response of Premixed Flames to Harmonic Velocity Disturbances," *Proc. Combust. Inst.*, **30**(2), pp. 1725–1732.
- [230] Preetham, S. H., and Lieuwen, T. C., 2007, "Response of Turbulent Premixed Flames to Harmonic Acoustic Forcing," *Proc. Combust. Inst.*, **31**(1), pp. 1427–1434.
- [231] Balachandran, R., Ayoola, B. O., Kaminski, C. F., Dowling, A. P., and Mastorakos, E., 2005, "Experimental Investigation of the Non Linear Response of Turbulent Premixed Flames to Imposed Inlet Velocity Oscillations," *Combust. Flame*, **143**(1–2), pp. 37–55.
- [232] Noiray, N., Durox, D., Schuller, T., and Candel, S., 2008, "A Unified Framework for Nonlinear Combustion Instability Analysis Based on the Flame Describing Function," *J. Fluid Mech.*, **615**, pp. 139–167.
- [233] Crocco, L., and Cheng, S.-I., 1956, "Theory of Combustion Instability in Liquid Propellant Rocket Motors," The Advisory Group for Aeronautical Research and Development North Atlantic Treaty Organization, Butterworths Scientific Publications, Oxford, UK.
- [234] Summerfield, M., 1951, "A Theory of Unstable Combustion in Liquid Propellant Rocket Systems," *J. Am. Rocket Soc.*, **21**(5), pp. 108–114.
- [235] Crocco, L., 1969, "Research on Combustion Instability in Liquid Propellant Rockets," *Symp. (Int.) Combust.*, **12**(1), pp. 85–99.
- [236] Sirignano, W. A., 2015, "Driving Mechanisms for Combustion Instability," *Combust. Sci. Technol.*, **187**(1–2), pp. 162–205.
- [237] Kashinath, K., Hemchandra, S., and Juniper, M. P., 2013, "Nonlinear Thermoacoustics of Ducted Premixed Flames: The Influence of Perturbation Convection Speed," *Combust. Flame*, **160**(12), pp. 2856–2865.
- [238] Friedman, A., and Shinbrot, M., 1968, "Nonlinear Eigenvalue Problems," *Acta Math.*, **121**, pp. 77–125.
- [239] Mennicken, R., and Möller, M., 2003, *Non-Self-Adjoint Boundary Eigenvalue Problems*, Vol. 192, Gulf Professional Publishing, Houston, TX.
- [240] Mehrmann, V., and Voss, H., 2004, "Nonlinear Eigenvalue Problems: A Challenge for Modern Eigenvalue Methods," *GAMM Mitt.*, **27**(2), pp. 121–152.
- [241] Betcke, T., Higham, N. J., Mehrmann, V., Schröder, C., and Tisseur, F., 2013, "NLEVP: A Collection of Nonlinear Eigenvalue Problems," *ACM Trans. Math. Software (TOMS)*, **39**(2), p. 1.
- [242] Güttel, S., and Tisseur, F., 2017, "The Nonlinear Eigenvalue Problem," *Acta Numer.*, **26**, pp. 1–94.
- [243] Schuermans, B., Bellucci, V., and Paschereit, C. O., 2003, "Thermoacoustic Modeling and Control of Multiburner Combustion Systems," *ASME Paper No. GT2003-38688*.
- [244] Bothien, M. R., Moeck, J. P., Lacarelle, A., and Paschereit, C. O., 2007, "Time Domain Modelling and Stability Analysis of Complex Thermoacoustic Systems," *Proc. Inst. Mech. Eng., Part A*, **221**(5), pp. 657–668.
- [245] Emmert, T., Meindl, M., Jaensch, S., and Polifke, W., 2016, "Linear State Space Interconnect Modeling of Acoustic Systems," *Acta Acust. United Acust.*, **102**(5), pp. 824–833.
- [246] Heiss, W. D., 2004, "Exceptional Points of Non-Hermitian Operators," *J. Phys. A: Math. General*, **37**(6), pp. 2455–2464.
- [247] Mensah, G., Magri, L., Silva, C., Buschmann, P., and Moeck, J., 2018, "Exceptional Points in the Thermoacoustic Spectrum," *J. Sound Vib.*, **433**, pp. 124–128.
- [248] Hryniw, R., and Lancaster, P., 1999, "On the Perturbation of Analytic Matrix Functions," *Integr. Equations Operator Theory*, **34**(3), pp. 325–338.
- [249] Roman, J. E., Campos, C., Romero, E., and Tomás, A., 2015, "SLEPc User's Manual," D. Sistemes Informàtics i Computació Universitat Politècnica de València, Valencia, Spain, Report No. DSIC-II/24/02.
- [250] Brebion, M. M., 2017, "Joint Numerical and Experimental Study of Thermo-Acoustic Instabilities," *Ph.D. thesis*, Université de Toulouse, Toulouse, France.
- [251] Buschmann, P., Mensah, G. A., Nicoud, F., and Moeck, J. P., 2019, "Solution of Thermoacoustic Eigenvalue Problems With a Non-Iterative Method," *ASME Paper No. GT2019-90834*.
- [252] Chandramoorthy, N., Wang, Q., Magri, L., Narayanan, S. H. K., and Hovland, P., 2017, "Sensitivity Analysis of Hydrodynamic Chaos in Combustion Using NILSS-AD," APS Division of Fluid Dynamics Meeting Abstracts.
- [253] Dennerly, P., and Krzywický, A., 1996, *Mathematics for Physicists*, Dover Publications, Mineola, NY.
- [254] Vogel, C. R., and Wade, J. G., 1995, "Analysis of Costate Discretizations in Parameter-Estimation for Linear Evolution-Equations," *SIAM J. Control Optim.*, **33**(1), pp. 227–254.
- [255] Bewley, T. R., 2001, "Flow Control: New Challenges for a New Renaissance," *Prog. Aerosp. Sci.*, **37**(1), pp. 21–58.
- [256] Giles, M. B., and Pierce, N. A., 2000, "An Introduction to the Adjoint Approach to Design," *Flow, Turbul. Combust.*, **65**(3/4), pp. 393–415.
- [257] Pierce, N. A., and Giles, M. B., 2004, "Adjoint and Defect Error Bounding and Correction for Functional Estimates," *J. Comput. Phys.*, **200**(2), pp. 769–794.
- [258] Hartmann, R., 2007, "Adjoint Consistency Analysis of Discontinuous Galerkin Discretizations," *SIAM J. Numer. Anal.*, **45**(6), pp. 2671–2696.
- [259] Berg, J., and Nordström, J., 2013, "On the Impact of Boundary Conditions on Dual Consistent Finite Difference Discretizations," *J. Comput. Phys.*, **236**(1), pp. 41–55.
- [260] Oden, J. T., 1979, *Applied Functional Analysis*, Prentice Hall, Upper Saddle River, NJ.
- [261] Kato, T., 1980, *Perturbation Theory for Linear Operators*, 2nd ed., Springer, Berlin.
- [262] Schrödinger, E., 1928, *Collected Papers on Wave Mechanics*, Blackie & Son Limited, Glasgow, UK.
- [263] Vishik, M. I., and Lyusternik, L. A., 1960, "The Solution of Some Perturbation Problems for Matrices and Self-Adjoint or Non-Self-Adjoint Differential Equations—I," *Russ. Math. Surv.*, **15**(3), p. 1.
- [264] Langer, H., and Najman, B., 1989, "Remarks on the Perturbation of Analytic Matrix Functions—II," *Integr. Equations Operator Theory*, **12**(3), pp. 392–407.

- [265] Sun, J.-G., 1990, "Multiple Eigenvalue Sensitivity Analysis," *Linear Algebra Appl.*, **137**, pp. 183–211.
- [266] Langer, H., and Najman, B., 1992, "Remarks on the Perturbation of Analytic Matrix Functions—III," *Integr. Equations Operator Theory*, **15**(5), pp. 796–806.
- [267] Lancaster, P., Markus, A. S., and Zhou, F., 2003, "Perturbation Theory for Analytic Matrix Functions: The Semisimple Case," *SIAM J. Matrix Anal. Appl.*, **25**(3), pp. 606–626.
- [268] Seyranian, A. P., and Mailybaev, A. A., 2003, "Interaction of Eigenvalues in Multi-Parameter Problems," *J. Sound Vib.*, **267**(5), pp. 1047–1064.
- [269] Seyranian, A. P., Kirillov, O. N., and Mailybaev, A. A., 2005, "Coupling of Eigenvalues of Complex Matrices at Diabolical and Exceptional Points," *J. Phys. A: Math. General*, **38**(8), p. 1723.
- [270] Evesque, S., Polifke, W., and Pankiewitz, C., 2003, "Spinning and Azimuthally Standing Acoustic Modes in Annular Combustors," *AIAA Paper No. 2003-3182*.
- [271] Moeck, J. P., Paul, M., and Paschereit, C. O., 2010, "Thermoacoustic Instabilities in an Annular Rijke Tube," *ASME Paper No. GT2010-23577*.
- [272] Moeck, J. P., 2010, "Analysis, Modeling, and Control of Thermoacoustic Instabilities," *Ph.D. thesis*, Technischen Universität Berlin, Berlin.
- [273] Noiray, N., Bothien, M., and Schuermans, B., 2011, "Investigation of Azimuthal Staging Concepts in Annular Gas Turbines," *Combust. Theory Modell.*, **15**(5), pp. 585–606.
- [274] Noiray, N., and Schuermans, B., 2013, "On the Dynamic Nature of Azimuthal Thermoacoustic Modes in Annular Gas Turbine Combustion Chambers," *Proc. R. Soc. A*, **469**(2151), p. 20120535.
- [275] Ghirardo, G., and Juniper, M. P., 2013, "Azimuthal Instabilities in Annular Combustors: Standing and Spinning Modes," *Proc. R. Soc. A*, **469**(2157), p. 20130232.
- [276] Bauerheim, M., Nicoud, F., and Poinsot, T., 2016, "Progress in Analytical Methods to Predict and Control Azimuthal Combustion Instability Modes in Annular Chambers," *Phys. Fluids*, **28**(2), p. 021303.
- [277] Ghirardo, G., Juniper, M. P., and Moeck, J. P., 2016, "Weakly Nonlinear Analysis of Thermoacoustic Instabilities in Annular Combustors," *J. Fluid Mech.*, **805**, pp. 52–87.
- [278] Bauerheim, M., Ndiaye, A., Constantine, P., Moreau, S., and Nicoud, F., 2016, "Symmetry Breaking of Azimuthal Thermoacoustic Modes: The UQ Perspective," *J. Fluid Mech.*, **789**, pp. 534–566.
- [279] Ghirardo, G., Di Giovine, C., Moeck, J. P., and Bothien, M. R., 2018, "Thermoacoustics of Can-Annular Combustors," *ASME Paper No. GT2018-75799*.
- [280] Balaji, C., and Chakravarthy, S. R., 2011, "Formulation of Combustion Acoustic Interaction Using Simultaneous Multiple Time and Length Scales and Combustion Instability Prediction in Turbulent Non-Premixed Half-Dump Combustor," 18th International Congress on Sound and Vibration (ICSV), Rio de Janeiro, Brazil, July 10–14.
- [281] Lighthill, J., 1978, "Acoustic Streaming," *J. Sound Vib.*, **61**(3), pp. 391–418.
- [282] Mariappan, S., and Sujith, R. I., 2011, "Modelling Nonlinear Thermoacoustic Instability in an Electrically Heated Rijke Tube," *J. Fluid Mech.*, **680**, pp. 511–533.
- [283] Chu, B. T., and Kovácsnay, L. S. G., 1958, "Non-Linear Interactions in a Viscous Heat-Conducting Compressible Gas," *J. Fluid Mech.*, **3**(5), pp. 494–514.
- [284] Silva, C. F., and Polifke, W., 2019, "Non-Dimensional Groups for Similarity Analysis of Thermoacoustic Instabilities," *Proc. Combust. Inst.*, **37**(4), pp. 5289–5297.
- [285] Mukherjee, N., and Shrira, V., 2017, "Intrinsic Flame Instabilities in Combustors: Analytic Description of a 1-D Resonator Model," *Combust. Flame*, **185**, pp. 188–209.
- [286] Steele, R. C., Cowell, L. H., Cannon, S. M., and Smith, C. S., 1999, "Passive Control of Combustion Instability in Lean Premixed Combustors," *ASME Paper No. 99-GT-52*.
- [287] Mongia, H. C., Held, T. J., Hsiao, G. C., and Pandalai, R. P., 2003, "Challenges and Progress in Controlling Dynamics in Gas Turbine Combustors," *J. Propul. Power*, **19**(5), pp. 822–829.
- [288] Richards, G. A., Straub, D. L., and Robey, E. H., 2003, "Passive Control of Combustion Dynamics in Stationary Gas Turbines," *J. Propul. Power*, **19**(5), pp. 795–810.
- [289] Sohn, C. H., and Park, J. H., 2011, "A Comparative Study on Acoustic Damping Induced by Half-Wave, Quarter-Wave, and Helmholtz Resonators," *Aerosp. Sci. Technol.*, **15**(8), pp. 606–614.
- [290] Noiray, N., and Schuermans, B., 2012, "Theoretical and Experimental Investigations on Damper Performance for Suppression of Thermoacoustic Oscillations," *J. Sound Vib.*, **331**(12), pp. 2753–2763.
- [291] Ghirardo, G., Boudy, F., and Bothien, M. R., 2018, "Amplitude Statistics Prediction in Thermoacoustics," *J. Fluid Mech.*, **844**, pp. 216–246.
- [292] Yang, D., Sogaro, F. M., Morgans, A. S., and Schmid, P. J., 2019, "Optimising the Acoustic Damping of Multiple Helmholtz Resonators Attached to a Thin Annular Duct," *J. Sound Vib.*, **444**, pp. 69–84.
- [293] Park, I. S., and Sohn, C. H., 2010, "Nonlinear Acoustic Damping Induced by a Half-Wave Resonator in an Acoustic Chamber," *Aerosp. Sci. Technol.*, **14**(6), pp. 442–450.
- [294] Jamieson, N. P., and Juniper, M. P., 2017, "Experimental Sensitivity Analysis of a Linearly Stable Thermoacoustic System Via a Pulsed Forcing Technique," *Exp. Fluids*, **58**(9), p. 123.
- [295] Aguilar, J. G., 2018, "Sensitivity Analysis and Optimization in Low Order Thermoacoustic Models," Ph.D. thesis, University of Cambridge, Cambridge, UK.
- [296] Giusti, A., Magri, L., and Zedda, M., 2018, "Flow Inhomogeneities in a Realistic Aeronautical Gas-Turbine Combustor: Formation, Evolution and Indirect Noise," *ASME Paper No. GT2018-76436*.
- [297] Chu, B. T., 1963, "Analysis of a Self-Sustained Thermally Driven Nonlinear Vibration," *Phys. Fluids*, **6**(11), p. 1638.
- [298] Yu, H., Jaravel, T., Juniper, M., Ihme, M., and Magri, L., 2019, "Data Assimilation and Optimal Calibration in Nonlinear Models of Flame Dynamics," *ASME Paper No. GT2019-92052*.
- [299] Traverso, T., Bottaro, A., and Magri, L., 2018, "Data Assimilation in Thermoacoustic Instability With Lagrangian Optimization," *EuroMech*, Vienna, Austria, Sept. 9–13.
- [300] Jaynes, E. T., 1957, "Information Theory and Statistical Mechanics," *Phys. Rev.*, **106**(4), pp. 620–630.
- [301] Constantine, P., 2015, *Active Subspaces: Emerging Ideas for Dimension Reduction in Parameter Studies*, Society for Industrial and Applied Mathematics, Philadelphia, PA.
- [302] Palies, P., Durox, D., Schuller, T., and Candel, S., 2010, "The Combined Dynamics of Swirler and Turbulent Premixed Swirling Flames," *Combust. Flame*, **157**(9), pp. 1698–1717.
- [303] Palies, P., Durox, D., Schuller, T., and Candel, S., 2011, "Nonlinear Combustion Instability Analysis Based on the Flame Describing Function Applied to Turbulent Premixed Swirling Flames," *Combust. Flame*, **158**(10), pp. 1980–1991.
- [304] Silva, C. F., Nicoud, F., Schuller, T., Durox, D., and Candel, S., 2013, "Combining a Helmholtz Solver With the Flame Describing Function to Assess Combustion Instability in a Premixed Swirled Combustor," *Combust. Flame*, **160**(9), pp. 1743–1754.
- [305] Stow, S. R., and Dowling, A. P., 2003, "Modelling of Circumferential Modal Coupling Due to Helmholtz Resonators," *ASME Paper No. GT2003-38168*.
- [306] Bonciolini, G., Ebi, D., Boujo, E., and Noiray, N., 2018, "Experiments and Modelling of Rate-Dependent Transition Delay in a Stochastic Subcritical Bifurcation," *R. Soc. Open Sci.*, **5**(3), p. 172078.
- [307] Shroff, G. M., and Keller, H. B., 1993, "Stabilization of Unstable Procedures: The Recursive Projection Method," *SIAM J. Num. Anal.*, **30**(4), pp. 1099–1120.
- [308] Waugh, I., Illingworth, S., and Juniper, M., 2013, "Matrix-Free Continuation of Limit Cycles for Bifurcation Analysis of Large Thermoacoustic Systems," *J. Comput. Phys.*, **240**, pp. 225–247.
- [309] Citro, V., Luchini, P., Giannetti, F., and Auteri, F., 2017, "Efficient Stabilization and Acceleration of Numerical Simulation of Fluid Flows by Residual Recombination," *J. Comp. Phys.*, **344**, pp. 234–246.
- [310] Magri, L., and Wang, Q., 2017, "Stability, Receptivity and Sensitivity of Linear, Periodic and Chaotic Flows: Application to a Thermoacoustic System," *APS Division of Fluid Dynamics Meeting Abstracts*.
- [311] McManus, K. R., Poinsot, T., and Candel, S. M., 1993, "A Review of Active Control of Combustion Instabilities," *Prog. Energy Combust. Sci.*, **19**(1), pp. 1–29.
- [312] Friedman, B., and Mishoe, L. I., 1956, "Eigenfunction Expansions Associated With Non-Self-Adjoint Differential Equation," *Pacific J. Math.*, **6**(2), pp. 249–270.
- [313] Sirkes, Z., and Tziperman, E., 1997, "Finite Difference of Adjoint or Adjoint of Finite Difference?," *Mon. Weather Rev.*, **125**(12), pp. 3373–3378.
- [314] Errico, R. M., 1997, "What is an Adjoint Model?," *Bull. Am. Meteorol. Soc.*, **78**(11), pp. 2577–2591.
- [315] Plessix, R. E., 2006, "A Review of the Adjoint-State Method for Computing the Gradient of a Functional With Geophysical Applications," *Geophys. J. Int.*, **167**(2), pp. 495–503.
- [316] Estep, D. J., 2004, "A Short Course on Duality, Adjoint Operators, Green's Functions, and a Posteriori Error Analysis," Course Notes, Colorado State University, Fort Collins, CO.
- [317] Ibragimov, N. H., 2006, "Integrating Factors, Adjoint Equations and Lagrangians," *J. Math. Anal. Appl.*, **318**(2), pp. 742–757.
- [318] Giles, M. B., and Süli, E., 2002, "Adjoint Methods for PDEs: A Posteriori Error Analysis and Postprocessing by Duality," *Acta Numer.*, **11**, pp. 145–236.
- [319] Claerbout, J., 2014, *Geophysical Image Estimation by Example*, Jon Claerbout, Stanford, CA.